Flight Mechanics and Control for an Unpowered Reusable Launch Vehicle

---

A Thesis presented to the Faculty of the Graduate School
University of Missouri

In Partial Fulfillment
Of the Requirements for the Degree

Master of Science

---

by
STEVEN MCKEE

Dr. Craig A. Kluever, Thesis Supervisor

MAY 2011

The undersigned, appointed by the dean of the Graduate School, have examined the thesis entitled

FLIGHT MECHANICS AND CONTROL FOR AN UNPOWERED REUSABLE LAUNCH VEHICLE

presented by Steven E. McKee,

a candidate for the Master of Science degree in Mechanical Engineering,

and hereby certify that, in their opinion, it is worthy of acceptance.

_____

Dr. Craig Kluever

_____

Dr. Roger Fales

_____

Dr. Mark Ellersieck

DEDICATION

I would like to dedicate this thesis to my family and friends who have encouraged me during my pursuit of an advanced degree.

To Anna, thank you for being my best friend. Thank you for always being there for me and for always making me smile. You always support me and are always willing to offer a helping hand. I cannot wait to spend the rest of my life with you.

To Dad, thank you for instilling in me a great sense of pride. Thank you for teaching me the meaning of hard work and dedication, and for teaching me to lead by example. But most of all, thank you for teaching me that if I am going to do something, I should always do it right.

To Mom, thank you for always being there for me to talk to. Whether our talks are about something important or nothing at all, they are always a bright spot during my day. Thank you for always providing me with the perspective I need and for always encouraging me to go above and beyond what anyone expects of me.

To Kevin, thank you for always providing the witty comments when we hang out together. You always find a way to make me laugh. Thank you for always being someone who I can go to when I need a little competition.

To Grandma and Grandpa McKee, thank you for always being involved and interested in whatever it is that I am doing in my life. I am so glad that I get to share everything with you both. I always look forward to hanging out with you, whether we are out on a hunting adventure or lounging around the house eating incredible food.

To Grandma and Grandpa Manter, thank you for financially supporting me throughout my college career. Without your help, I would not be where I am today.

To my friends, I could not ask for a better group of individuals to be involved in my life. You all are always just a phone call away and we always manage to have a great time together. Thank you for being so supportive of my academic interests yet always knowing when to tell me that I need a break.

ACKNOWLEDGEMENTS

This thesis would not have been possible without the help and guidance of many people who contributed significant assistance towards the completion of my research.

To my professor, mentor, and advisor Dr. Craig Kluever, I would like to extend my thanks for accepting me first as a freshman in the Discovery Fellows program, second as an Undergraduate research student, and finally, as your Graduate Research Assistant. My five years of researching and studying under your direction has been invaluable in my academic progress and development. You created an environment that allowed me to thrive and I will always be thankful towards you for that.

To the brilliant minds at Barron Associates, Inc, I thank you for funding my graduate research and providing insight into which new idea to pursue next.

To Dr. Roger Fales, I thank you for your excellent coursework pertaining to control-design.

To Dr. John Miles, I thank you for getting me involved in the MSGC program and further developing my knowledge of Aerospace Engineering.

To my colleagues, namely Aaron Rosengren and John Wagner, who have furthered my understanding of control-design through countless hours studying for tests and working on homework, I thank you greatly. A large amount of my programming knowledge can be attributed to you both.

To my bride-to-be, Anna McLaughlin, I thank you for proofreading and editing this thesis. For your continued support and motivation, I cannot thank you enough.

To my friend, Bret Wiley, for his technological savvy and computer genius, I am very thankful.

TABLE OF CONTENTS

LIST OF FIGURES

Figure Page

LIST OF TABLES

Table Page

NOMENCLATURE

AR	=	aspect ratio
a	=	acceleration, ft/s^2
b	=	wingspan, ft
C_D	=	drag coefficient
C_{D0}	=	zero-lift drag coefficient
C_L	=	lift coefficient
D	=	drag force, lb_f
E	=	energy, ft·lb_f
e	=	span efficiency factor
G_R	=	HAC radius error gain, ft^{-1}
G_{RD}	=	HAC radius rate gain, rad·s/ft
g	=	Earth's gravitational acceleration, 32.174 ft/s^2
H	=	constant value bias scale factor
h	=	altitude above runway, ft
$\boldsymbol{I}$	=	identity matrix
K	=	lift-induced drag coefficient parameter
k_θ	=	angular gain value, rad
k_R	=	radial gain value, ft^{-1}
L	=	lift force, lb
Ma	=	Mach number
m	=	vehicle mass, slugs
$PSHA$	=	heading angle relative to the HAC, deg
$\boldsymbol{Q}$	=	controllability matrix
$\bar{q}$	=	dynamic pressure, lb/ft^2
R	=	instantaneous turn radius, ft
R_F	=	final HAC radius, ft
R_2	=	quadratic coefficient for HAC radius, ft/deg^2
S	=	vehicle reference area, ft^2
S	=	groundtrack range, ft
t	=	time, s
V	=	airspeed, ft/s

W	=	weight, lb_f
X_HAC	=	HAC location in x-direction, ft
x	=	downtrack position along runway centerline, ft
y	=	crosstrack position with respect to runway centerline, ft
$\%OS$	=	percent overshoot
α	=	angle of attack, deg
β	=	inverse scale height, ft^{-1}
γ	=	flight path angle, deg
δ	=	angular vehicle position, deg
λ	=	eigenvalues
ϕ	=	bank angle, deg
ρ	=	atmospheric density, $slugs/ft^3$
θ	=	angular elevation from nominal, deg
ψ	=	heading angle, deg
ω_n	=	natural frequency, rad/s
ζ	=	damping ratio

Subscripts

actual	=	instantaneous calculated value
ALI	=	approach and landing interface
BIAS	=	bias bank angle value
CL	=	closed-loop
error	=	error value
f	=	final value
H	=	horizontal
HAC	=	heading alignment cone
MAX	=	maximum value
OL	=	open-loop
offset	=	offset distance value
ref	=	reference value
SL	=	straight line value
s	=	settling time
WLE	=	wings-level equivalent
0	=	initial value

ABSTRACT

A new trajectory planning strategy has been developed to aid in allowing a reusable launch vehicle to complete the Terminal Area Energy Management (TAEM) phase of reentry. Using the new trajectory planning and tracking strategy, the reusable launch vehicle will complete TAEM with a higher degree of accuracy than what has been accomplished in the past. The reusable launch vehicle will also be better prepared to adapt to unpredictable conditions, which in the past were a hindrance to an accurate and safe reentry.

The new strategy is composed of two distinct components. The first component provides the vehicle with a new way to track the Heading Alignment Cone (HAC) using dynamic gain values. The new dynamic gains values are found through a combination of linearization, state-space representation, and pole-placement. The second component provides the vehicle with an extremely accurate groundtrack predictor. The groundtrack predictor allows the vehicle to accurately determine an ideal trajectory to the next reentry phase, Approach and Landing. The groundtrack predictor utilizes a combination of HAC size and location modifications in order to provide the vehicle with an accurate prediction.

CHAPTER 1

INTRODUCTION

A new method of trajectory tracking and control has been developed in order to improve both lateral and longitudinal performance of reusable launch vehicles. In one of the most critical stages of reentry flight, Terminal Area Energy Management (TAEM), the vehicle must quickly and efficiently negate any position or heading error that has been inherited, prior to Approach and Landing Interface (ALI) occurring. The vehicle must be able to effectively follow a planned route, recognizing and correcting any errors with respect to trajectory in real-time. Also, a new method of range prediction and calculation has been developed. With a superior model to predict maximum possible range for the vehicle a more accurate and reliable trajectory model may be used during the TAEM phase of flight.

1.1 Background and History

In the recent past, the most common type of vehicle reentering Earth's atmosphere from space has been NASA's Space Shuttle, henceforth referred to as the Shuttle. The Shuttle can be generally classified as a reusable launch vehicle (RLV). The Shuttle is a glider with very poor aerodynamic characteristics. The lack of an ideal aerodynamic profile can be attributed to the need for the Shuttle to withstand incredible heating and force as it reenters the atmosphere. Much of the basis for new and developing technology relating to current and future vehicles is derived from documents concerning the Shuttle.

As an RLV with lifting capability is returning from space, there are five stages of flight that it must pass through before safely reaching touchdown at a runway. The final three stages of flight occur within Earth's atmosphere and are the stages in which error correction and range prediction is critical. The three stages are known as the entry phase, the TAEM phase, and the approach and landing (A&L) phase.

While the vehicle is still in the extreme outer range of Earth's atmosphere the vehicle will have a known energy value. The RLV's energy will decrease due to drag and will eventually match up with a predetermined energy value denoting that the vehicle has entered the TAEM stage of flight. This phase of flight is the second to last phase before landing at the runway. The energy of the vehicle is simply calculated using the altitude and velocity of the vehicle. Some documents are very general, such as Lockheed Martin [1], which defines the TAEM phase of flight as when the velocity of the vehicle drops below 3000 ft/s, or approximately Mach 3. Hull et al. [2] are even more general in its description of when TAEM starts, stating "[TAEM] begins after the vehicle has

entered the atmosphere and heating constraints are no longer a concern." One particular document from NASA [3], is much more specific in its parameters for TAEM. Moore [3] states that TAEM begins when the Shuttle reaches a speed of Mach 2.5 and an altitude of 85,000 ft. Throughout this document the definition of TAEM provided by Moore will be utilized.

There are four subphases of flight within TAEM, as seen in Fig. 1. First, if the energy of the vehicle is deemed to be excessive, the vehicle will execute S-turns to bleed the excess energy. An S-turn is merely a series of bank reversals used to slow the velocity of the vehicle while decreasing its altitude. This maneuver is very effective for decreasing the energy of the vehicle. Next, the vehicle proceeds to the second subphase of TAEM known as the acquisition. This subphase is characterized by the vehicle obtaining the correct heading in order to fly to a tangent point of the Heading Alignment Cone (HAC). After the correct heading value is obtained, the vehicle maneuvers to that heading value and flies a straight, wings-level path to the desired tangent point of the HAC.

The third subphase of TAEM is defined by the vehicle flying the HAC profile. The HAC is an imaginary cone with the point of the cone on or below the ground and the base extending upward. As the vehicle flies the HAC profile the altitude of the vehicle is decreasing, meaning that when the vehicle starts flying on the HAC it is tracing a larger radius than when it finishes flying the HAC. The vehicle is spiraling downward, tracing the surface of the cone until the end of this subphase of flight. Viewed from above, the spiral turn profile is very apparent. Figure 1 illustrates the spiral nature of the HAC with a simple view from above.

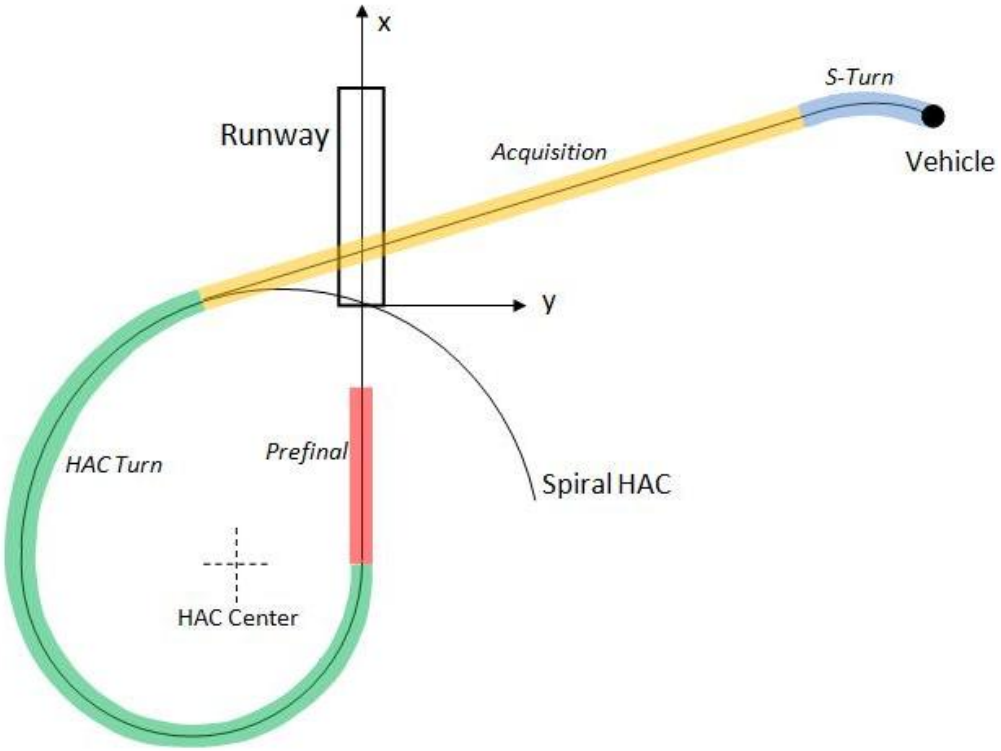

Fig. 1. Simple illustration of the spiral HAC and the four subphases of flight during TAEM.

It should be noted that there are two different options for the HAC subphase of flight depending on the overall energy of the vehicle. Ideally, the vehicle will have enough energy to fly an overhead HAC. This means that the vehicle will cross over the imaginary extended runway line in order to fly a HAC profile on the opposite side of the runway from where the vehicle began TAEM. An overhead HAC requires the vehicle to fly at least 180 deg on the HAC. Figure 1 provides an illustration of an overhead HAC. If the vehicle does not have enough energy to complete an overhead HAC turn, the vehicle will be required to complete a direct HAC turn. A direct HAC turn occurs when the vehicle does not cross the imaginary extended runway line, but rather the HAC is on the same side of the runway as the vehicle when it began TAEM. A direct HAC requires the vehicle to fly a turn of less than 180 deg. Overall, the distance, and therefore energy,

covered by a direct HAC is much less than an overhead HAC. Figure 2, provided by Vernis et al. [4], demonstrates the four different possible HAC locations, simplified as cylinders. Figure 2 also shows a three-dimensional view of a vehicle completing the TAEM phase of flight by utilizing a direct HAC turn. It should be noted that all four possible HAC locations are shown in Fig. 2. Within Fig. 2, HAC 3 and HAC 4 should be utilized only if it is desired that the vehicle land with the wind. This situation is rare and in nearly all cases HAC 1 or HAC 2 will be used.

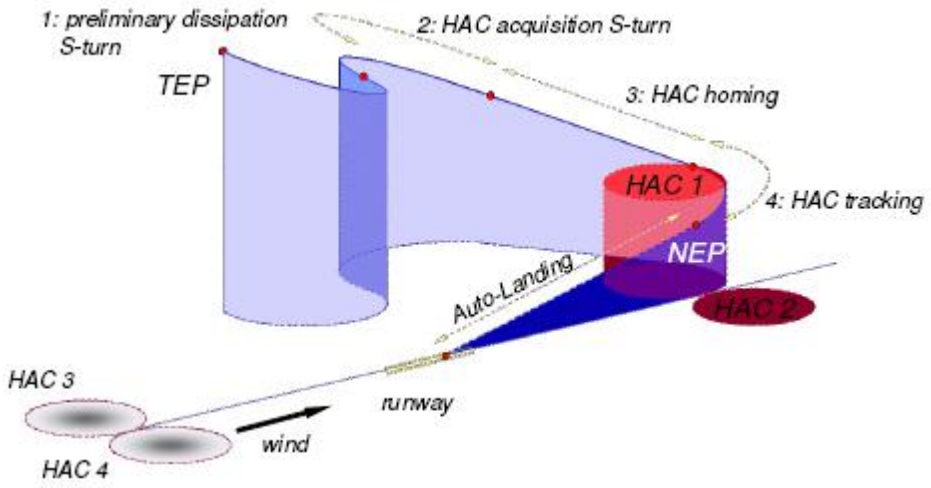

Fig. 2. Illustration of a three-dimensional view of the TAEM phase. In this case, the HAC is simplified to a cylinder. Also, the vehicle's energy has required it to complete a direct HAC [4].

The fourth and final subphase of TAEM is the prefinal phase of flight. Ideally, as the vehicle leaves the HAC its heading will be aligned with the runway. The prefinal phase of flight denotes the straight line path flown from the end of the HAC to ALI. The vehicle completes the prefinal subphase while flying with wings-level. By definition, ALI occurs when the vehicle reaches an altitude of 10,000 ft [5]. The occurrence of ALI also signals the end of the TAEM phase of flight.

1.2 Previous Work

1.2.1 Original NASA Guidance

According to NASA and documented by Moore [3], the TAEM phase of flight was initially developed to be used as an energy controller for the Shuttle. It is intuitive that a vehicle reentering Earth's atmosphere would need to dissipate the majority of its energy before attempting to land safely. The TAEM phase of flight was initially designed with this requirement in mind.

As the Shuttle was progressing through the TAEM stage, the lateral flight component would be controlled by the bank angle magnitude and direction. The bank angle would be modified in order to allow the Shuttle to attempt to fly a prescribed trajectory. Any cross-range error would be damped out using bank angle as the correcting control. Longitudinal motion, or the vertical channel, of the Shuttle was controlled mainly by the angle of attack. The vertical channel was also primarily responsible for the energy and altitude control. Speed was regulated by using a speedbrake and by monitoring dynamic pressure.

When the TAEM portion of flight was initially developed, there was a need for some control to guide the Shuttle in-line with the runway. Many models, using varying bank methods, were analyzed and a simple mixture of a few models was developed further. The direct HAC method was the basis for the design. It should be noted that the HAC, in its early stages, was only a cylinder and not a cone. This allowed the separation of lateral and longitudinal control; bank angle and angle of attack were used,

respectively. In the early days of TAEM, if the Shuttle had too much energy, instead of using an overhead HAC, the Shuttle would simply fly away from the target for a prescribed amount of time until energy levels were acceptable. When the energy was determined to be at an acceptable level the Shuttle would then fly towards the direct HAC, complete the TAEM phase, and successfully move on to the Approach and Landing phase.

It was determined a few years later that the choice of using an overhead HAC, as well as a direct HAC, would provide the Shuttle with more options when it came to weather avoidance [3]. By using an overhead HAC the Shuttle could come in at a much higher altitude to avoid weather disturbances and still bleed off the necessary amount of energy and altitude as it was flying the much longer path of the overhead HAC. While storm avoidance was the initial driving force behind the push for an overhead HAC, one positive side effect was that the Shuttle would now be able to fly a path that would dissipate more energy than the nominal direct HAC. This would prevent the Shuttle from having to fly away from the target until an acceptable energy level was reached. The margin for error with flying away from the target until the Shuttle has reached the correct energy level is extremely minimal and any small calculation error would result in the Shuttle not having enough energy to reach the runway safely. Having two different HAC options would increase the margin for error, whether that error is in making calculations, predicting weather, or predicting winds. Moore named this method Optional TAEM Targeting (OTT) [3].

With the OTT change came a few other changes to the general HAC profile. These changes were used by NASA beginning in the 1980's and are documented by

Moore [3]. The most significant and major change was the HAC being changed from a cylinder to a cone. Flying the profile of a cone, as can be seen in Fig. 3, the Shuttle would be flying a smaller radius at each increasing instant of time. Viewed from above in two dimensions the Shuttle would be tracing a spiral. Another change allowed the Shuttle to fly a HAC using a turn greater than 360 deg. This change allowed the Shuttle to bleed off extra energy because of the increased distance that it would fly.

Using these new parameters for the TAEM phase of flight NASA attempted to control the path and trajectory of the Shuttle. When the Shuttle reached the correct requirements to be considered flying the TAEM portion of reentry, the pilot would switch the logic to either the overhead HAC or the direct HAC. This decision depended solely on the energy of the vehicle. It should be noted that this decision was not made automatically by a computer, but rather by a human. This is the first of many decisions that had the potential to introduce some degree of error to the trajectory problem. It also should be noted that the HAC, whether it be direct or overhead, had static dimensions as well as location. The HAC was always located in the same place relative to the runway and was always the same size.

After a HAC had been chosen, a groundtrack predictor attempted to accurately predict the distance the Shuttle would need to fly in order to make it safely to the runway. The groundtrack predictor was essentially composed of the four distinct parts that make up the TAEM phase of flight. Using the equations of motion appropriate for the Shuttle, it was very difficult to accurately predict the groundtrack for the S-turn and HAC phase of TAEM because the bank angle of the Shuttle is dynamic. Also, in the vertical channel, the flight path angle is not constant. In order for the groundtrack predictor to be accurate

for these subphases of TAEM the angles would need to be predictable as a known function of some known parameter. In order to simplify, for the S-turns, the Shuttle used the current velocity and an average value of bank angle in order to calculate the groundtrack. For the HAC, a very complicated set of geometry was used along with an estimation of HAC starting velocity for the Shuttle. Also, since the velocity changes significantly as the Shuttle traveled around the HAC, a function to represent velocity was estimated. Another variable was introduced here named PSHA. Seen in Fig. 3, this variable, the heading angle relative to the HAC, represented the turn-to-go angle between the Shuttle's current position and the runway line. This PSHA variable would be extremely easy to calculate if the HAC was a cylinder; there would be a direct and linear relationship between PSHA and true heading angle. However, since the HAC is a spiral, there is no linear relationship and PSHA must be either estimated or calculated in real-time as the Shuttle progresses around the HAC.

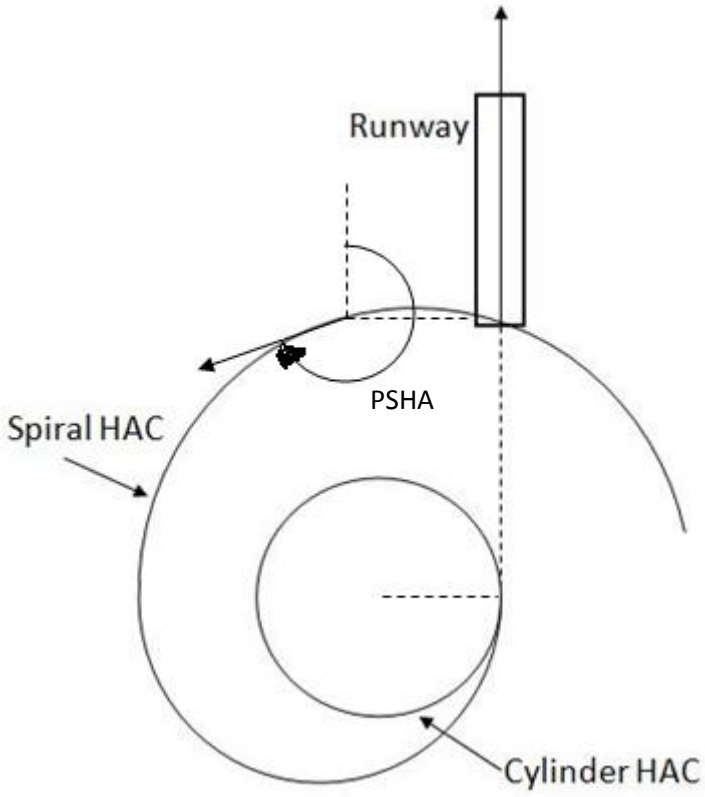

Fig. 3. Simple illustration of the difference between a cylinder and spiral HAC.

Calculating anything in real-time is going to put a significant extra load on the equipment that must complete the task, and is therefore not desirable. It should be noted that PSHA also depends significantly on how tight the HAC spiral is. After all of this estimation is complete, it is easy to see how there is a need for a more accurate method of landing the Shuttle.

The acquisition and prefinal phases of TAEM were more accurately predicted because the Shuttle was flying "wings-level." Also, the flight path angle is nearly constant for these subphases as dynamic pressure was maintained at a near constant value.

While the groundtrack predictor was determining the estimated range to the runway, energy calculations were being performed. Many different scenarios using

varying bank angle profiles were used to calculate energy. At one extreme, the energy was calculated for the Shuttle if it were to fly as efficiently as possible. This efficiency would be characterized by flying with wings-level at the correct flight path angle and angle of attack to produce the maximum lift-to-drag ratio. This was considered the maximum energy that the Shuttle was capable of. At the other extreme, the minimum energy for the Shuttle was calculated in the same manner. The maximum and minimum energy were then used to "constrain the altitude controller [3]." Knowing the energy envelope, it was then possible to create a vertical profile for the Shuttle to track in the TAEM phase. This vertical profile corresponded to the Shuttle following and trying to track a nominal dynamic pressure profile. Since dynamic pressure is dependent on velocity and atmospheric density it is intuitive that this would be an ideal parameter to track. Velocity determines kinetic energy, and altitude, which causes atmospheric density to vary, determines potential energy.

After the groundtrack predictor has estimated the necessary range-to-go, the subphases of TAEM must be completed. The names of the subphases are shown in Fig. 1. While the S-turn and acquisition phase were calculated in a fairly straightforward manner, the completion of the HAC turn required the use of many complex equations and processes. The Shuttle transitioned from the acquisition phase to the HAC turn phase when it was within 10% of the HAC turn radius [3]. At this point, the Shuttle was outside of the HAC, meaning that the distance from the HAC center to the vehicle was greater than the HAC turn radius. It should be noted that the HAC turn radius varies with altitude; the HAC turn radius that is compared with the distance to the vehicle is

calculated using the altitude of the vehicle as a variable. Accordingly, the values for each of these parameters are directly comparable.

After the Shuttle was within 10% of the HAC radius, multiple angle measurements were taken. The angle measured from the vehicle to the HAC center was recorded as well as the angle from the vehicle to the nearest HAC tangent point. Using these angle measurements it was possible to determine the PSHA value for the Shuttle. The PSHA value, along with the HAC location variables, was then used to calculate the distance from the center of the HAC to the Shuttle [1]. Through many complex equations PSHA was also used to calculate the predicted distance around the HAC, which was used for the groundtrack predictor. The PSHA value was updated in real time and new values for the Shuttle position were determined.

Knowing the distance from the HAC center to the vehicle is critical. The difference was taken between this distance and the nominal HAC radius resulting in a radial error value. Similarly, the radial turning rate that the Shuttle was supposed to be flying at was compared with the calculated radial turning rate. After these rate values were differenced a new variable called the radial rate error value was determined. Based on these radial and radial rate error values, the Shuttle would bank right or left in order to negate as much of the error as possible. This banking maneuver was completed based on the nominal HAC bank value for the Shuttle, referred to as the open-loop banking command. This open-loop term was calculated using the velocity, radial rate, and radial position of the Shuttle. A closed-loop banking term was added to the open-loop term in order to provide the Shuttle with better tracking. The closed-loop term was comprised of the radial and radial rate error values. The two error values were weighted with constant

gain values [1]. The gain values allowed the controller to not be overly dominating but still provide the Shuttle with an appropriate amount of closed-loop banking. This method of calculating the bank for the Shuttle was continued throughout the HAC turn subphase until it was determined that the Shuttle was ready to transition to the prefinal subphase. The Shuttle transitioned to prefinal flight when it was within 5 deg of the runway centerline.

1.2.2 Flatness-Based Guidance

One of the more modern ideas for how to control a vehicle entering the atmosphere during the TAEM phase of flight involves the theory known as differential flatness. The differential flatness theory was first developed by Fliess et al. [6] purely in a mathematical sense. Morio et al. [7] applied this theory to the multiple nonlinear equations governing the flight of a winged reentry vehicle in the hopes that the nonlinear equations could be uncoupled. The model was inverted using a method called Nonlinear Dynamic Inversion in order to provide estimates for the many states of the system. The control inputs used for the system were bank angle, angle-of-attack, and airbrake deflection. Using these new strategies the model was then tested to see if it was indeed "flat." According to Morio et al., "The main contribution of this work is to demonstrate that the nonlinear vehicle model is flat and that using this property, a global guidance scheme can be designed without having to uncouple in-plane and out-of-plane dynamics, as it is done currently with most guidance schemes [7]." Using the control inputs mentioned previously, the outputs of the system were determined to be downrange, crossrange, and altitude. After manipulating the nonlinear equations of motion for the

vehicle using the inputs and outputs, it was determined that the model is indeed flat and invertible. This model is then tracked using a method similar to a proportional-integral-derivative (PID) controller.

Like the Shuttle guidance design before it, the flatness theory guidance scheme made a few assumptions. First, the Earth was viewed as locally flat. Second, it was assumed that the Earth was non-rotating. These are two assumptions that seem to be uniform throughout all guidance and navigation schemes and can be accepted as standard.

Morio et al. completed a Monte Carlo analysis using the differential flatness theory and it seems that the results are acceptable. It was found that for 95% of the trials run, the error at the nominal exit point was less than 150 ft [7]. The nominal exit point was defined to be the point where the vehicle exits the HAC turn.

1.2.3 Fuzzy Logic Guidance

One idea that has been recently developed by Burchett [8] is the use of fuzzy logic to control a vehicle upon reentry to Earth's atmosphere, namely during the TAEM phase of flight. Unlike the previously mentioned flatness-based guidance, fuzzy logic steers the control laws away from using dynamically inverted equations and precise mathematical models. Using the law of conservation of momentum, fuzzy logic separates the motion of the vehicle into three distinct components. "Vehicle groundtrack is controlled primarily by bank angle, the altitude is controlled by normal acceleration, and the dynamic pressure is controlled by either the flight path angle, or changing the coefficient of drag by extending drag devices [8]."

There are many different parameters that must be estimated using fuzzy logic. A couple of these parameters include the size and location of the HAC. It is also known that the problem at hand is constrained by a nominal final condition. This final condition is that the vehicle must have an altitude of approximately 10,000 ft when it is approximately 20,000 ft downrange from the runway. The vehicle also must have a flight path angle of about 30 deg at this point.

Much like the Shuttle TAEM procedure, the phases of flight are separated into four subphases. However, while the Shuttle guidance logic tells the Shuttle to point at a tangent point of the HAC during the acquisition phase, fuzzy logic tells the vehicle to point at the direct center of the HAC [8]. Fuzzy logic then relies on the pilot to implement 89 different rules "to intercept and fly the HAC [8]." Bank angle of the vehicle is solely dependent on the pilot's decisions along with the 89 rules mentioned.

While this may not be the most precise method to land a reusable launch vehicle, the method is successful. Using varying initial conditions the vehicle was always able to safely reach the runway for touchdown. One glaring drawback to using this method is that the vehicle seems to be flying at the maximum extents of its available bank angle during a significant portion of the TAEM phase. With the bank angle essentially maxed out there is little room for error during the TAEM stage of flight.

1.2.4 Energy-Tube Guidance

Ridder et al. [9] has completed a recent study concerning TAEM navigation and control. Focusing specifically on the vertical channel, this paper constructs the idea that a possible vertical profile must be created. This is done off-line and preflight and

determines the vehicles maximum range vertical profile as well as the maximum dive vertical profile. The maximum range vertical profile is determined by flying the vehicle at the vehicle's maximum lift-to-drag ratio. Both profiles are illustrated as dynamic pressure as a function of altitude. Knowing the flight profiles for the vehicle at both extremes, Ridder et al. now specifies that the vehicle should fly a nominal vertical profile that essentially splits the difference between the maximum range and maximum dive profiles.

Ridder et al. [9] continues on to specify different methods of using energy of the vehicle as the deterministic factor as to which flight trajectory should be flown. It is said that since energy is always decreasing this is the optimal variable to track as the vehicle completes the TAEM phase of flight. Once an optimal trajectory is found off-line there is still a need to track this optimal trajectory in real time. It should be noted that as a result of the initial planning the initial states for the vehicle are well known.

Ridder et al. has decided to use the angle of attack for the vehicle as the variable that directly controls the vertical profile for the vehicle. This is the variable that will be tracked and controlled. Ridder et al. employs the use of a proportional-derivative controller using feedback terms related to dynamic pressure. Both the perturbation of the dynamic pressure and the rate of change of the dynamic pressure are used as the feedback controller variables and added to the open-loop angle of attack value. The dynamic pressure perturbation and rate of change variables are gained by gains related to their respective variables. These gains are determined using a genetic algorithm, the details of which will not be included here.

There seems to be a slight downfall with using this method of control tracking. The gains that are used to modify the dynamic pressure perturbation and rate of change variables are always different for different initial vehicle states. The gains are not constant and must be recalculated during the online simulation every time the initial states for the vehicle change. This seems to be only a small inconvenience, however. Because of the inability to use a constant set of gains for all initial states, Ridder et al. [9] suggests using one set of gains for several different initial states. While this may negatively affect the results of the simulation, the robustness of the program will still be intact.

Using all of the vertical profile calculations an energy-tube concept was developed. This concept generally states that, depending on the energy state of the vehicle, the vehicle will be encapsulated by a certain "drag tube," which corresponds to a specified trajectory. There are many "tubes" that allow the vehicle to have a range of initial states but still reach ALI with the correct energy and flight characteristics. It is ideal to fly at the bottom of the chosen "tube" in order to minimize energy loss.

1.3 Current Work

The main problem with the original TAEM tracking method is the lack of variability when it comes to adapting to off-nominal vehicle conditions. The Shuttle has a very limited number of reference trajectories to choose from in order to adapt to the variable vehicle conditions at the start of TAEM. A few of the main variable vehicle conditions include the velocity, altitude, and position of the vehicle at the initialization of

TAEM. For example, the Shuttle is only able to choose from two possible HAC locations, one on each side of the runway centerline. Depending on what general direction the Shuttle is entering TAEM from, the best HAC location is chosen. It should be noted that the two possible HAC locations are set the same distance away from the runway, essentially fixing the length of the prefinal subphase. The fixed locations of the two possible HAC's does not aid in allowing the Shuttle to adapt to off-nominal vehicle conditions. Also, the size and shape of the HAC are fixed within the Shuttle's stored reference trajectories. Again, this does not allow the Shuttle to adjust to nonstandard conditions. In summary, if the Shuttle transitions to the TAEM phase with an energy level greater than the prescribed energy and at a position closer to the runway than the prescribed position, the Shuttle is unable to modify its path in order to complete a safe and accurate landing.

It has been determined that the original TAEM tracking method could be improved upon, thus allowing the vehicle to more accurately and precisely follow a prescribed trajectory. Also, the new tracking method would modify the HAC location and size on-line and in real-time. This would allow the vehicle to transition to TAEM with any possible initial conditions and still successfully and accurately complete the transition to Approach and Landing.

In addition, a new method for predicting the groundtrack range for a vehicle has been developed, which is considerably simpler than the groundtrack predictor method initially used by NASA. While this new method may be simpler, a high degree of accuracy is still maintained. The original method required the numerical integration of multiple energy equations in order to determine the groundtrack range through the S-

turns and around the HAC. The new method uses a simple relation in order to effectively scale the maximum range of the vehicle. It should be noted that the maximum range for the vehicle occurs when the vehicle flies in a straight line with wings-level. The scale factor is solely dependent on the bank angle of the vehicle as it completes the S-turns or the HAC turn.

Figure 4 illustrates one possible scenario as the vehicle plans to complete the TAEM phase of flight. The four different subphases are color-coded in order to help distinguish between them. The groundtrack shown in Fig. 4 represents the actual groundtrack range for the vehicle. Using the new simple scaling method that was developed, it is possible to determine the wings-level equivalent range of the vehicle by multiplying the actual groundtrack range by the scaling factor. It should be noted that only the S-turn and HAC turn portions of TAEM should be modified by the scaling factor. The acquisition and prefinal portions of flight are already being flown with wings-level.

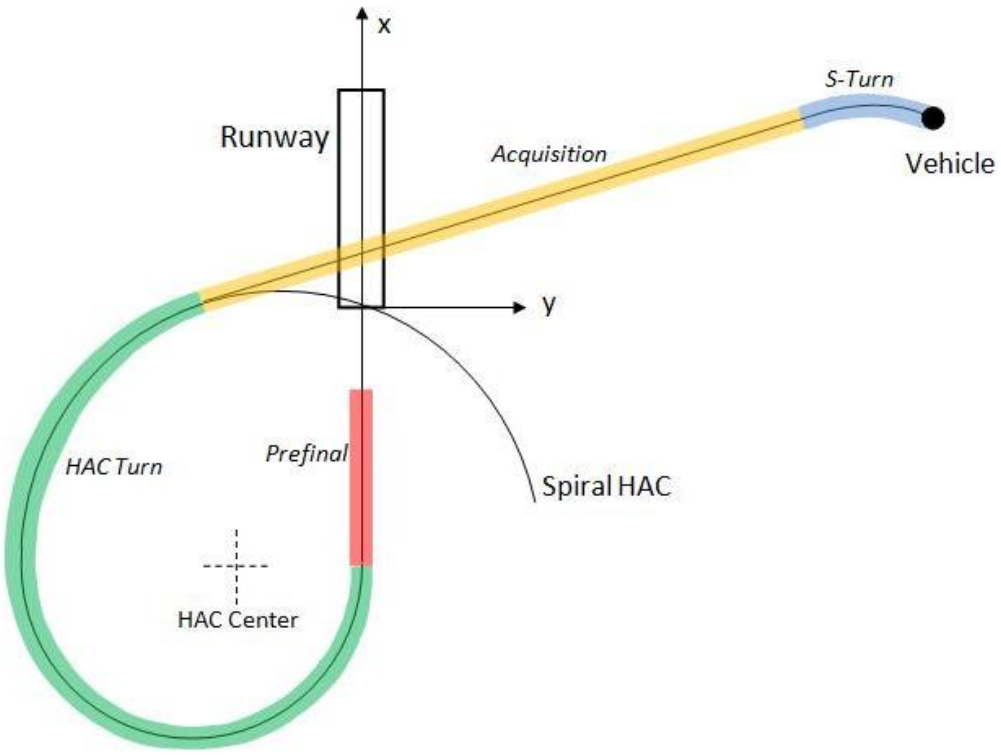

Fig. 4. Simplified example trajectory for the vehicle. The different subphases of flight are color-coded appropriately and represent the actual groundtrack range values for the vehicle.

A new method for tracking the HAC, as a cone, has also been developed. This new method increases the accuracy of HAC tracking for the vehicle considerably. One of the most intuitive illustration factors for accuracy is the plot relating radial error of the vehicle as it travels around the HAC to either time or PSHA. Knowing the equations of motion for the vehicle, two states for the vehicle were chosen. One differential equation for each state was determined using the equations of motion for the model. The states were determined to be radial position and the heading angle of the vehicle with respect to PSHA.

Instead of attempting to solve the differential state equations, the equations were simplified by the linearization process. The differential equations were linearized with respect to the two states, as well as the input, which for this case was bank angle. The

newly linearized equations were evaluated at the nominal state values. The result of this process yields a state-space representation of the system, namely the ***A*** and ***B*** matrices. With the ***A*** and ***B*** matrices now known the system can be evaluated in a number of different ways. For this particular application the goal was to evaluate and modify the system using pole-placement. The use of pole-placement would result in the creation of a gain matrix; one gain for each of the two states of the system. The gains would then be applied to the perturbations of the states. The control law would then basically be comprised of two components, the open-loop portion and the closed-loop portion. The open-loop portion would provide the base value for bank angle, which is the input required to complete a HAC turn, while the closed-loop portion would essentially provide error correction for the system. The perturbation from the nominal state would be gained by the newly created gain matrix.

Pole-placement was accomplished by using a balancing method to choose the desired natural frequency and damping ratio. Choosing these variables allowed for the control of system variables such as the percent overshoot, settling time, and rise time.

It should be noted that the pole-placement process was not just completed once, offline; NASA originally calculated gain values in this manner. The gain values calculated by NASA were static throughout the entire trajectory. The new process was performed on line each time the guidance control was updated, roughly every second during the TAEM phase of flight. Therefore, the gain matrix is dynamic as TAEM is being flown. This facet of the control law allows the vehicle to fly a more precise and accurate trajectory. Since the ***A*** and ***B*** matrices are dependent on the velocity of the vehicle, these ***A*** and ***B*** matrices are changing with the changing vehicle velocity. Since

the ***A*** and ***B*** matrices are dynamic with time, the gain matrix is also dynamic and provides varying levels of error correction throughout the trajectory. Ideally, the gain matrix will provide a little amount of correction when the perturbation, or error, is small, and a larger amount of correction when the perturbation is large.

Pole-placement, however, was not enough to provide perfect tracking for a complex shape such as a cone. With the need for another closed-loop tracking term to perfect the turn, a bias value was introduced with respect to the bank angle. This bias value was added to the open and closed-loop terms for the bank angle. There were many different methods tested for how to compute the bias value including a constant term, a term that was linear with respect to PSHA, and a term that was quadratic with respect to PSHA. Ultimately, a value that was exponential with respect to PSHA was chosen. The strategy for this bias value was to use a value that was large at the beginning of the HAC turn, when the turn acted most like a spiral. Towards the end of the HAC, when the cone begins to act more like a cylinder, the bias value was not required to be as large.

1.3.1 Advantages

There are many advantages to using the new method of guidance during the TAEM phase of flight. The analytic groundtrack predictor is much simpler in that multiple numerical integrations do not have to be performed. The groundtrack can be predicted using a simple scale factor placed on the maximum range-to-go for the vehicle. This simple scale factor has a direct relationship to the bank angle of the vehicle. Because of the simplicity of the new groundtrack predictor, the load placed on the on-board computer system is very insignificant when compared to the previous load, which

included the necessity to complete multiple numerical integrations on-line and in real-time.

The method of using pole-placement to obtain a closed-loop term for control of the bank angle is extremely advantageous because of the fact that the poles for the system may be chosen. This allows the user to determine the amount of damping the system should have, as well as other aspects such as settling time, rise time, and percent overshoot. By balancing these system parameters, an ideal trajectory can be followed with a high level of precision. In addition to pole-placement, a bias value placed on the bank angle will significantly help the performance of the vehicle when it is completing the HAC turn.

Overall, the new method of trajectory planning and tracking is much more advanced than the method currently used by the Shuttle. The new method will allow for the HAC location and size to be determined on-line and in real-time, as opposed to the Shuttle method, which only employs two possible reference trajectories. Using the new method, the vehicle will have an infinite number of possible reference trajectories and one will be chosen based on the vehicle conditions as it reaches TAEM.

CHAPTER 2

FLIGHT MECHANICS

2.1 Equations of Motion

There are six key equations of motion that are associated with flight of the vehicle during the TAEM stage of reentry. The equations of motion for three-dimensional motion of the vehicle are

$$\dot{V} = \frac{-D}{m} - g\sin\gamma \tag{1}$$

$$\dot{\gamma} = \frac{L\cos\phi}{mV} - \frac{g}{V}\cos\gamma \tag{2}$$

$$\dot{\psi} = \frac{L\sin\phi}{mV\cos\gamma} \tag{3}$$

$$\dot{h} = V\sin\gamma \tag{4}$$

$$\dot{x} = V\cos\gamma\cos\psi \tag{5}$$

$$\dot{y} = V\cos\gamma\sin\psi \tag{6}$$

These equations of motion apply to the model of the system assuming the Earth is simplified to be flat and non-rotating. The flat-Earth simplification is accurate because the vehicle is beginning the TAEM phase of flight at a relatively low altitude. Also, in order to assume the Earth is not rotating, the TAEM stage of flight must occur relatively quickly. This simplification is valid because over the course of reentry the TAEM stage of flight lasts a relatively short amount of time.

The positive x-axis is located along the runway centerline. Specifically, the positive x-axis begins at the start of the runway, or the runway threshold. The positive y-axis is also located at the runway threshold and points to the right of the runway on approach. The vehicle's heading angle relative to the runway is measured clockwise from the positive x-axis. Figure 5 illustrates a simplified model of the HAC as it relates the runway. It should be noted that the *x'* and *y'* axes are responsible for illustrating the center of the HAC.

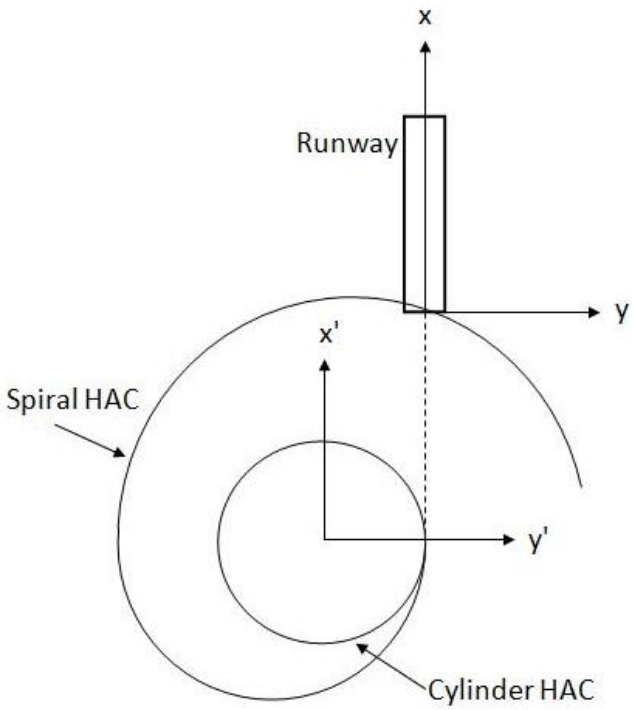

Fig. 5. Simplified illustration of the HAC relative to the runway.

2.2 Atmospheric Model

An underlying common thread between all simulations was the model of the atmosphere. The U.S. Standard Atmosphere of 1976 was used. This model is responsible for specifying the density of the atmosphere at varying altitudes. The model is comprised of raw data which, like the model, is extremely reliable. The raw data is organized in a look-up table. When given an altitude, the look-up table is able to produce the corresponding atmospheric density. A significant difference in the raw data is observed when the vehicle passes from the stratosphere to the troposphere at approximately 36000 ft.

One critical parameter that could be determined using the atmospheric model was the dynamic pressure on the vehicle at any possible vehicle speed. The dynamic pressure is solely a function of vehicle velocity and atmospheric density. Since atmospheric density is a function of altitude, Fig. 6 illustrates the dynamic pressure profile for the vehicle when plotted against altitude. Multiple constant values of velocity were used to create the dynamic pressure profiles shown in Fig. 6; these velocity values are identified by utilizing the legend within Fig. 6. The atmospheric model is represented indirectly through each dynamic pressure profile. Generally, an acceptable dynamic pressure value is less than 200 psf. Figure 6 illustrates an acceptable dynamic pressure value when the altitude and velocity of the vehicle are large. The dynamic pressure is able to maintain a reasonably constant value as altitude and velocity decrease, which corresponds well with the system model. The model of the system requires the vehicle to initially have a high velocity and high altitude. The velocity and altitude decrease as the vehicle progresses

through TAEM. The model parameters will be explained in further detail in subsequent chapters.

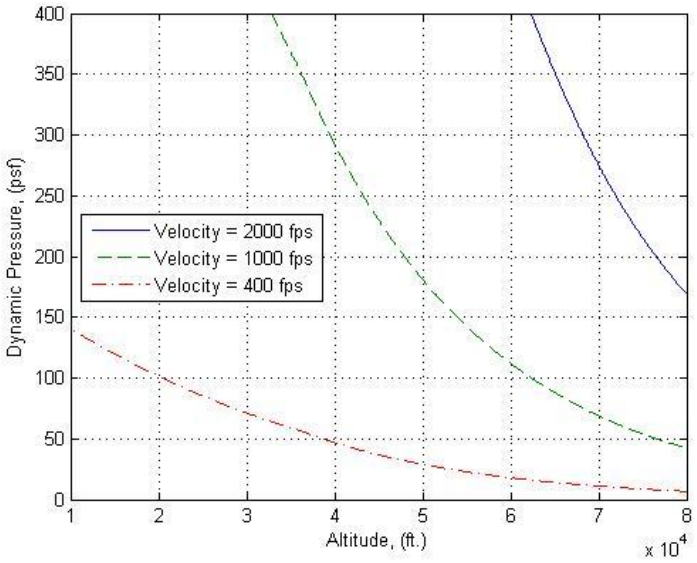

Fig. 6. Dynamic pressure versus altitude for multiple vehicle velocity values.

2.3 Vehicle Model

In order to create a realistic simulation there is a need for a model of a realistic vehicle. There is no shortage of data from many different test vehicles. First, there is data from the Space Shuttle, which NASA has relied upon for many years. There are a few downfalls with using the Space Shuttle data, however. The Space Shuttle is not an aerodynamically efficient vehicle mainly because of its delta wings. The Space Shuttle does less gliding and flying on reentry than it does falling. While the small delta wings excel during supersonic flight, the high stall angle of attack value requires a large angle of attack for the Shuttle to exhibit significant lift. The profile of the curve for the coefficient of lift with respect to angle of attack linearly increases until the critical angle

of attack is reached. At this point, if angle of attack is increased any further, the vehicle will begin to lose lift and stall. It is possible for the Space Shuttle to exhibit a relatively high value for angle of attack before it stalls. Figure 7 shows a typical illustration of the lift coefficient, C_L, plotted against vehicle angle of attack, α.

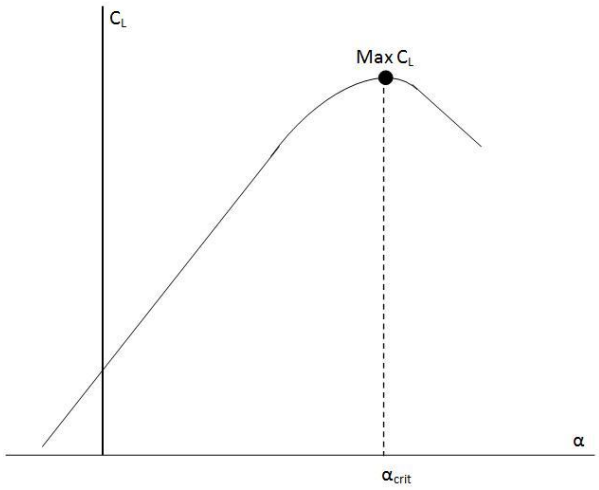

Fig. 7. General plot of coefficient of lift versus angle of attack for a vehicle traveling at some Mach number.

Many test vehicles have been developed for NASA with the intent of being the next Space Shuttle. Some of these vehicles include the X-33, the X-34, and the X-37. The many vehicles that have been developed have not just been rough first attempts. Each vehicle has undergone rigorous testing in a virtual world in order to determine flight simulation data. For the sake of this simulation, a vehicle was essentially created from the large amount of raw data available from other vehicle testing. This vehicle, while not real in a physical sense, possesses many realistic attributes from various vehicles that have preceded it. It should be noted that this simulation was created with variability in mind. It is easy to input different values for the many different vehicle parameters in order to customize the simulation to fit a specific actual or faux vehicle.

The dynamic inputs to Eqs. (1-6) include the lift and drag forces placed on the vehicle. These inputs, along with the many components of the lift and drag forces, are calculated using Eqs. (7-14). The vehicle model is heavily dependent on the definition of variables such as the planform area of the vehicle, the mass of the vehicle, and the aerodynamic profile of the vehicle. The equations demonstrating all of the coupled relationships may be seen as Eqs. (7-14). Using Eq. (7) with a known vehicle velocity, one can solve for and calculate the lift coefficient.

$$L = \frac{1}{2}\rho V^2 S C_L \tag{7}$$

Using the calculated lift coefficient as well as the zero-lift drag coefficient, C_{D0}, with the vehicle dependent variable *K*, one is able to calculate the coefficient of drag, or the drag polar equation, shown by Eq. (8).

$$C_D = C_{D0} + K C_L^2 \tag{8}$$

Equation (8) is the traditional equation used to calculate the coefficient of drag. However, in search of a more accurate model, a cubic equation was used and is represented by Eq. (9).

$$C_D = c_0 + c_1 C_L + c_2 C_L^2 + c_3 C_L^3 \tag{9}$$

In the traditional sense, the zero-lift drag coefficient would correspond to the c_0 coefficient and the variable *K* would correspond to the c_2 coefficient. The other leading coefficients within Eq. (9) were determined though curve fitting the aerodynamic vehicle data.

The zero-lift drag coefficient is a constant solely dependent on vehicle geometry.

$$K = \frac{1}{\pi e AR} \tag{10}$$

The variable *K* is calculated using Eq. (10), where *e* is the span efficiency factor and *AR* is the aspect ratio for the vehicle. The span efficiency factor for this vehicle model usually ranges in value from 0.8 to 0.9.

$$AR = \frac{b^2}{S} \tag{11}$$

Aspect ratio is calculated using Eq. (11), where *b* is the wingspan of the vehicle. The span efficiency factor is a variable that is completely dependent on vehicle and wing geometry, as is the aspect ratio. With the drag coefficient now calculated it is possible to calculate the drag force, *D*, exerted on the vehicle using Eq. (12).

$$D = \frac{1}{2}\rho V^2 S C_D \tag{12}$$

This equation for drag force is very similar to the lift force, *L*, equation, Eq. (7). Both lift and drag force equations contain the dynamic pressure equation, Eq. (13).

$$\bar{q} = \frac{1}{2}\rho V^2 \tag{13}$$

By combining Eqs. (7) and (12), it is possible to determine the maximum lift-to-drag ratio. When completed using the traditional drag coefficient equation, Eq. (8), it is easy to see that after some simplification the maximum lift-to-drag ratio is solely dependent on vehicle geometry. Similarly, when using Eq. (9), the maximum lift-to-drag ratio is based solely on vehicle geometry; however, the equations are much more complex and are not shown here.

$$(L/D)_{MAX} = \frac{1}{2\sqrt{C_{D0}K}} \tag{14}$$

In an attempt to demonstrate the model of the vehicle that will be used throughout the remainder of this paper, many plots were created in order to illustrate some of the

aerodynamic characteristics. The first plot, shown as Fig. 8, illustrates the lift coefficient plotted against the drag coefficient. The cubic function representing the drag coefficient was determined to be non-continuous over the range of Mach numbers correlating to the TAEM phase of flight. The inability to fit a continuous curve through the drag coefficient caused it to be treated as a piecewise function. For this research, a different drag coefficient was used depending on if the vehicle Mach number was greater or less than 0.9. It is easily seen when observing Fig. 8 that a different cubic function is used for the drag coefficient when Mach number is 2.0 as compared to the drag coefficient when Mach number is 0.7 or 0.4. It should be noted that the altitude values that correspond to the Mach numbers are values that approximately correlate with the high-fidelity simulation.

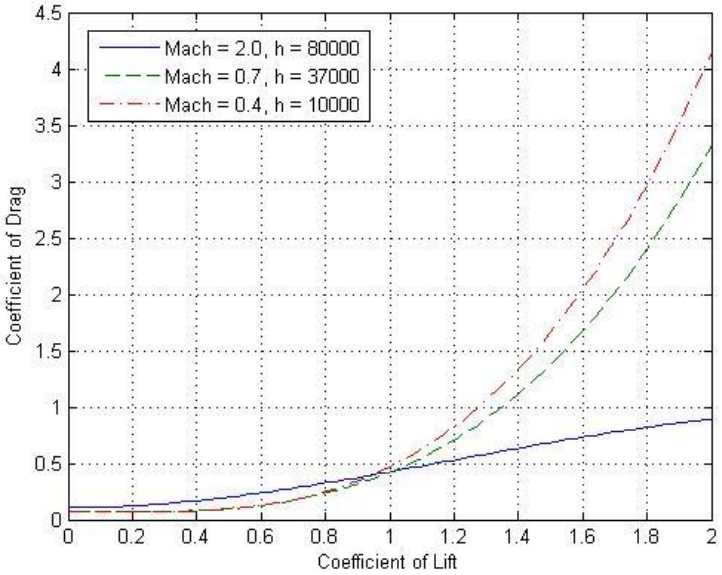

Fig. 8. C_L versus C_D.

The coefficient of lift plotted against angle of attack creates a flight profile for the vehicle. This angle of attack plot illustrates the lift created by the vehicle at all possible

angles of attack. The angle of attack plot will also vary with vehicle Mach number and altitude. It can be seen in Fig. 9 that multiple vehicle velocity values were used in order to create multiple angle of attack profiles.

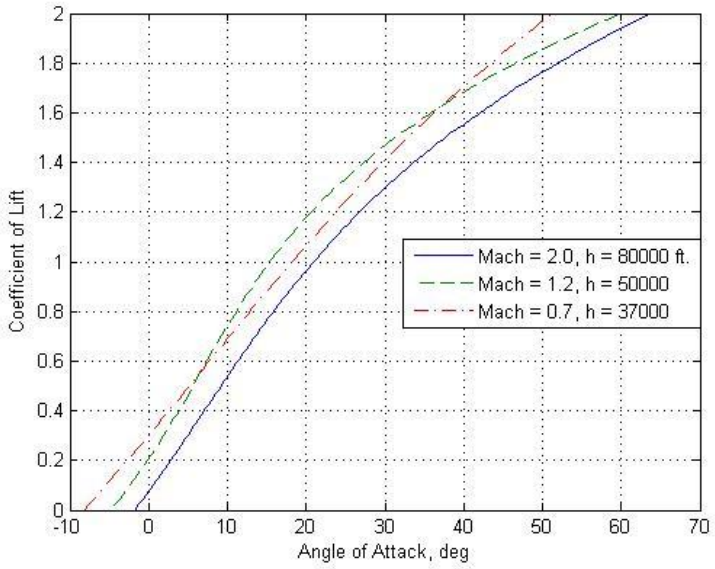

Fig. 9. Coefficient of lift versus angle of attack for the vehicle model being simulated with this research. The different curves correspond to different vehicle Mach numbers and altitudes.

From the vehicle data, it was possible to determine the lift-to-drag ratio, *L/D*, for the vehicle at any Mach number. Perhaps even more critical, it was possible to determine the maximum possible lift-to-drag ratio for the vehicle at any given Mach number. Figure 10 illustrates the maximum lift-to-drag ratio for the vehicle model compared against Mach number. It can be seen from Fig. 10 that the maximum lift-to-drag ratio appears to be a piecewise function depending on vehicle Mach number. The shape of the maximum lift-to-drag ratio function is heavily dependent on the vehicle-specific aerodynamic model. As a result of the drag coefficient increasing, the maximum lift-to-drag ratio decreases, which is exhibited by Fig. 10. Figure 10 also clearly shows the discontinuity that exists at a Mach value of 0.9. While there are other discontinuities over the range of

Mach numbers, the discontinuity when Mach number is equal to 0.9 is due to the zero-lift drag coefficient. The other discontinuities seen in Fig. 10 can be attributed to the aerodynamic model of the vehicle.

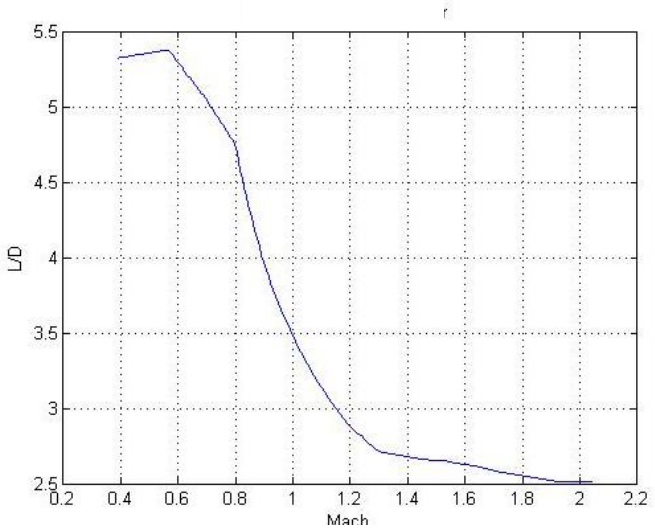

Fig. 10. Maximum lift-to-drag ratio versus vehicle Mach number.

CHAPTER 3

LATERAL GUIDANCE

A new method of lateral tracking for a vehicle reentering the atmosphere has been developed. This method applies to the vehicle when it is the TAEM stage of flight. The initial subphases of flight for the vehicle will be very similar to the original Shuttle guidance; however, there will be new and unique characteristics to each of the subphases.

When the vehicle is deemed to have the energy level necessary to be within the TAEM phase an onboard program will be executed, which will determine the maximum range for the vehicle. This component of the reentry guidance package will be explained in further detail in a subsequent chapter. After the initial maximum range program is executed and a HAC location and size have been determined, it is time for the vehicle to begin attempting to fly the prescribed lateral trajectory for heading control.

3.1 S-turn and Acquisition Phases of TAEM

Ideally, and for the initial explanation, it is assumed that the vehicle will possess an energy level sufficient enough to complete an overhead HAC turn but not too much to require an excessive number of S-turns during the beginning to TAEM. Assuming these parameters, once the vehicle enters TAEM it will complete a banked turn in order to be oriented with the nearest tangent point on the HAC. Assuming decent execution of the phase of flight before TAEM, this first banked turn to the HAC tangent point should be a small, nearly insignificant, maneuver. However, even if the first turn for the vehicle is large enough to be significant, all of the possible scenarios have been accounted for within the guidance and navigation programs.

After the completion of the first banked S-turn, the vehicle is now pointed at a HAC tangent point. The vehicle will fly with wings-level at the maximum lift-to-drag ratio to the HAC tangency point. This acquisition phase of TAEM is preferably completed at a linearly increasing dynamic pressure. The angle-of-attack for the vehicle will be varied in order to maintain this linear dynamic pressure. The speedbrake on the vehicle also helps with maintenance of the dynamic pressure. Also, it is assumed that the vehicle will maintain a nearly constant flight path angle of approximately -9 deg throughout the TAEM phase of flight. It should also be noted, that while vehicle dynamics were taken into account, the vehicle was treated as a point mass throughout these calculations. This is a simplification that has been proven to be effective while not detracting from the end results. At this point, with the vehicle at a location ten percent further from the HAC center than the HAC radius and aimed at the original HAC tangent

point, switching logic will allow the vehicle to begin flying the HAC turn portion of TAEM.

3.2 HAC Turn Phase of TAEM

A new HAC tracking technique for the vehicle has been developed and begins as the vehicle enters the HAC turn subphase of TAEM. It should be noted that this technique was originally developed using the basic equations required to track and fly the perimeter of a circle. However, since flight of the vehicle does not occur in just one plane, the vertical component of flight made these basic circle-tracking equations applicable to a cylinder. In order to allow the vehicle to track and fly a more complicated spiral, or cone, the equations for radial distance and heading angle-to-go were modified slightly. Because the vehicle begins the HAC turn with a greater velocity than when it ends the HAC turn, flying the profile of a cone allows the vehicle to complete the turn with a constant bank angle. Simple dynamics state that the radius of a turn is large when completed at a high velocity, while maintaining a constant bank angle. The radius of a turn is small when completed at a low velocity with that same constant bank angle. Since the vehicle begins the HAC turn at a high velocity and ends the HAC turn at a low velocity a spiral, or cone, is traced by the trajectory as opposed to a circle, or cylinder.

The strategy used to track the spiral HAC included using an open-loop bank angle term that was modified by system feedback in order to correct any error. First, the open-loop bank angle for the vehicle was determined. This open-loop bank angle term represents the bank angle that the vehicle must nominally fly at in order to complete a

turn of a known radius. This open-loop bank angle term is generally not as accurate as it could be with the help of an additional closed-loop bank angle term. The closed-loop term provides feedback from the system and helps to correct errors, thus resulting in a fully controlled vehicle. The open-loop bank angle was determined by applying $\Sigma F = ma$ to the vehicle in the normal flight path direction, as well as to the side forces of the vehicle for a general banked circular turn. When applying $\Sigma F = ma$ to the vehicle in the direction normal to the flight path, the resulting equation is

$$mV\dot{\gamma} = L\cos\phi - W\cos\gamma \tag{15}$$

where W represents the weight of the vehicle. As a reminder, the vehicle is a glider and, therefore, thrust is not a term that will be used in any of the $\Sigma F = ma$ equations. Equation (15) is simplified by dividing through by the mass of the vehicle and assuming that the rate of change of the flight path angle for the vehicle is approximately zero. The resulting equation is viewed as

$$\frac{L}{m} = \frac{g\cos\gamma}{\cos\phi} \tag{16}$$

Newton's Second Law is then applied to the side forces of the vehicle during a general banked turn.

$$mV\cos\gamma\dot{\psi} = L\sin\phi \tag{17}$$

Equation (17), which is actually just a manipulated version of Eq. (3), is simplified first by recognizing that the velocity of the vehicle in the horizontal direction is expressed as

$$V_H = V\cos\gamma \tag{18}$$

Additionally, it should be noted that the turning rate of the vehicle, $\dot{\psi}$, is equivalent to

$$\dot{\psi} = \frac{V_H}{R} \tag{19}$$

by definition [10], where *R* represents the instantaneous radial position of the vehicle. The simplification of Eq. (17), along with the usage of Eq. (16) may be viewed as

$$\dot{\psi} = \frac{g cos\gamma}{cos\phi} \frac{sin\phi}{V_H} = \frac{V_H}{R} \tag{20}$$

When solving Eq. (20) explicitly for the open-loop bank angle the result is

$$\phi_{OL} = \tan^{-1}\left(\frac{V_H^2}{R\, g \cos\gamma}\right) \tag{21}$$

In order to track and fly a prescribed trajectory there is a need for a dynamic controller. The first step towards accomplishing a controlled vehicle is to specify the states of the vehicle. It was determined that the states of the vehicle would be the radial position of the vehicle and heading angle of the vehicle with respect to the nominal. The vehicle states are shown by Eq. (22).

$$\vec{x} = \begin{bmatrix} \theta \\ R \end{bmatrix} \tag{22}$$

A simple diagram of the system, which explicitly defines the vehicle states, may be viewed as Fig. 11. Figure 11 illustrates the HAC simplified as a circle. The x and y coordinate system is placed at the center of the HAC for this illustration. As a reference, according to Fig. 11, the vehicle is currently on the HAC with no radial error. However, the vehicle is flying away from the prescribed path as shown by the positive value of theta. Ideally, θ should be zero. Figure 11 merely illustrates one possible scenario out of many for the vehicle.

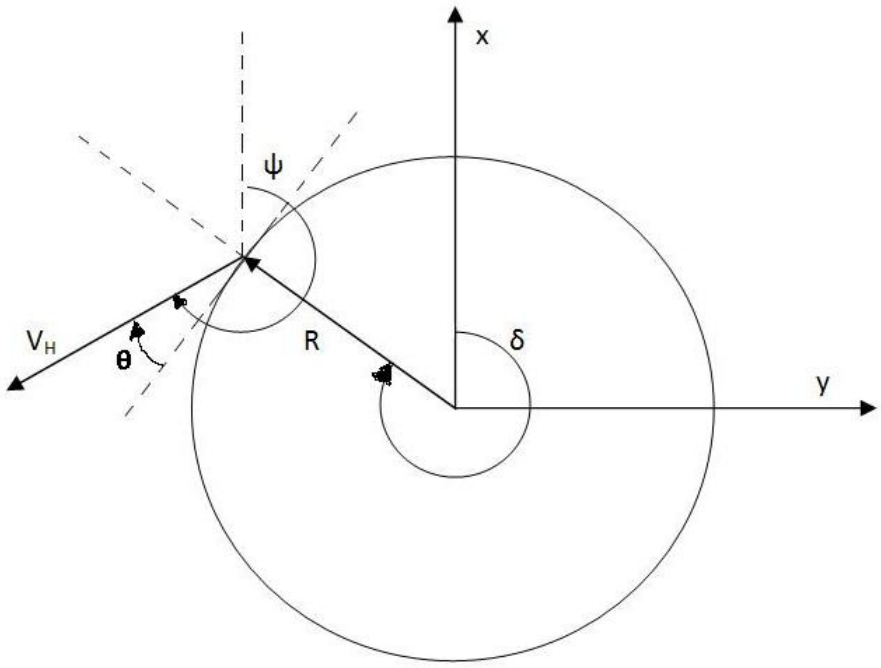

Fig. 11. Simple schematic of the simplified HAC. This is merely used to help visualize the variables with respect to the HAC.

As shown by Fig. 11, the vehicle has a known velocity, which is represented by the variable V_H. It should be pointed out that due to the three-dimensional nature of this problem and the fact that only the lateral plane is currently being examined, the vertical component of velocity can presently be ignored. The horizontal component of the velocity is the only element of the velocity that is applicable in order to laterally track the HAC. The horizontal component of velocity, V_H, was determined previously using Eq. (18).

As shown by Fig. 11, θ is a variable that is ideally equal to 0 deg. The heading angle of the vehicle, ψ, is eventually driven to 0 deg at the end of the HAC turn; therefore, the angular position of the vehicle, δ, is driven to 90 deg. This conclusion drawn from observing Fig. 11 is shown in equation form by

$$\delta = \psi + (90° - \theta) \tag{23}$$

When working to control a system it is easier to drive a variable to zero rather than to a nominal value. Because of this, the first state variable for the system will be θ. Since vehicle heading angle with respect to the nominal is a state variable it is required that an equation for the rate of change for that variable is acquired. Determining a rate of change equation for θ is done by taking the derivative of Eq. (23) with respect to time and then solving for $\dot{\theta}$.

$$\dot{\theta} = \dot{\psi} - \dot{\delta} \tag{24}$$

The rate of change for the radial state variable was found in a simpler manner. By looking at Fig. 11, it was determined that the change in radial position was a direct result of the sine component of the horizontal velocity of the vehicle. The radial rate of change was determined through simple trigonometric relations and is shown as

$$\dot{R} = V_H \sin\theta \tag{25}$$

With the rate of change equations determined for each of the state variables, it is now required that these equations be expressed in terms of either the state variables, constants of the system, or variables that vary with time but are measured parameters of the system. With the purpose of completing Eq. (24) using the aforementioned requirements, Eq. (17) illustrates the variables used to complete the equation for rate of change of the heading angle for the vehicle.

$$\dot{\delta} = -\frac{V_H}{R}\cos\theta \tag{26}$$

Equation (26) achieves the same goal of specifying the variables needed to complete the equation for rate of change for the angular position of the vehicle. After solving Eq. (17) for $\dot{\psi}$, the resulting expanded version of Eq. (24) may be viewed as

$$\dot{\theta} = \frac{L \sin \phi}{m V_H} + \frac{V_H}{R} cos\ \theta \tag{27}$$

It should be pointed out that Eq. (27) is a nonlinear equation because of the lift force term. As one might remember from Eq. (7), lift is a function of many nonlinear terms, namely atmospheric pressure, the square of the velocity of the vehicle, and the lift coefficient of the vehicle. Even though Eq. (27) is nonlinear, it is a function which contains only variables that are either state variables or inputs, constants of the system, or variables that are measured and known.

The rate of change equation for radial position, Eq. (25), is already expressed in terms of a state variable of the system and a measured variable. Because of this, Eq. (25) and Eq. (27) are the nonlinear rate of change equations for the state variables.

Chartres et al. [11] contends that the best way to solve the guidance problem at hand is by using these nonlinear equations. Much like this model, Chartres et al. uses bank angle as a control input; however, in Chartres' model, angle of attack and speedbrake deflection are also used. According to Chartres et al., optimizing a nonlinear system using the previously mentioned control inputs and a sequential programming algorithm, NLPQL, produces an accurate and precise solution to the control problem. This method is completed by first determining a function to be minimized. Using this minimized function, along with constraint equations and the initial and final states of the vehicle, a fourth order Runga-Kutta solver was applied to the multiple nonlinear differential equations. According to Chartres et al., this method yielded optimal results for a great number of varying initial vehicle conditions.

Unlike Chartres et al., this paper will not attempt to solve the nonlinear differential equations in order to develop bank angle control. Rather, the equations will

be linearized in an attempt to simplify the solution process. It has been determined that the linearizing process does not add a significant amount of error to the trajectory.

3.2.1 Linearization and State-Space Representation

The end goal for the lateral tracking portion of the HAC turn phase is to establish a control system that provides excellent tracking of a spiral HAC. In order to reach that goal the system must be able to be represented by a state-space system. The states for the system have already been chosen and the equations for the system have already been detailed; however, in order for a state-space representation of the system to be correct, the equations representing the system must be linear. Therefore, in order to cooperate with the requirements for a state-space representation, the equations representing the system will be linearized.

The first step in linearizing this problem is defining the perturbation variables. This is done by Eq. (28), where the nominal values θ^* and R^* are equal to 0 deg and the radius of the nominal HAC, R_F, respectively.

$$\delta\vec{\eta} = \begin{bmatrix} \theta - \theta^* \\ R - R^* \end{bmatrix} \tag{28}$$

Intuitively, the perturbation variables are the variables within the system that are to be driven to zero. The variables θ and R within Eq. (28) represent the values at that particular instant in time.

$$\delta u = \phi - \phi^* \tag{29}$$

Equation (29) illustrates the perturbation variable for the input of the system, bank angle. The nominal value for bank angle is equal to the bank angle required to complete the

HAC turn at any accompanying value of R_F. If the vehicle were following the path of a cylinder, this nominal value of bank angle would be known. However, in order to track a cone this nominal bank angle value is unknown. If this nominal value is unknown, it is impossible to determine the $\boldsymbol{B}$ matrix. This situation will be remedied shortly.

$$\delta\dot{\eta} = \boldsymbol{A}\delta\vec{\eta} + \boldsymbol{B}\delta u \tag{30}$$

The general equation representing a linearized system can be viewed as Eq. (30). This equation, needing to be completed, contains many parts. The first component of Eq. (30) is the $\boldsymbol{A}$ matrix.

$$\boldsymbol{A} = \begin{bmatrix} \frac{\partial f_1}{\partial \theta} & \frac{\partial f_1}{\partial R} \\ \frac{\partial f_2}{\partial \theta} & \frac{\partial f_2}{\partial R} \end{bmatrix}_* \tag{31}$$

The $\boldsymbol{A}$ matrix, Eq. (31), has four components for this particular case, each component made up of a partial derivative. For this case, f_1 is equivalent to Eq. (27). The function f_2 is equivalent to Eq. (25).

$$\boldsymbol{B} = \begin{bmatrix} \frac{\partial f_1}{\partial \phi} \\ \frac{\partial f_2}{\partial \phi} \end{bmatrix}_* \tag{32}$$

The $\boldsymbol{B}$ matrix, Eq. (32), is composed of two components in this case, both of which are calculated in a similar manner as those components that made up the $\boldsymbol{A}$ matrix. All of the elements within both the $\boldsymbol{A}$ and $\boldsymbol{B}$ matrices are evaluated at the nominal values defined previously, as denoted by the * subscript.

Each partial derivative evaluated at the nominal conditions for both $\boldsymbol{A}$ and $\boldsymbol{B}$ matrices can be seen as Eqs. (33-38).

$$\frac{\partial f_1}{\partial \theta} = -\frac{V_H}{R^*}\sin\theta^* = 0 \tag{33}$$

$$\frac{\partial f_1}{\partial R} = -\frac{V_H}{R^{*2}}\cos\theta^* = -\frac{V_H}{R^{*2}} \tag{34}$$

$$\frac{\partial f_2}{\partial \theta} = -V_H \cos\theta^* = V_H \tag{35}$$

$$\frac{\partial f_2}{\partial R} = 0 \tag{36}$$

$$\frac{\partial f_1}{\partial \phi} = \frac{L\cos\phi^*}{m V_H} \tag{37}$$

$$\frac{\partial f_2}{\partial \phi} = 0 \tag{38}$$

The result of combining all of the different elements made up by Eqs. (33-38) is

$$\begin{bmatrix}\delta\dot{\theta}\\ \delta\dot{R}\end{bmatrix} = \begin{bmatrix}0 & -\frac{V_H}{R^2}\\ V_H & 0\end{bmatrix}\begin{bmatrix}\delta\theta\\ \delta R\end{bmatrix} + \begin{bmatrix}\frac{L\cos\phi}{m V_H}\\ 0\end{bmatrix}\delta\phi \tag{39}$$

Equation (39) is merely Eq. (30) simplified in terms of variables that are either measured or constant. There is one exception to this statement, however. The lift force term as well as the bank angle term is still present in the ***B*** matrix. This is a situation that requires a remedy mainly because of the uncertainty of the value for the bank angle at any particular turning radius. Therefore, the goal is to express the lift force term and the bank angle term in terms of variables that are either known or can be measured, much like the velocity and radius terms that compose the rest of the ***A*** and ***B*** matrices.

When looking to simplify the ***B*** matrix, one equation that is extremely useful actually comes from the equations of motion that govern the motion of the vehicle during reentry. Equation (2) contains the $\frac{L\cos\phi}{\boldsymbol{m}}$ portion of Eq. (39), of which we are trying to simplify. Since it is assumed that the flight-path angle of the vehicle during TAEM is relatively constant, it can be said that the rate of change of the flight-path angle is negligible. Essentially, this means that Eq. (2) can be set equal to zero. This is what Eq.

(40) does, along with multiplying both sides of the equation by the velocity of the vehicle.

$$V\dot{\gamma} = \frac{L\cos\phi}{\boldsymbol{m}} - g\cos\gamma = 0 \tag{40}$$

Simplifying Eq. (40) gives the explicit term that is trying to be substituted for in Eq. (39). This simplification is plainly shown as

$$\frac{L\cos\phi}{\boldsymbol{m}} = g\cos\gamma \tag{41}$$

The final state-space representation of the system is shown in equation form by

$$\begin{bmatrix}\delta\dot{\theta}\\ \delta\dot{R}\end{bmatrix} = \begin{bmatrix}0 & -\frac{V_H}{R^2}\\ V_H & 0\end{bmatrix}\begin{bmatrix}\delta\theta\\ \delta R\end{bmatrix} + \begin{bmatrix}\frac{g\cos\gamma}{V_H}\\ 0\end{bmatrix}\delta\phi \tag{42}$$

Equation (42) is expressed solely in terms of variables that are either measured or known.

Before any more progress was achieved there was a need to see if this system was, in fact, controllable. If the system proves to not be controllable there is no point in proceeding because a new method of solving the trajectory problem needs to be adopted. According to Ogata [12], "a system is said to be controllable at time t_o if it is possible to transfer the system from any initial state $\mathbf{x}(t_o)$ to any other state in a finite interval of time by means of an unconstrained control vector." It is also known, and Ogata agrees, that controllability is a requirement for certain control-design operations, such as pole-placement. Since the overall goal is to create a pole-placement controller for the trajectory of the vehicle during the HAC turn subphase of flight, it is necessary that the system recently created is controllable.

$$Q = [\boldsymbol{B} \quad \boldsymbol{AB} \quad \boldsymbol{A^2B} \quad \cdots \quad \boldsymbol{A^{n-1}B}] \tag{43}$$

Using Eq. (43), the controllability of the system was determined. By definition, a system is controllable if and only if Q has full rank. This means that the columns of the newly

created Q matrix must be linearly independent. After evaluating Eq. (43) using the $\boldsymbol{A}$ and $\boldsymbol{B}$ matrices of the system it was determined that the system is, indeed, controllable. The evaluation of the Q matrix is shown as

$$Q = \begin{bmatrix} \frac{g\cos\gamma}{V_H} & 0 \\ 0 & g\cos\gamma \end{bmatrix} \tag{44}$$

It is also of interest to determine if the second order system is stable and damped. This is done by finding the eigenvalues of the $\boldsymbol{A}$ matrix.

$$det\,[\lambda \boldsymbol{I} - \boldsymbol{A}] \;=\; det \begin{bmatrix} \lambda & \frac{V_H}{R^2} \\ -V_H & \lambda \end{bmatrix} = 0 \tag{45}$$

The eigenvalues of the system are found by using Eq. (45), where $\boldsymbol{I}$ is the identity matrix and λ represents the eigenvalues of the system. After Eq. (45) is solved for the eigenvalues it was determined that both eigenvalues were imaginary. Specifically, $\lambda_{OL} = \pm j\frac{V_H}{R}$, where j denotes the fact that the term is imaginary. Since both open-loop eigenvalues are imaginary, by definition, the open-loop second-order system is marginally stable and undamped.

Since the open-loop response of the system is marginally stable and undamped there is a high probability that the open-loop response will not provide an ideal solution. In fact, since the response is undamped, the radial position error of the vehicle will oscillate depending on the sine and cosine functions of the natural frequency of the response. The natural frequency of the response is dependent on the velocity and position of the vehicle. The undamped nature of the response will not allow the radial position error to be damped to zero. In order to create a stable response that damps out the radial position error and heading angle error, feedback needs to be inserted into the system. Feedback is inserted in the form of a closed-loop bank angle response term.

3.2.2 Closed-Loop Bank Angle

With confirmation that the system is controllable it is possible to proceed in using pole-placement in an attempt to control the trajectory of the vehicle. First, the closed-loop $\boldsymbol{A}$ matrix, $\boldsymbol{A_{CL}}$, is calculated.

$$\boldsymbol{A_{CL}} = \boldsymbol{A} - \boldsymbol{BK} \tag{46}$$

Unlike the open-loop, or standard, $\boldsymbol{A}$ matrix, the closed-loop $\boldsymbol{A}$ matrix contains feedback terms that act as gains for each state of the system. These gains are applied to the perturbations of the state variables in order to help control the system.

$$\boldsymbol{A_{CL}} = \begin{bmatrix} 0 & -\frac{V_H}{R^2} \\ V_H & 0 \end{bmatrix} - \begin{bmatrix} \frac{g\cos\gamma}{V_H} \\ 0 \end{bmatrix} [k_{\boldsymbol{\theta}} \quad k_R] \tag{47}$$

Equation (46) illustrates the general process of obtaining the closed-loop $\boldsymbol{A}$ matrix. Equations (47) and (48) are explicit in showing the details of obtaining the closed-loop $\boldsymbol{A}$ matrix.

$$\boldsymbol{A_{CL}} = \begin{bmatrix} -\frac{k_\theta g\cos\gamma}{V_H} & -\frac{V_H}{R^2} - \frac{k_R g\cos\gamma}{V_H} \\ V_H & 0 \end{bmatrix} \tag{48}$$

It is intuitive that $k_{\boldsymbol{\theta}}$ represents the gain that will be applied to the $\delta\theta$ state variable. Similarly, k_R corresponds to the gain that will be applied to the δR state variable.

The next step in the pole-placement process is to determine the eigenvalues, λ, of the closed-loop $\boldsymbol{A}$ matrix. This is done using

$$det\,[\lambda \boldsymbol{I} - \boldsymbol{A_{CL}}] = det \begin{bmatrix} \lambda + \frac{k_\theta g\cos\gamma}{V_H} & \frac{V_H}{R^2} + \frac{k_R g\cos\gamma}{V_H} \\ -V_H & \lambda \end{bmatrix} = 0 \tag{49}$$

After completing all of the necessary algebraic steps and setting the corresponding determinant equation equal to zero the result is

$$det\,[\lambda \boldsymbol{I} - \boldsymbol{A_{CL}}] \;=\; \lambda^{\mathbf{2}} + \frac{k_\theta g\cos\gamma}{V_H}\lambda + \frac{V_H^2}{R^2} + \; k_R g\cos\gamma = 0 \tag{50}$$

Under different circumstances, only the eigenvalues of the system would be of interest in order to tell if the system is stable. However, there are two additional unknown gain values that are contained within Eq. (50). These are the variables that are of interest, in this case. Since the system is a second-order, damped, and stable system, by definition, Eq. (50) can be compared with

$$\lambda^{\mathbf{2}} + \; 2\zeta\omega_n\lambda + \; \omega_n^2 = 0 \tag{51}$$

As can be seen, the different components of Eqs. (50) and (51) compare favorably. Since the gain terms are the terms of interest, the similar components of Eqs. (50) and (51) were set equal to each other. The gain terms were then solved for, explicitly.

$$k_\theta = \frac{2\zeta\omega_n V_H}{g\cos\gamma} \tag{52}$$

$$k_R = \frac{1}{g\cos\gamma}\left(\omega_n^2 - \frac{V_H^2}{R^2}\right) \tag{53}$$

Equations (52) and (53) are still not complete because undamped natural frequency, ω_n, and damping ratio, ζ, are unknown. These two variables have a significant effect on the response of the system and must be adjusted by the user. There is no "correct" value for each of the two variables; however, there must be a balance that is struck between them. If the natural frequency value is too large the system will exhibit a large transient response before the damping effect has enough time to negate it. If the damping ratio is too small the steady-state response time of the system will be too large, as well as the percent overshoot. A guess-and-check process was established to determine the

combination of natural frequency and damping ratio that affected the system in the most positive manner.

It should be noted that the new gain values are dynamic with respect to time. Each time the program is called in real time to assist with trajectory planning and navigation the gain values will be updated based on the current velocity and position of the vehicle. This new strategy replaces the static gain strategy that has been employed by NASA since the 1970's. Dynamic gains allow for better real-time tracking of the HAC, as will be shown by the forthcoming results.

After the gains were determined for each of the state variables another issue was encountered. Historically, the bank angle of the reentry vehicle has contained a closed-loop term that contains static gains. These static gains have historically been expressed in terms of radial error and radial rate error. The new dynamic gains are expressed in terms of radial error and angular heading error. There must be a conversion performed in order for the new dynamic gains to be effective with the previous HAC tracking method. By evaluating the motion of a vehicle traveling around a circular path, the conversion between radial rate error and angular heading error is as simple as dividing the angular heading error by the horizontal velocity of the vehicle. The gain conversions are illustrated as Eqs. (54) and (55). The gains are applied to the perturbation values for radial position and radial rate, as can be seen in Eq. (56). Equation (56) represents the closed-loop bank angle term.

$$G_{\dot{R}} = \frac{k_\theta}{V_H} \tag{54}$$

$$G_R = k_R \tag{55}$$

$$\phi_{CL} = G_R \delta R + G_{\dot{R}} \delta \dot{R} \tag{56}$$

3.2.3 Bank Angle Bias Strategy

While the pole-placement control-design procedure was effective in limiting the amount of error as the vehicle traveled around the HAC, there was still a need for a fine-tuning mechanism that negated nearly all of the radial position and rate error. This mechanism is presented in the form of a bank angle bias strategy. The concept behind this strategy is simple. An accompanying simple schematic of an overhead view of the trajectory is shown in Fig. 12.

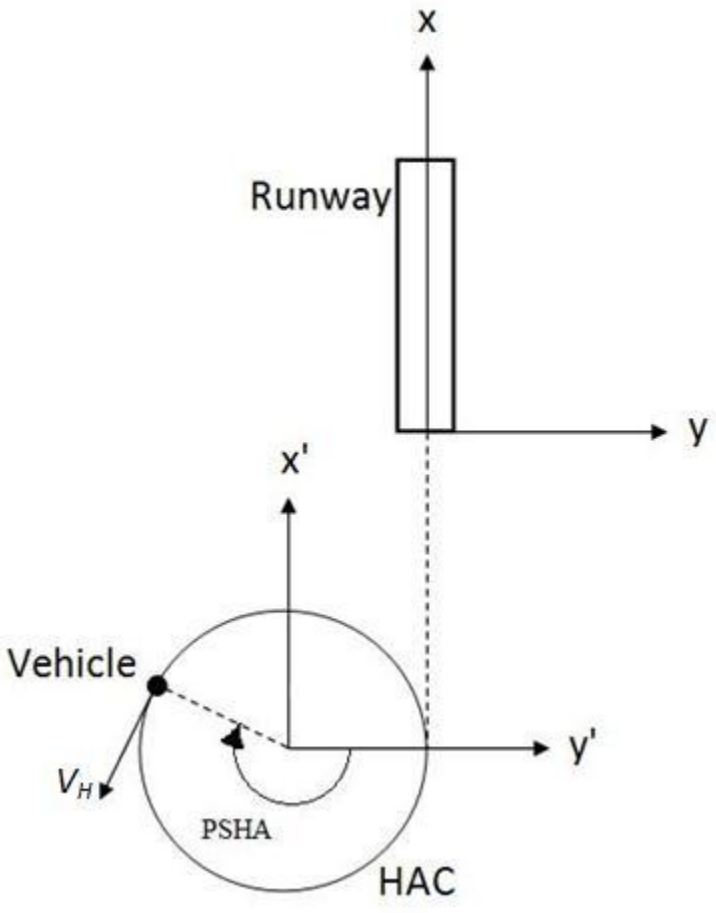

Fig. 12. Simple illustration of PSHA as it relates to the HAC and the runway. It should be noted that in this illustration the HAC is simplified to a cylinder.

When the PSHA angle-to-go is large during this simulation the spiral is large and the vehicle is not banked at a large enough angle to be able to follow the trajectory effectively. However, when the PSHA angle-to-go is small the spiral essentially turns into a circle. This point occurs just before the vehicle transitions from the HAC turn to the prefinal phase. At this point, the vehicle is banked at the correct angle to follow the nearly circle trajectory. There is a need for an additional bank angle term that will considerably increase the bank angle of the vehicle at the start of the HAC turn while progressively becoming less and less effective as the vehicle travels around the HAC. The previous statement assumes an overhead HAC, which means the vehicle must complete a turn of at least 180 deg. Simply put, when the vehicle has a greater turn angle-to-go, the bank angle bias value will be greater. When the vehicle has a smaller turn angle-to-go, the bank angle bias value will be relatively smaller.

Multiple approaches were taken when examining this problem. At first, a constant bank angle bias term was employed to make sure this strategy would work within the simulation. The constant bias term, shown as Eq. (57a), simply added a couple of degrees of bank to the overall bank angle term. This bias term was applied as a constant throughout the HAC turn, meaning that the bias term was independent of PSHA. For this illustration, it should be noted that the vehicle was completing an overhead HAC turn to the left. Due to the sign convention, this means that the overall bank angle value will be negative to complete a left-hand turn. Because of this, the bank angle bias term is negative, making the overall bank angle term more negative. It should also be noted that the variable H is a constant value representing an angle of only a few degrees. This H variable is used throughout the bank angle bias equations.

$$\phi_{BIAS} = -H \tag{57a}$$

A linear bank angle bias term was also tested. This linear term accomplished the goal of being large when the PSHA value was large and small when the PSHA value was small. It should be noted that PSHA is measured in degrees. Again, the PSHA variable is explicitly shown in Fig. 12. Shown as Eq. (57b), this term proved to be a considerable upgrade than just using a constant value for the bank angle bias term. Similarly, a quadratic function with respect to PSHA was tested. This is shown as Eq. (57c).

$$\phi_{BIAS} = -\frac{H}{270^{\circ}} PSHA \tag{57b}$$

$$\phi_{BIAS} = -\frac{H}{145800^{\circ}} PSHA^2 - \frac{H}{540^{\circ}} PSHA \tag{57c}$$

Finally, a bank angle bias value that was an exponential function of PSHA was tested. This bank angle bias term was computed using another variable, *a*, which was chosen by the user in order to obtain the best results possible. Equation (57d) illustrates this exponential function.

$$\phi_{BIAS} = -He^{a(PSHA-270^{\circ})} \tag{57d}$$

For all of the different versions of Eq. (57) it can be seen that the recurring theme includes using 270 deg. This value was chosen by the user and seemed to yield the best results. This is because, when completing an overhead HAC turn, the vehicle will always have to travel at least 180 deg around the HAC. Rarely will the vehicle have to complete a HAC turn greater than 360 deg. Because of these factors, a balance was struck and the value of 270 deg was settled on.

3.2.4 Complete HAC Turn Bank Angle

After the completion of all of the separate terms that make up the total bank angle for the vehicle at any instant in time, all of the terms needed to be compiled. This is done using simple addition and is illustrated as Eq. (58). Equation (58) is composed of three different bank angle term equations, namely Eqs. (21), (56), and (57).

$$\phi = \phi_{OL} + \phi_{CL} + \phi_{BIAS} \tag{58}$$

It should be noted that the many versions of the bank angle bias term, Eq. (58), were tested extensively and the ideal bias term will be determined at a later point in time.

3.3 Prefinal Flight Phase

The HAC turn is considered complete when the vehicle reaches the point where the heading angle is within 5 deg of the runway centerline. After the HAC turn is complete a logic operator switches the navigation of the vehicle to the prefinal phase. During the prefinal phase the vehicle should optimally be flying with a negligible bank angle. However, due to position error of the vehicle as it is leaving the HAC turn the prefinal phase is required to employ a controller, which will modify the bank angle of the vehicle in order to negate any position error. This method is similar to the method utilized by the HAC turn, though it is much simpler.

Crosstrack position and crosstrack rate of change for the vehicle were determined to be the two control states for this portion of TAEM. Observing the strategy utilized by

Moore [3], these states were modified by static gains in order to create a makeshift closed-loop controller. This general bank controller may be seen as

$$\phi = -K_y y - K_{\dot{y}} \dot{y} \tag{59}$$

In an attempt to create a better response from the vehicle the same method from the HAC turn of obtaining dynamic gains was used. Using simple dynamics it was determined that

$$\dot{y} = V_H \sin \psi \tag{60}$$

$$\ddot{y} = V_H \dot{\psi} \cos \psi \tag{61}$$

represent the velocity and acceleration equations in the y-direction for the vehicle. After simplifying and applying the equations to a state-space representation the resulting system may be viewed as

$$\begin{bmatrix} \delta \dot{y} \\ \delta \ddot{y} \end{bmatrix} = \begin{bmatrix} 0 & 1 \\ 0 & 0 \end{bmatrix} \begin{bmatrix} \delta y \\ \delta \dot{y} \end{bmatrix} + \begin{bmatrix} 0 \\ g \cos \gamma \end{bmatrix} \delta \phi \tag{62}$$

The process of creating the state-space representation of the system was completed using the same procedure as section 3.2.

After completing the process of determining the closed-loop poles of the system, which was the same process carried out for the HAC turn using Eqs. (46-53), it was found that the gains for the prefinal phase could be represented by

$$K_y = \frac{2\zeta \omega_n}{g \cos \gamma} \tag{63}$$

$$K_{\dot{y}} = \frac{{\omega_n}^2}{g \cos \gamma} \tag{64}$$

Much like the gains used for the HAC turn, the prefinal gains were calculated with the end goal being that these gains would be updated as the vehicle was completing the prefinal phase. Ideally, dynamic gains should improve vehicle tracking of the prefinal trajectory. The one possible downfall to this dynamic gain strategy is that the prefinal

phase of TAEM is not long enough for the dynamic gains to show any significant improvement over the standard static gains. This possible downfall will be tested and from this testing the appropriate gains will be found and utilized.

It should be noted that there was no attempt to constrain the prefinal gains in order to create a continuous bank angle transition between the HAC turn subphase and the prefinal subphase. Because of this, there is a possibility for a small discontinuity in the commanded bank angle to occur between the two subphases. However, currently the Shuttle uses a logic program that creates a fade between the two discontinuous bank angle values. This fader logic could be utilized in order to create a continuous commanded bank angle function between the two subphases.

CHAPTER 4

LATERAL GUIDANCE RESULTS

The major component of the TAEM phase of flight that was modified in the lateral plane was the HAC turn subphase. Because of this, the HAC turn was isolated from the remainder of the trajectory. This was done by simulating the environment created by the original model and applying this new environment to only the HAC turn.

4.1 HAC Model Simplification

One notable difference in the model is the fact that the vehicle is now only traveling at subsonic speeds, unlike the beginning of the TAEM phase in which the vehicle travels at supersonic and transonic speeds. Because of the relatively slower speeds of the vehicle the drag coefficient equation, Eq. (9), is simplified. Equation (9), which varies indirectly because of Mach number, does not need to be changed but rather

it is merely simplified. While Eq. (9) does not directly vary with Mach number, the vehicle's aerodynamic characteristics vary with Mach number and the drag coefficient varies with changing vehicle dynamics.

One other significant difference between the simplified HAC simulation and the full TAEM simulation is that the vehicle is given a constant flight path angle of negative 14 deg for the simplified simulation. The primary reason for doing this is because the simplified simulation was not given access to the complex programs that related lateral and longitudinal motion. Even with a constant flight path angle, the simplified simulation is a good representation of the full TAEM simulation. First of all, the linearized equations used to compute the gains for the HAC turn were calculated using the assumption of a constant flight path angle. As will be seen, this is a good approximation as there is not much variation to the flight path angle within the full TAEM simulation.

The remainder of the vehicle model is constant with the more thorough TAEM model detailed in Chapter 2. Even though the model remains consistent the process of isolating the HAC turn from the rest of the TAEM trajectory will introduce some error to the model. This is because the simplified model no longer relies on all of the detailed programs that predict the groundtrack for the vehicle. Specifically, the PSHA for the vehicle, which is updated constantly while the vehicle is flying the TAEM trajectory, was estimated for the simplified HAC-only simulation. This estimation for PSHA was proven to be accurate after simple geometric calculations. The angle from the positive x'-axis of the runway to the vehicle was calculated using the known vehicle position. The PSHA value for the vehicle was calculated by simply subtracting 90 deg from this angular vehicle position. Essentially, the estimated PSHA value for the vehicle was determined to

be the angle from the positive y'-axis to the vehicle. This can be seen from the simple sketch viewed as Fig. 12. After extensive testing and comparison of the simplified model with the full TAEM model it was determined that the simplified model would be sufficient to provide accurate results. After the results were obtained from the simplified model the results would be applied to the full TAEM model in order to check for accuracy.

4.1.1 Simplified Simulation Characteristics

After determining that the simplified simulation would provide accurate results to apply to the full TAEM simulation a test case was created. First, the vehicle was positioned on the HAC with no radial error. The vehicle was positioned so that it would complete a 270 deg turn. In other words, the initial PSHA angle-to-go was 270 deg. The vehicle was also given the correct heading angle in order to follow the planned spiral path. If the vehicle were just following a simplified cylinder then the heading angle would be equivalent to the PSHA value at all points around the HAC. However, since the HAC is a spiral the heading angle needed to be modified slightly. For the vehicle's heading angle to match the prescribed heading angle of the spiral HAC it was determined that the radial rate of change for the vehicle needed to match the radial rate of change for the spiral. Using geometry within the model along with vehicle dynamics it was possible to explicitly solve for the initial heading angle of vehicle. This was done using Eqs. (65-70). First, it should be noted that the reference radius was calculated using

$$R_{ref} = R_F + R_2 PSHA^2 \tag{65}$$

The radial turn rate values were then set equal to each other in an attempt to eventually solve for the heading angle of the vehicle.

$$\dot{R}_{actual} = \dot{R}_{ref} \tag{66}$$

The actual calculated radial turn rate, $\dot{R}_{actual}$, was determined merely through geometry. The reference radial turn rate, $\dot{R}_{ref}$, was calculated by first taking a derivative of Eq. (65). In order to match the units of the actual calculated radial turn rate multiple factors were inserted as well as a factor that converted radians to degrees. After all of the manipulation the resulting equation was determined to be

$$-\frac{(x_{actual}\dot{x} + y_{actual}\dot{y})}{R_{actual}} = -\frac{(2V_H R_2 PSHA)}{R_{ref}}\left(\frac{180}{\pi}\right) \tag{67}$$

It should be noted that the negative signs in front of both radial rate equations prove that the vehicle is spiraling inward; the radius is getting smaller as the vehicle travels around the HAC.

Simple geometry was used to calculate the current x and y positions of the vehicle, as well as the radial position, R_{actual}. The current velocity of the vehicle in the x and y directions is also known using the simple equations

$$\dot{x} = V_H \cos\psi \tag{68}$$

$$\dot{y} = V_H \sin\psi \tag{69}$$

It was assumed that R_{actual} was equal to R_{ref}, which further simplifies Eq. (67). The PSHA value of the vehicle is known as well as the R_2 value for the spiral. The horizontal velocity value for the vehicle does not need to be known since it will cancel out when combining Eq. (67) with Eqs. (68) and (69). The result yields the required heading angle for the vehicle when the vehicle is positioned with a known PSHA value.

$$x_{actual}\cos\psi + y_{actual}\sin\psi = 2R_2 PSHA\left(\frac{180}{\pi}\right) \tag{70}$$

Equation (70) contains only one unknown that must be solved for, vehicle heading angle.

4.1.2 Universal Simulation Results

Initial simulations using the simplified model resulted in very similar results for many of the measured variables. Variables that did not change significantly with respect to the pole-placement strategy included the Mach number profile, the dynamic pressure profile, and the general shape of the bank angle and angle of attack profiles. These simulation parameters may be viewed as Figs. 13-16.

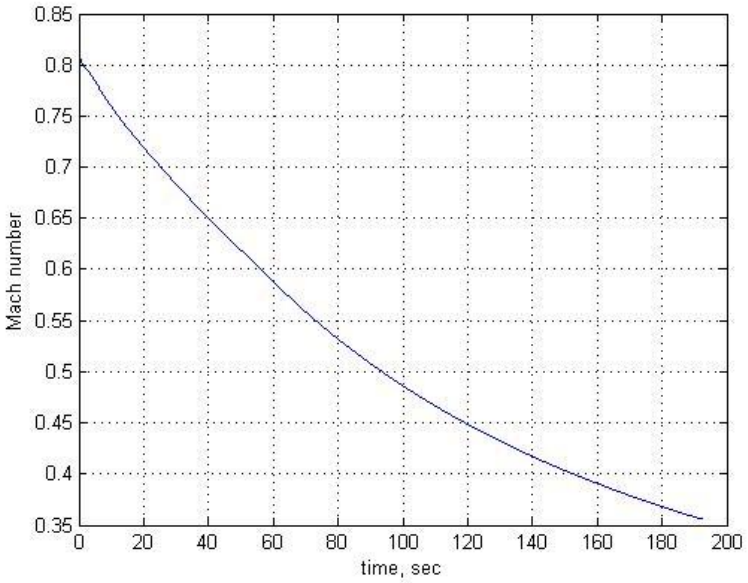

Fig. 13. Vehicle Mach number versus time for the simplified simulation.

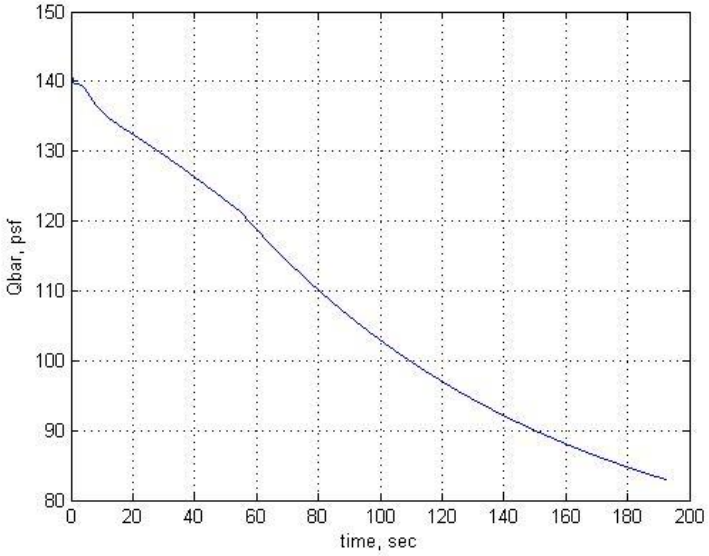

Fig. 14. Dynamic pressure versus time for the simplified simulation.

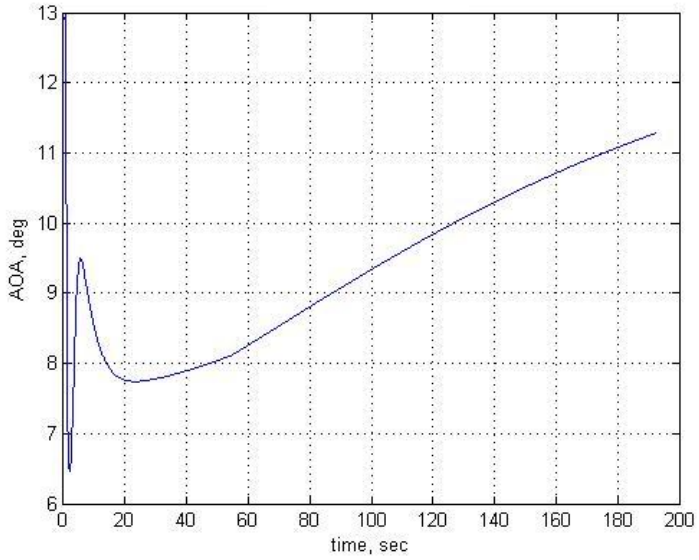

Fig. 15. Vehicle angle of attack versus time for the simplified simulation.

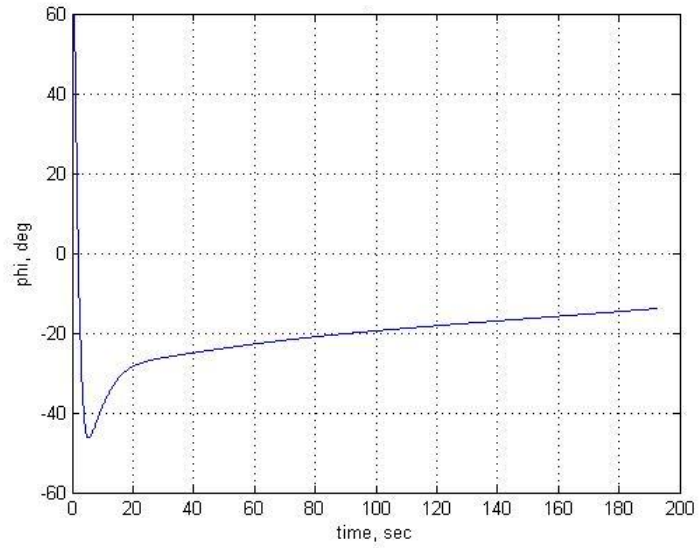

Fig. 16. Vehicle bank angle versus time for the simplified simulation.

It can be easily seen from Fig. 13 that the vehicle is traveling at subsonic speeds throughout the entire HAC turn. Figure 13 also illustrates the fact that the speed of the vehicle is nearly linearly decreasing. This linear speed change accurately represents the HAC turn during the full TAEM simulation and also lends itself to the linear decrease in dynamic pressure shown in Fig. 14. Figure 15 illustrates the angle of attack for the vehicle during the HAC turn. Besides the transient response at the beginning of the profile, the vehicle angle of attack is very representative of the full TAEM simulation. The bank angle profile, shown in Fig. 16, is accurate enough for this simplified simulation. Ideally, the bank angle would be constant around the HAC; however, Fig. 16 illustrates a profile that does not change an extreme amount during the HAC. This bank angle profile will be acceptable for initial testing purposes.

4.1.3 Iteration of Natural Frequency and Damping Ratio

Using the simplified HAC-only environment, different combinations of natural frequency and damping ratio were employed in order to determine the combination that negated the most radial position error during the trajectory. It should be noted that during this testing the bank bias value was not added to the bank angle command term. Only the natural frequency and damping ratio were used to control the system. While many combinations were tested and evaluated, the combinations shown in Table 1 represent a cross-section of some of the better results. All combinations of natural frequency and damping ratio tested outside of those shown in Table 1 were not shown due to the fact that the results were not within acceptable limits.

Table 1. Absolute error results based on varying natural frequency and damping ratio.

ω_n (rad/s)	ζ	Y-error at end of HAC (ft)	Max error during HAC (ft)
0.2	0.7	23	1000
0.2	0.8	36	1100
0.2	0.9	50	1200
0.3	0.7	10	675
0.3	0.8	16	750
0.3	0.9	22	825
0.4	0.7	6	500
0.4	0.8	9	575
0.4	0.9	12	625
0.5	0.7	4	400
0.5	0.8	6	450
0.5	0.9	8	500

Table 1 illustrates the maximum amount of radial position error, in feet, as the vehicle travels around the HAC. More importantly, Table 1 shows the radial position

error of the vehicle at the end of the HAC, also in feet. Ideally, both of these values will be small, which would indicate a vehicle traveling around a prescribed HAC and ending the HAC on the runway centerline. However, while 1,000 ft may sound like a large amount of radial error, since the scale of this trajectory is so great, 1,000 ft of error is not extremely large. Similarly, error on the scale of approximately 20 ft at the end of the HAC turn is exceptionally small.

Since all of the results presented in Table 1 would be acceptable under normal circumstances there must be another deciding factor employed in order to choose the ideal poles for the simulation. The vehicle's trajectory should be damped a significant amount. This is intuitive when one thinks about the dynamics of the vehicle. It is obviously easier for the vehicle to make one banked turn in order to correct the trajectory in order to match the nominal path rather than oscillating back and forth about the nominal path. Every oscillation about the nominal path means another bank reversal, which introduces more and more error into the system. Logic requires a large damping ratio to be employed, in this case, 0.9.

After the damping ratio for the system is chosen, a natural frequency also must be chosen. Ideally, the natural frequency should not be overly large in order to minimize the transient response of the system. A large transient response could introduce spikes to the bank angle command, which would cause unnecessarily large bank angles for the vehicle during the initial stages of the HAC turn. Because of this, the natural frequency was chosen to be 0.3 rad/s.

It can be seen using

$$t_s = \frac{4}{\omega_n \zeta} \tag{71}$$

$$\%OS = e^{\zeta\pi/\sqrt{1-\zeta^2}} \quad (72)$$

that the time response and percent overshoot for this system is acceptable. Equation (71) results in a settling time for the system of 14.81 seconds. Relative to the amount of time required to complete the HAC, which is nearly 200 seconds, this value is fairly small. Equation (72) results in a percent overshoot for the system of 0.15%. This is an extremely small value and is due to the fact that the damping ratio is so large.

4.1.4 Iteration of Maximum Bank Angle Bias Value

With values of natural frequency and damping ratio chosen it is possible to begin fine tuning the results. This fine tuning process was completed using the bank angle bias strategy described in section 3.2.3. Much like the testing of natural frequency and damping ratio, the most radical results from bank angle bias testing were omitted from the results. The radical results were tested in order to help hone in on bank angle bias values that produced acceptable amounts of error. The results from the many simulations were obtained using maximum bank angle bias values of 2, 3, and 4 deg. Four different strategies were employed when testing this method. A constant bank angle bias value was tested along with a linearly decreasing bias value. The linear bias value decreased with respect to PSHA. Also, decreasing quadratic and exponential functions were tested. In the case of the exponential function, one tuning parameter was kept constant for these trials. This tuning variable, *a*, which can be seen in Eq. (57d), was set to a value of 0.001. The results from testing may be seen in Table 2.

Table 2. Absolute error results from varying maximum bank angle bias value.

Bias type[1]	Max bias value (deg)	Y-error at end of HAC (ft)	Max y-error during HAC (ft)
Constant	2	10	800
Constant	3	4	800
Constant	4	2	800
Linear	2	22	800
Linear	3	21	800
Linear	4	21	800
Quadratic	2	10	500
Quadratic	3	4	350
Quadratic	4	1.5	200
Exponential[2]	2	10	800
Exponential[2]	3	4	800
Exponential[2]	4	2	800

[1] Note: ω_n and ζ are equal to 0.3 and 0.9, respectively, for all trials.
[2] Note: a = 0.001 for all exponential trials.

As can be seen from Table 2, the best error results are produced by the quadratic function using a maximum bank angle bias value of 4 deg. Even though the quadratic function seems to produce the best results it was still possible to produce better results using the exponential function by tuning the variable *a*. This process was completed and the results may be seen in Table 3. Like the trials for varying the maximum bank angle bias value, the natural frequency and damping ratio were kept at the chosen values of 0.3 and 0.9, respectively. Also, the best trial was chosen from Table 2 for the exponential function, which results in Table 3 showing the results using 4 deg as the maximum bank angle bias value.

Table 3. Absolute error results from varying the tuning variable a for the exponential function.

$a^{1,2}$	Y-error at end of HAC (ft)	Max y-error during HAC (ft)
0.1	7	800
0.01	1	800
0.001	2	800
0.0001	2	800

[1] Note: ω_n and ζ are equal to 0.3 and 0.9, respectively, for all trials.
[2] Note: Maximum bias value is 4 deg for all trials.

Table 3 illustrates the fact that by setting the tuning variable, *a*, to 0.01 better results are produced than when using the quadratic function. However, the maximum error value using the quadratic function is four times smaller than when using the exponential function. The maximum error value is not nearly as significant as the error at the end of the HAC. The maximum error value is specific to the simplified model. Since the vehicle was placed on the HAC with no radial error and no heading error the initial gains applied to the system were negligible. Because of this, the bank angle of the vehicle was set to be equal to the open-loop bank angle, which was calculated with a significant amount of error the first time through the process. With no feedback terms to help correct the open-loop bank angle the vehicle initially flies away from the HAC before correcting back to the prescribed trajectory. This process is illustrated in Fig. 17.

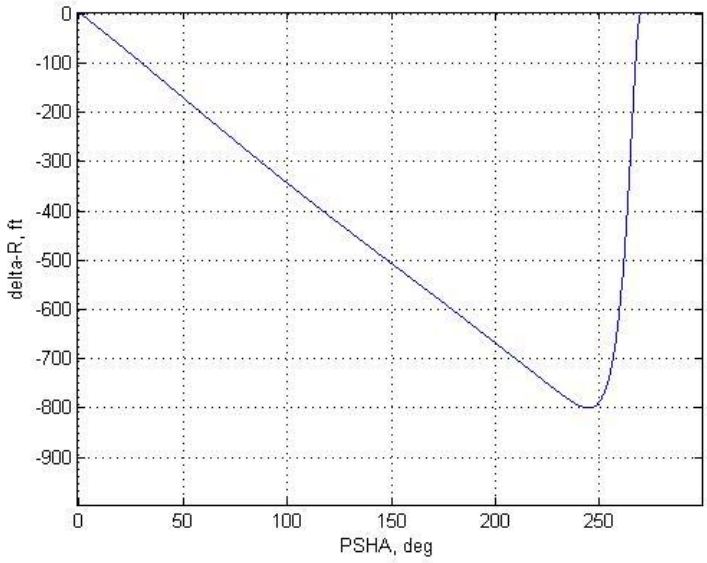

Fig. 17. Vehicle radial position error versus PSHA. This figure corresponds to an exponential bank angle bias function with a = 0.01.

4.1.5 Ideal Pole-Placement and Bank Angle Bias Parameters

The results of the testing done in sections 4.3.1 and 4.3.2 led to a solution that optimizes the radial position error of the vehicle when the vehicle reaches the end of the HAC turn. Regarding the pole-placement control design, the natural frequency of the system was chosen to be 0.3 rad/s and the damping ratio was chosen to be 0.9. The maximum bank angle bias value was chosen to be 4 deg and an exponential function was chosen to relate the bank angle bias value to PSHA. The tuning variable, *a*, was chosen to be 0.01. By using these values for the parameters of the system the vehicle will finish the simulated HAC turn with 1 ft of radial position error. Figure 18 illustrates the simplified HAC trajectory from a top-down view.

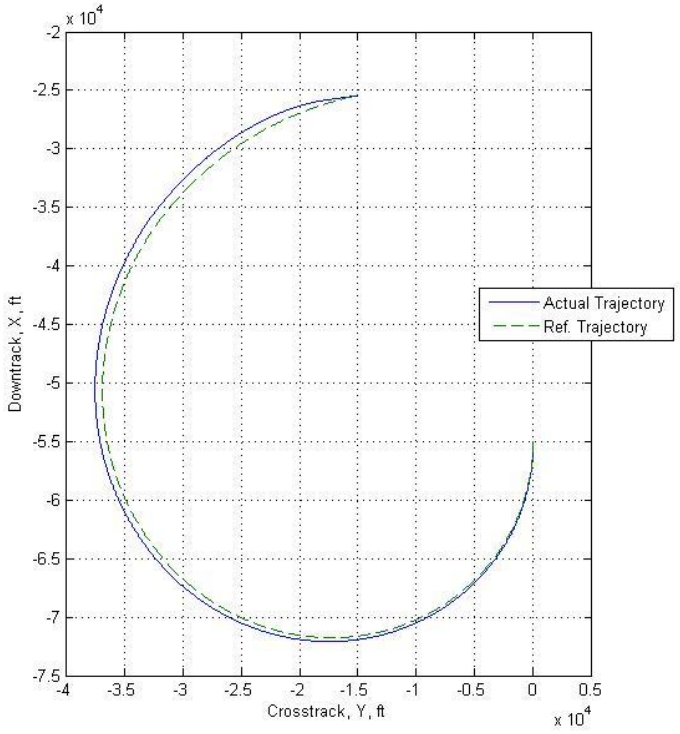

Fig. 18. Vehicle groundtrack from a top-down viewpoint.

The final critical requirement of the HAC turn is to correctly align the vehicle with the centerline of the runway at the end of the HAC turn. Recall that ideally both vehicle states will be driven to zero. One of the vehicle states was the heading of the vehicle with respect to the nominal, θ. During the simplified simulation, the angle θ was tracked and plotted compared to the nominal. Because of the spiral nature of the HAC the nominal value of θ is relatively large at the start of the HAC turn and decreases as PSHA decreases. Ideally, the angle θ will be negligible at the end of the HAC. Coupled with negligible radial position error, the vehicle's heading will be along the runway centerline. Figure 19 illustrates the nominal θ profile along with the actual θ for the vehicle. After the initial transient dies out the tracking of the nominal profile is exceptionally good. At the end of the HAC turn the θ value is very small.

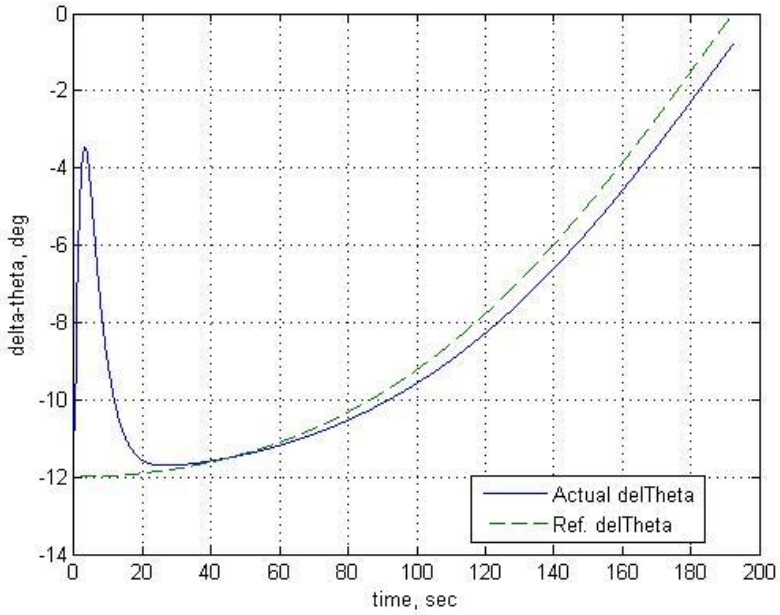

Fig. 19. Nominal and actual values of the state variable θ plotted against time during the HAC turn.

4.1.6 HAC Turn Completion with Inherited Error

The pole-placement and bank angle bias values provided the vehicle with good tracking as the vehicle completed the HAC turn. In order to further test the robustness and accuracy of the control design provided to the vehicle, radial position error and radial rate error were introduced to the simulation. First, 1,000 ft of radial position error was introduced to the vehicle at the beginning of the HAC. The controller sufficiently deals with the error, as can be seen in Fig. 20. Figure 21 shows the radial position error of the vehicle with respect to time. At the end of the HAC turn the radial position error of the vehicle is only 1.25 ft. Figure 22 shows the nominal and actual values of θ associated with this trajectory. It should also be noted that since the vehicle started off with a significant amount of position error the gains for the system did not initialize at zero. By not starting the feedback terms at zero the vehicle was able to use a more accurate initial

bank angle. Because of this, the vehicle did not fly away from the HAC before correcting back onto the correct trajectory.

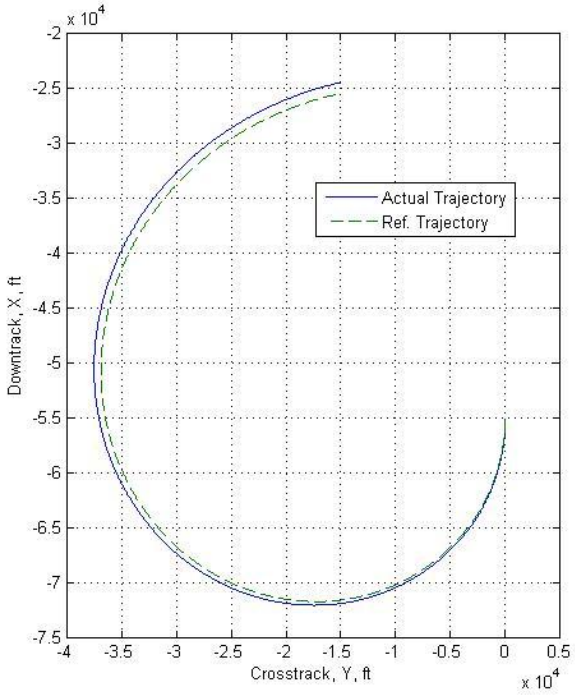

Fig. 20. Groundtrack for the vehicle with an initial position error of 1000 ft.

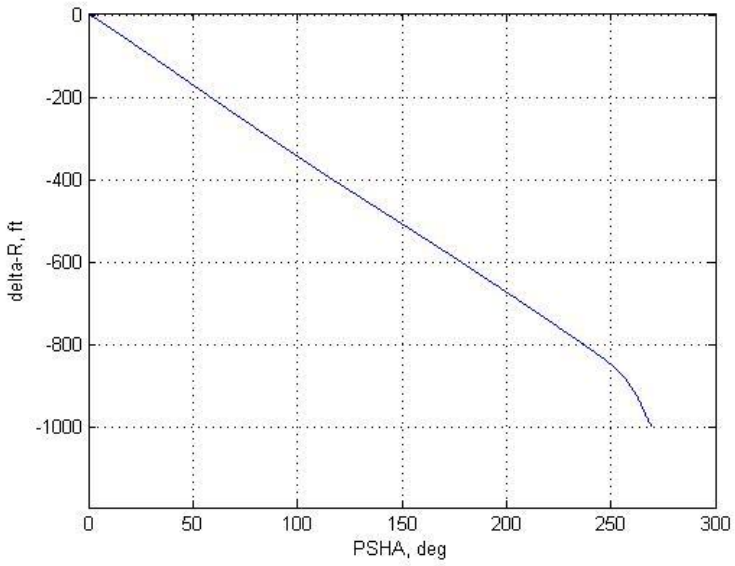

Fig. 21. Radial position error for the vehicle when starting with 1000 ft of error.

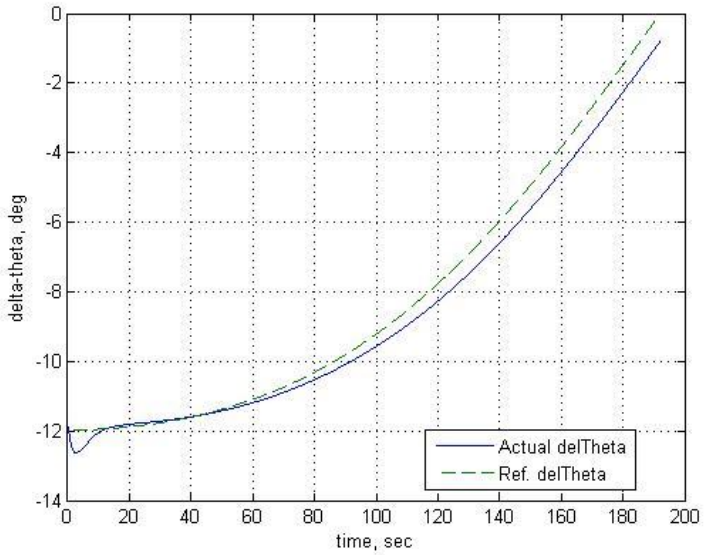

Fig. 22. Heading angle error with respect to the nominal when starting with 1000 ft of error.

After radial position error was introduced to the vehicle the initial heading angle of the vehicle was modified in order to make the vehicle initially fly in with the wrong heading angle. Twenty deg of heading angle error was introduced to the system. The initial radial position error was set back to zero. Figures 23-25 illustrate the groundtrack for the vehicle, the radial position error, and the heading angle error, respectively. The radial position error for the vehicle at the end of the HAC is only 1.10 ft.

In order to further test the robustness of the control design, radial position error and heading angle error were introduced to the system at the same time. One thousand feet of radial error along with 20 deg of heading angle error produced a vehicle trajectory, which can be analyzed by viewing Figs. 26-28. Figure 27 shows the radial position error for the vehicle, which is only 1.45 ft at the end of the HAC turn.

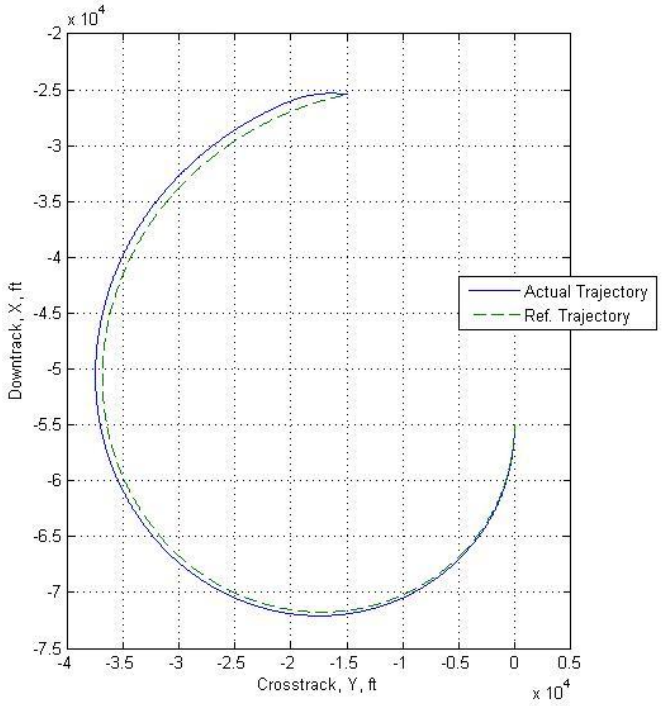

Fig. 23. Groundtrack for the vehicle with an initial heading angle error of 20 deg.

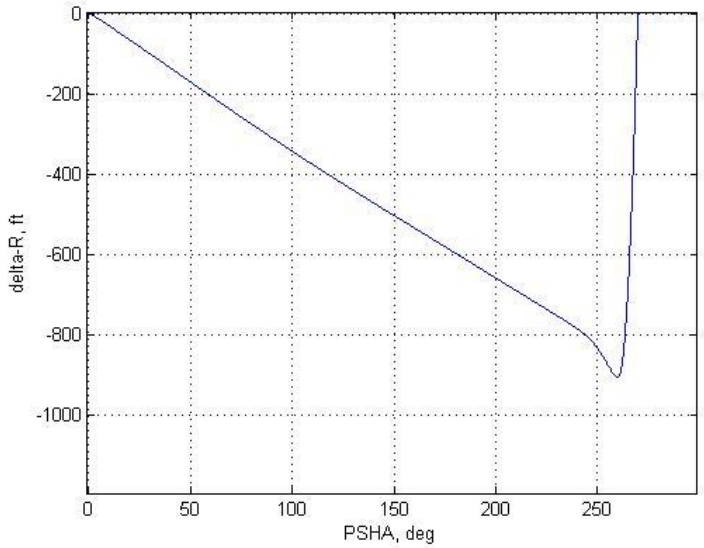

Fig. 24. Radial position error for the vehicle when starting with a 20 deg heading angle error.

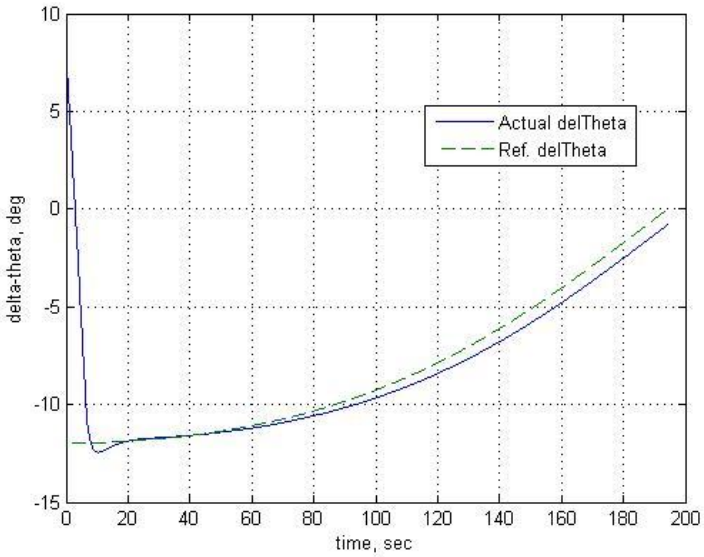

Fig. 25. Heading angle error with respect to the nominal when starting with 20 deg of heading angle error.

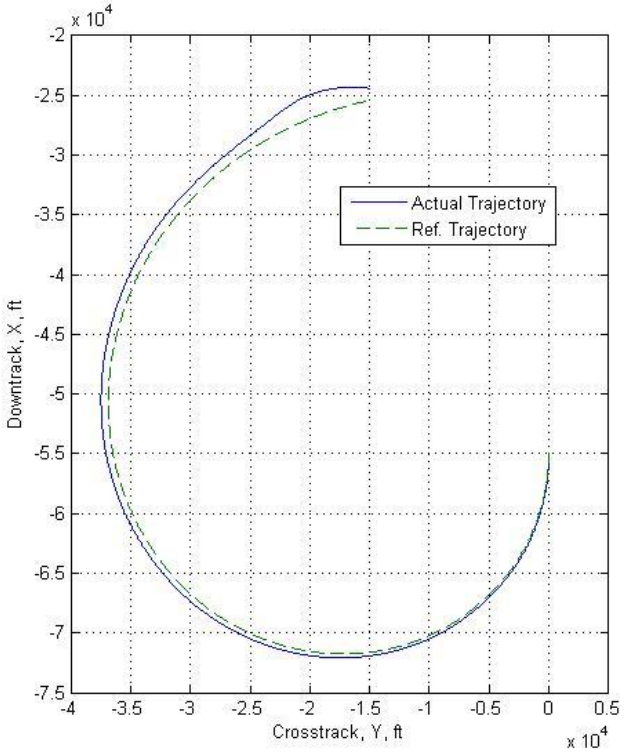

Fig. 26. Groundtrack profile for the vehicle when initialized with 1000 ft of position error and 20 deg of heading angle error.

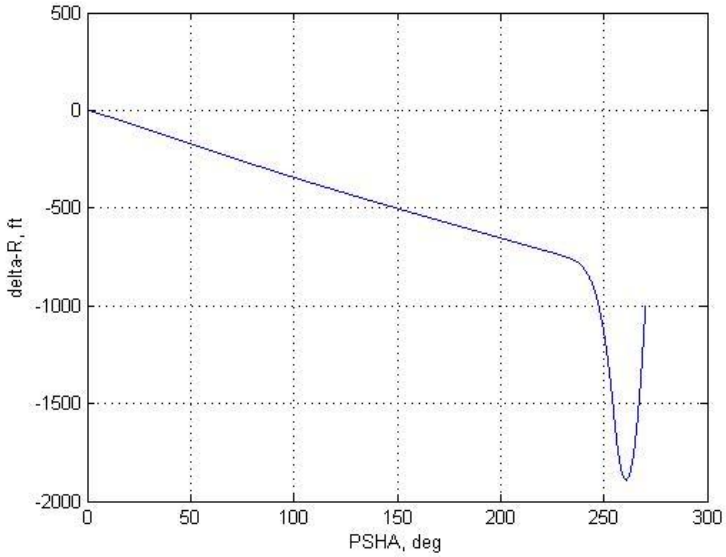

Fig. 27. Radial position error for the vehicle when initialized with 1000 ft of position error and 20 deg of heading angle error.

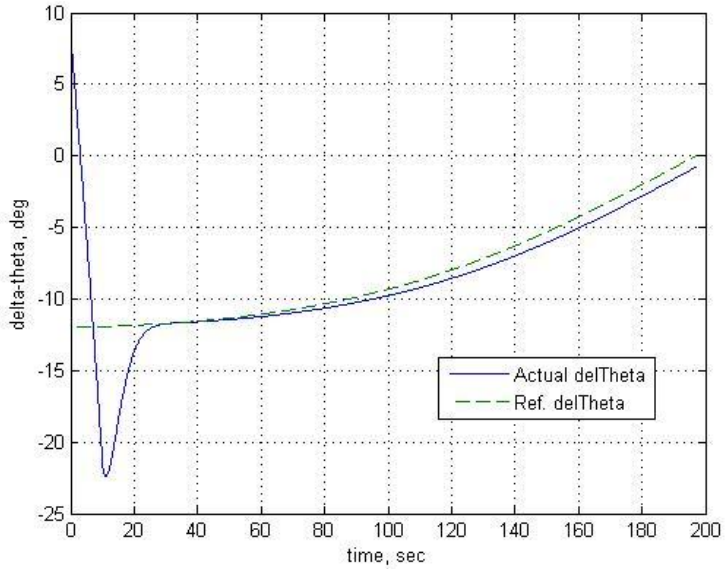

Fig. 28. Heading angle error with respect to the nominal for the vehicle when initialized with 1000 ft of position error and 20 deg of heading angle error.

The test cases illustrated by Figs. 20-28 highlight the ability of the control design law to negate any error introduced to the system. At this point, it was determined that the control design law was ready to be applied to the full TAEM simulation. While the

results will not be an exact replication of the results produced by the simplified HAC simulation, they will be close enough to still provide an optimal solution to the trajectory problem.

4.2 Full TAEM Simulation

The pole-placement parameters and bank angle bias value provided an accurate and well-damped response for the vehicle as it traveled around the simplified simulation of the HAC turn. Because of the success of these parameters they will be applied directly to the full TAEM simulation.

4.2.1 Environment

The full TAEM simulation makes use of a series of interconnected programs. The first program that is called has the responsibility of setting the initial conditions for the TAEM phase of flight. For this simulation, the vehicle is defined to be the HLV vehicle. Defining characteristics for the HLV vehicle may be found in Table 4. Also, runway characteristics such as altitude and direction are defined. The vehicle velocity is initially set at 2,000 ft/s and the altitude is set at 80,000 ft. The initial position and heading angle of the vehicle are initially set at a location locally south-east of the runway and pointing at 266 deg, measured clockwise from the local north direction. These values of position and heading angle will be modified in order to test a wide variety of cases. The HAC location and size is defined initially; however, the HAC will vary in size and location

depending on the energy of the vehicle. The nominal bank angle for the vehicle as it travels around the HAC is set to 30 deg. The limits on the vehicle regarding bank angle are set at plus or minus 60 deg. Finally, the gains for all phases of flight are initialized. The initial gains for the HAC turn portion of TAEM are calculated using estimates for velocity and flight path angle and inserting these values into Eqs. (52) and (53). The initial estimation of the HAC gains is a valid estimation because after the first iteration the velocity and flight path angle will be measured. The new measured velocity and flight path angle values are used to calculate the second set of HAC gains. The gains are updated continuously in this manner.

Along with the initial conditions for the simulation being set, the final conditions otherwise known as the conditions at ALI are defined. The vehicle conditions at touchdown at the runway are known. By propagating the results backwards from touchdown to ALI, it is possible to define the vehicle conditions at ALI. This propagation is able to be performed because during the ALI phase of flight the dynamic pressure of the vehicle is kept at a relatively steady value. Since the altitude at ALI is known then the velocity of the vehicle at ALI can be solved for. At this point, enough information is known that it is possible to calculate the energy of the vehicle at ALI. Knowing all of this information about the vehicle at ALI creates a target point in which to aim for at the beginning of the TAEM phase.

Once all of the information about the vehicle is known it is possible to begin calculating information concerning the trajectory of the vehicle. Using geometry, a program is able to determine the angle from the vehicle to the center of the HAC and to the closest tangent point of the HAC. Also, while the vehicle is still in the initial stages of

TAEM, PSHA is calculated. Each of these angle measurements is updated continuously throughout TAEM.

After the angle calculations are performed the three-dimensional high-fidelity simulation is completed. This simulation is responsible for determining the values for all of the states of the vehicle over the course of the TAEM trajectory. The states of the vehicle are set as altitude, velocity, flight path angle, heading angle, x-position, y-position, and energy-to-weight ratio. Another variable that is tracked is the groundtrack distance covered by the vehicle. Two separate programs are responsible for determining the lateral and longitudinal control of the vehicle. The lateral trajectory of the vehicle is controlled by the bank angle of the vehicle. This lateral control program is where the new bank angle gain values are calculated. This is also where the new bank angle bias is applied to the simulation. The longitudinal control program uses a quasi-equilibrium glide solver in order to determine the optimal path of the vehicle. This quasi-equilibrium glide solver is a program that solves for the steady-state of the vehicle assuming a constant dynamic pressure and a constant flight path angle. The most significant output of the longitudinal control program is the angle of attack at which the vehicle should be flying. Angle of attack is the control variable that is tracked.

Once the trajectory of the vehicle is calculated and the many states of the vehicle are known it is possible to start analyzing and optimizing the trajectory. One program in particular is accountable for varying the size and shape of the HAC depending on the energy and states of the vehicle. This program, which determines and plans groundtrack, will be discussed further in Chapters 5 and 6. Once the optimal HAC location and size are determined the bank angle of the vehicle is modified using the lateral control program

in order to accurately track the optimal HAC turn. The ideal result of these many programs working together is an optimal trajectory for the vehicle during the TAEM phase.

4.2.2 Trials

For the trial cases presented in this section it should be noted that only lateral guidance about the HAC turn was being evaluated. The groundtrack planner and controller presented in Chapters 5 and 6 will be responsible for optimizing the entire TAEM trajectory. A constant bank angle value initialized at 30 deg was applied to the simulation. The HAC location and size are free to vary as long as the turn that is completed is performed while trying to track the open-loop bank angle. The open-loop bank angle is calculated using the velocity of the vehicle and size of the HAC, as shown by Eq. (21). The radial position error and the radial rate error of the vehicle will cause the vehicle to either add or subtract bank based on the closed-loop response of the system. This closed-loop response, along with the bank angle bias value, will help negate any error in the states of the vehicle and track the open-loop bank value.

For all trials the location of the runway is at the origin, specifically X_{RW} = 0 and Y_{RW} = 0. For the first trial, the x-location of the vehicle is approximately 32,000 ft downrange of the runway. The y-location of the vehicle is 319,500 ft to the right of the runway, if viewed from a top-down perspective. Generally, the vehicle is located south-east of the runway. The initial heading angle of the vehicle is 266.8 deg, measured clockwise from the local north direction. The initial location of the center of the HAC is

approximately 58,000 ft downrange of the runway and 6,000 ft to the left of the runway. The final radius of the HAC, R_F, is initially set to 6,000 ft. The R_2 value for the HAC is initially 0.1 ft/deg^2.

Using the initial conditions for the first trial the groundtrack planner, which will be discussed later, modified the HAC to have a radius of 11,700 ft at a location approximately 99,000 ft downrange of the runway. The HAC is also located 11,700 ft left of the centerline of the runway. The spiral shape of the HAC is dictated by the R_2 value, which was modified to 0.0909 ft/deg^2. The groundtrack for the vehicle, as seen from above, is presented as Fig. 29. Figure 29 illustrates the initial position of the vehicle, HAC location, and HAC size as well as shows the ideal tracking of the vehicle to the nominal HAC profile.

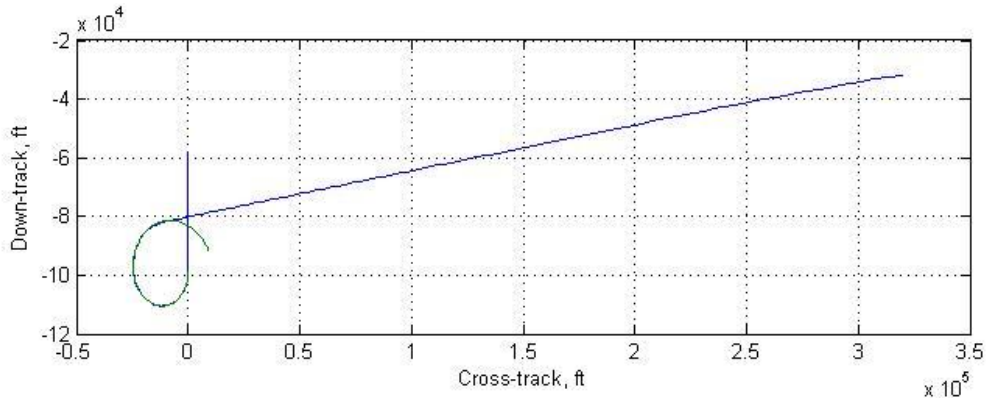

Fig. 29. View of the vehicle groundtrack from above. Illustration of the initial position of the vehicle, HAC location, and HAC size.

It can be seen, after zooming in on Fig. 29, that the vehicle position error at the end of the HAC turn is approximately 7 ft. There is a minimal amount of crosstrack rate error. However, there is enough crosstrack rate error to cause the vehicle to slightly overshoot the runway centerline during the prefinal subphase. The vehicle overshoots the runway centerline by approximately 40 ft; however, the vehicle correctly completes a

banking maneuver in order to return to the centerline quickly. The dynamic gains employed during the prefinal phase are responsible for this quick return to the runway centerline. Figure 30 shows a zoomed in view of the end of the HAC turn and Fig. 31 illustrates the slight overshoot during the prefinal subphase. Figure 30 and 31 were obtained from Fig. 29.

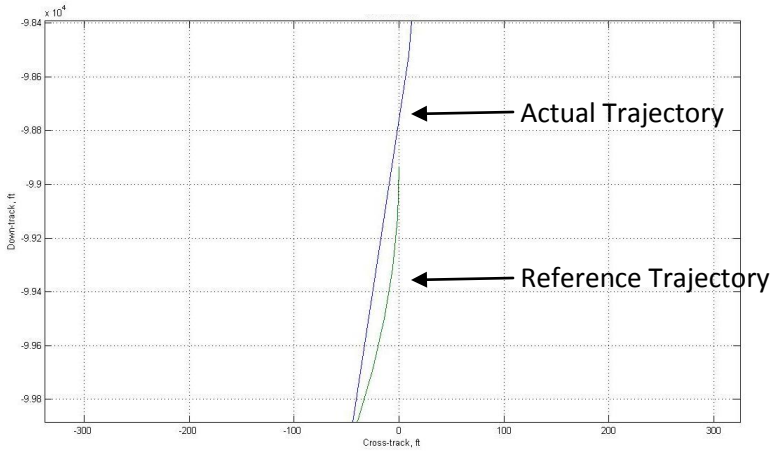

Fig. 30. Zoomed-in view of Fig. 29. Illustrates the slight positional error of the vehicle at the end of the HAC turn.

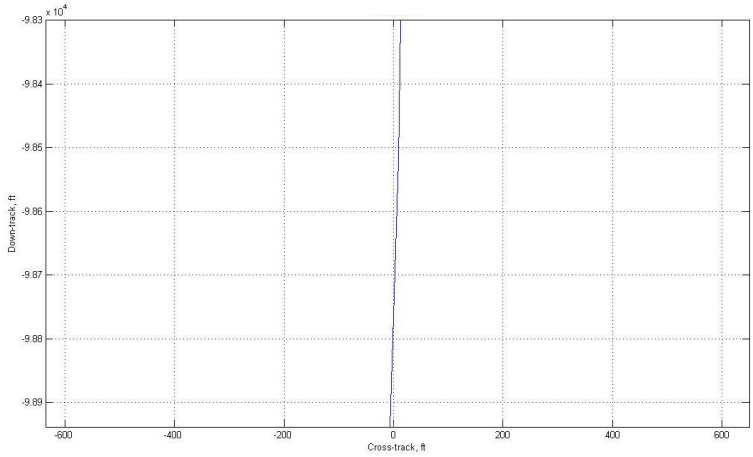

Fig. 31. Zoomed-in view of Fig. 29. Illustrates the slight overshoot of the vehicle during the prefinal phase. Ideally, the vehicle should track the runway centerline, denoted in this figure by the zero value on the crosstrack axis.

The overshoot that occurs during the prefinal subphase is damped out quickly by the control-design that is employed by the lateral controller. The accuracy of the simulation is exhibited by the final crosstrack position of the vehicle. The vehicle transitions to ALI with a crosstrack position of 0.0129 ft. The crosstrack position error of the vehicle, after nearly 80 miles of flight within the TAEM envelope, is a miniscule 0.01 ft.

Many other trials were completed in order to ensure the robustness of the simulation. The initial position of the vehicle was varied significantly as well as the heading angle of the vehicle. Four of these trials may be viewed within Fig. 32. Figure 32 illustrates four initial positions of the vehicle, all at a radically different location. Each initial position, denoted on Fig. 32 by their respective number, requires the vehicle to complete a unique HAC turn, which will help to show the versatility of the simulation. It should be noted that the actual HAC turn as well as the nominal HAC turn was shown within Fig. 32.

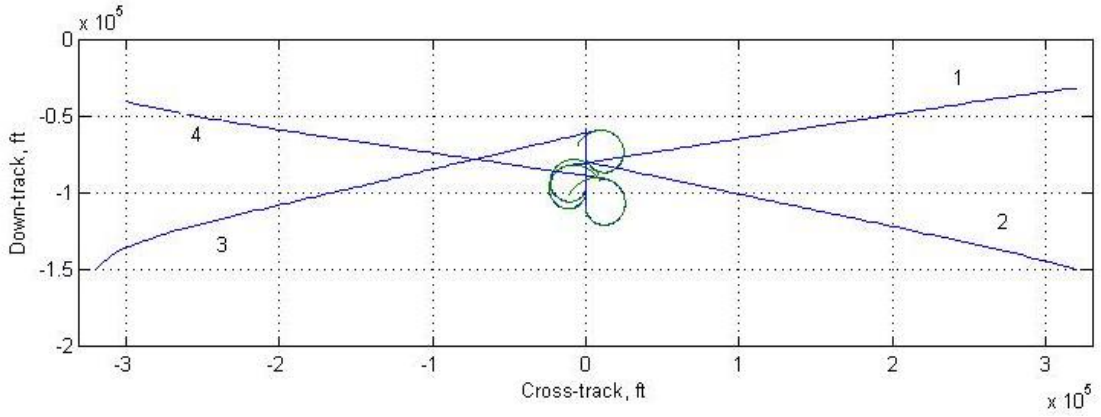

Fig. 32. Illustration of four unique vehicle trajectories. The tracking for each trial is extremely accurate.

The numerical results from the four trials are shown in Table 4. As can be seen in Table 4, the final crosstrack error for the vehicle is extremely small. The vehicle position error at the end of the HAC is also small, suggesting good tracking of the nominal HAC

turn. The overshoot of the runway centerline during the prefinal subphase is at an acceptable level for all of the trials.

Table 4. Numerical lateral trajectory results from the four radical position trials as labeled on Fig. 30.

Trial Number	X_o (ft)	Y_o (ft)	ψ_o (deg)	PSHA (deg)	Y-error at end of HAC (ft)	Max y-overshoot (ft)	Final y-error (ft)
1	-32,000	320,000	266	261	7	40	0.0129
2	-150,000	320,000	290	281	6	50	0.0209
3	-150,000	-320,000	40	285	4	60	0.6246
4	-40,000	-300,000	110	261	7	25	0.0001

After observing Table 4, it can be seen that the HAC turn that was completed for each trial was similar in the sense that each trial required a HAC turn between 260 and 285 deg. In order to further diversify the trials that were tested, two additional trials were completed. These two additional trials had initial positions near the centerline of the runway and were helpful in determining how the system would react when the required HAC turn possessed a PSHA value of nearly 180 and 360 deg. Figure 33 shows the initial positions for the two trials, labeled with the appropriate trial number, as well as the trajectory for the subphases that make up TAEM. It should be noted that the nominal HAC turns were shown for each trial along with each trajectory. The nominal HAC turn is the HAC turn that was tracked throughout the actual turn.

Table 5 presents the critical lateral numerical data for trial 5 and 6. It can be seen from Table 5 that the goal of requiring the vehicle to complete HAC turns with PSHA values of approximately 180 and 360 deg was successfully accomplished. Even with PSHA values near the limits of the simulation, the vehicle was able to fly a very accurate trajectory. It should be noted that when the PSHA value is less than 180 deg or more than

360 deg, there is logic within the simulation that places the HAC on the other side of the runway centerline. When the HAC is placed on the other side of the runway centerline the goal of obtaining data near the PSHA limits is not accomplished. Because of this simulation limitation, the PSHA values were not able to be extremely close to the 180 and 360 deg limits.

The final crosstrack error for the vehicle during trials 5 and 6 was miniscule. The vehicle position error at the end of the HAC turn was also very small for each trial. The error level during the prefinal subphase is acceptable for each trial. The overshoot error during the prefinal subphase was successfully damped out well before the transfer to ALI.

Table 5. Numerical lateral trajectory data from trials 5 and 6, as labeled on Fig. 31.

Trial Number	X_o (ft)	Y_o (ft)	ψ_o (deg)	PSHA (deg)	Y-error at end of HAC (ft)	Max y-overshoot (ft)	Final y-error (ft)
5	-400,000	-50,000	3	352	6	55	0.0181
6	200,000	10,000	170	187	12	65	0.0005

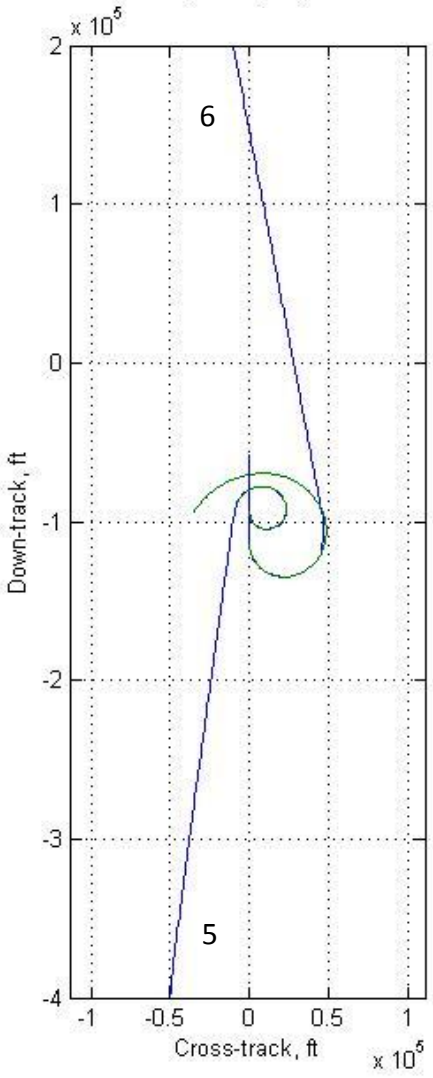

Fig. 33. Illustration of two unique vehicle trajectories. These trials require the vehicle to complete HAC turns of approximately 180 and 360 deg.

CHAPTER 5

GROUNDTRACK PREDICTION

The groundtrack prediction component may be the most important of the many programs that make up the TAEM simulation. Quite simply, the groundtrack predictor is responsible for determining if it is possible for the vehicle to safely reach the runway from its current position and state. The groundtrack predictor finds and iterates on initial estimates for the physical components of the reference trajectory, namely the HAC size, location, and orientation such that a plausible trajectory for the vehicle can be determined.

5.1 Initial Trajectory Determination

When the vehicle first reaches the point during reentry when it is considered to be flying within the TAEM phase, an initial program is run in order to calculate the

maximum possible range for the vehicle. This maximum range is determined only after a few conditions are placed on the vehicle. The initial simulation begins with the vehicle flying with wings-level, meaning that no banking maneuvers will be performed. No matter what heading angle the vehicle enters TAEM at, this heading angle will remain constant throughout the initial simulation. Also, the vehicle will fly at the angle of attack which will maximize the lift-to-drag ratio. By following these procedures, the simulation will be able to analytically determine the maximum possible range for the vehicle. It should be pointed out that the maximum range is found using only numbers and formulas. The maximum range trajectory is not actually flown.

After the maximum range for the vehicle is determined analytically, the actual range to be flown to ALI is computed. The TAEM phase is split into the familiar four subphases for this range calculation. Figure 34 illustrates the four subphases, color-coded appropriately. Figure 34 also shows details of the trajectory such as the final radius, the instantaneous spiral radius, and the corresponding PSHA value. It should be remembered that the instantaneous radius is calculated using the final radius and the PSHA-to-go values, Eq. (65).

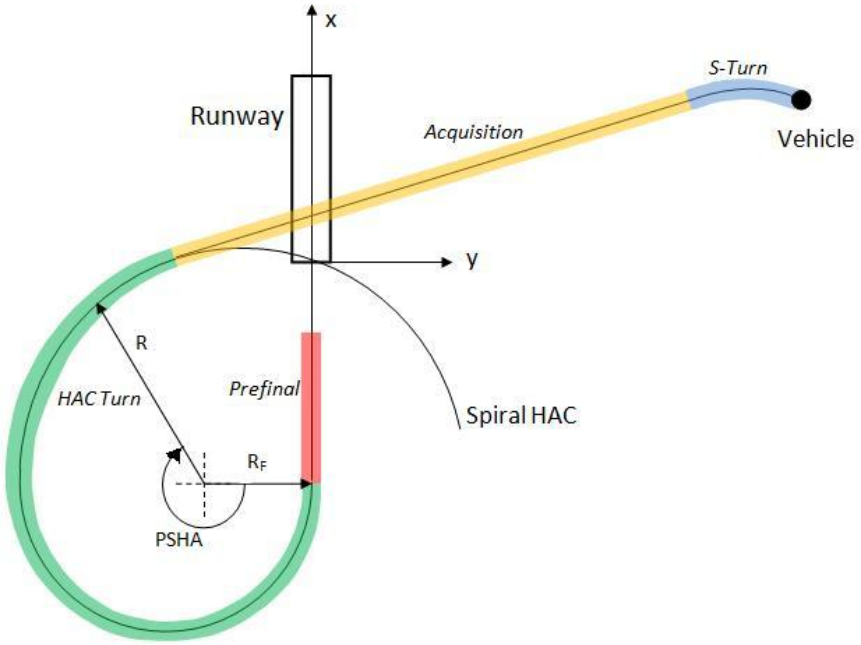

Fig. 34. Overhead illustration of TAEM. The four subphases are color-coded appropriately.

The actual range is determined using complicated geometry inherited from Moore [3]. Using the Shuttle's geometric groundtrack method along with a new range "scaling" method, a new groundtrack planner was able to be developed. This scaling method will be applied to each of the actual S-turn and HAC turn ranges, which will, on paper, lengthen the range for each of these subphases. It should be noted that the range for each of the subphases is not actually being lengthened yet, but is just being interpreted in a different frame of reference. The new frame of reference is named the wings-level equivalent reference and the new range is named the wings-level equivalent (WLE) range. As an example, if the WLE range for the HAC turn were to be multiplied by the new scaling factor, the result would be the actual calculated range of the HAC turn for the vehicle. The same principle is applied to the S-turn subphase. The acquisition and prefinal phases do not need to be scaled as these subphases are already being flown with

the same characteristics of flight, wings-level flight at the maximum lift-to-drag ratio, as the initially calculated maximum possible range trial. Figure 35 illustrates this scaling concept. In order to best compare the range values for each of the subphases, the trajectory was straightened out. The same colors that were used in Fig. 34 are used in Fig. 35. As can be seen in Fig. 35, the acquisition and prefinal subphases have the same length because neither of these subphases need to be scaled. The S-turn and HAC turn subphases have different lengths when looking at the actual and WLE ranges. For this visual example, the actual range is about 85% of the length of the WLE range. This is assuming a bank angle of approximately 30 deg.

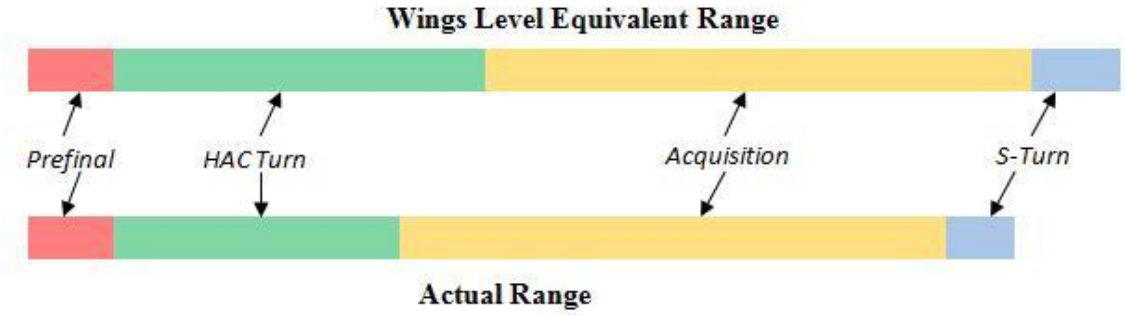

Fig. 35. Simple comparison of the actual range versus the wings-level equivalent range for each of the four subphases of flight.

With the maximum possible range and the WLE range of the vehicle known, it is possible to present the goal of this simulation modification. The main goal is to accurately match the maximum possible range with the WLE range for the vehicle. Matching the two ranges is done by modifying the WLE range by either moving the HAC or changing the size of the HAC.

Matching the two ranges requires the calculation of the final HAC radius, the quadratic coefficient of the HAC radius, and the HAC location in the x-direction.

Ultimately, these parameters are dependent upon the HAC turn bank angle that is calculated. After the ranges are matched successfully within the groundtrack planner, the parameters used to complete the range matching are used as initial estimates within the high-fidelity simulation environment. Good estimates obtained from the groundtrack planner will result in a high-fidelity simulation solution that will converge quickly to the planned trajectory. Within the high-fidelity simulation environment the quick execution of trajectory programs is essential to an accurate, and ultimately safe, TAEM phase.

In summary, when the vehicle enters TAEM the maximum possible range for the vehicle is calculated via numerical integration of the equations of motion. The maximum possible range is calculated using the current vehicle states and assuming the vehicle will be flying with wings-level and at maximum lift-to-drag ratio. After the maximum range is found, the actual range to ALI is found analytically using inherited equations. Then, within the groundtrack planner program, the actual range is modified by a simple scaling factor. The simple scaling factor translates the actual range to a WLE range. The WLE range is compared to the initially calculated maximum possible range. The groundtrack planner program is responsible for modifying either the HAC location or size in order to accurately match the WLE range to the initially calculated maximum range. When these two ranges are accurately matched, the corresponding HAC location and size estimates produced by the groundtrack predictor are given to the high-fidelity simulation. The high-fidelity simulation uses the estimates for HAC location and size when numerically determining the best possible trajectory to ALI.

5.2 Simplified Scaling Strategy

The acquisition phase and the prefinal subphase of TAEM are both very straightforward to deal with. Both of these subphases are executed with an ideal bank value of zero. Also, during these subphases the vehicle is flying at the maximum lift-to-drag ratio. Both of these characteristics were exhibited in the initial simulated flight where the maximum range for the vehicle was calculated. Because of this, the ranges associated with these subphases may be directly subtracted from the overall maximum range of the vehicle. The remaining portion of the maximum range is to be applied to the S-turn and the HAC turn. However, since banking maneuvers are required to complete the S-turn and HAC turn, the range for these subphases cannot be directly subtracted from the maximum vehicle range. A scaling factor must be applied to the nominal distance required to complete the turns in order to express the nominal turn range in terms of the WLE range for the vehicle. Multiplying the actual range by the scaling factor will result in the WLE range, which can be directly compared to the maximum possible range.

The first step in determining a scaling factor for the range of the vehicle was to start with the most general equation of motion relating to the range of the vehicle. The rate of change for the groundtrack, $\dot{S}$, was determined to simply be the horizontal velocity component of the vehicle.

$$\dot{S} = V \cos\gamma \tag{73}$$

Equation (73) was integrated with respect to time before the derivative with respect to energy was found. The equation for the "energy height" of the vehicle is shown as Eq. (74).

$$E = \frac{V^2}{2g} + h \tag{74}$$

After taking the derivative of Eq. (74) with respect to time and combining the result with Eq. (73), the simplified result is shown as

$$\frac{dS}{dE} = \frac{V\cos\gamma}{-DV/mg} \tag{75a}$$

It should be noted that Eq. (75b) is merely the simplified version of Eq. (75a), with the addition of the lift-to-drag ratio term, which will be helpful at a later point in the derivation.

$$\frac{dS}{dE} = -\frac{mg\cos\gamma}{L}\left(\frac{L}{D}\right) \tag{75b}$$

The right hand side of Eq. (75b) is familiar in the sense that if the flight-path angle is assumed to be constant, Eq. (2) can be used to simplify the $L\cos\phi = mg\cos\gamma$ portion of the equation. After the simplification,

$$\frac{dS}{dE} = -\left(\frac{L}{D}\right)\cos\phi \tag{75c}$$

the result is still a function of energy because of the lift-to-drag ratio. Equation (75c) is then integrated with respect to energy in order to find the range for the vehicle.

$$S = -\int_{E_o}^{E_f}\left(\frac{L}{D}\right)\cos\phi \; dE \tag{76}$$

This integration step is illustrated by Eq. (76), which is the governing equation for this simplification.

When applied to the initial case where the vehicle does not bank in order to find the maximum possible range, the bank angle in Eq. (76) is set to zero and the result, with the switch in the integral limits, is

$$S_{WLE} = \int_{E_f}^{E_o} \left(\frac{L}{D}\right) dE \tag{77}$$

On the other end of the spectrum, when the vehicle is allowed to bank in order to complete the necessary S-turn and HAC turn, the result is

$$S_{ACTUAL} = \cos\phi \int_{E_f}^{E_o} \left(\frac{L}{D}\right) dE \tag{78}$$

The cosine of the bank angle is able to be moved out in front of the integration sign because that term is assumed to be a constant value. The subscripts *WLE* and *ACTUAL* represent the wings-level equivalent range and the actual calculated range, respectively.

After examining Eqs. (77) and (78), it can be seen that S_{ACTUAL} is a function of S_{WLE}. This relation is explicitly shown using

$$S_{WLE} = \frac{S_{ACTUAL}}{\cos\phi} \tag{79}$$

The result of this derivation of a simple method to relate WLE range to actual range for a banked turn has proved to be extremely valuable for constructing a simple groundtrack planner. Equation (79) is proved further after observing Fig. 35. It is clearly seen within Fig. 35 that the WLE range is approximately 15% greater than the actual range for the S-turn and HAC turn portions of flight. This is because $\frac{1}{\cos\phi}$ is approximately equal to 1.15 when the bank angle is 30 deg.

5.3 Strategy 1: Moving the Location of the HAC

There are two possible strategies that may be employed in order to accomplish the overall goal of matching the maximum possible range to the WLE range for the vehicle. The first strategy includes physically moving the location of the HAC in the x-direction. For example, if the WLE range is greater than the maximum possible range for the vehicle, then the HAC will be moved closer to the runway. Conversely, if the WLE range is less than the maximum possible range, then the HAC will be moved away from the runway. This will create a longer WLE range-to-go for the vehicle and will help the vehicle to match its maximum possible range. In both examples, the size of the HAC will remain approximately constant. Since the size of the HAC will not change significantly, the bank angle that the vehicle is required to fly at will remain at approximately 30 deg. It should be noted that the location of the HAC in the y-direction will always be equivalent to the final radius of the HAC, R_F. This allows the vehicle to finish the HAC turn and be aligned with the centerline of the runway.

A very simple method for modifying the location of the HAC in the x-direction was employed. The variable responsible for making sure the two range values accurately match is the range error value. This value is calculated using

$$S_{ERROR} = S_{MAX} - S_{WLE} \tag{80}$$

and is equal to the difference between the maximum possible range, S_{MAX}, and the WLE range, S_{WLE}.

If the error between the two ranges is positive it is required that the HAC is moved away from the runway. This will lengthen the WLE range until it matches within 100 ft of the maximum possible range. In order to accomplish this, the range error value was multiplied by 95 percent and added to the initial HAC location value. The new value represented the new HAC location in the x-direction. This process may be viewed as

$$X_{HAC_n} = X_{HAC_{n-1}} + 0.95S_{ERROR} \tag{81}$$

If the error was a positive value then the HAC would be moved away from the runway, as desired. If the error value was a negative value then the HAC would be moved towards the runway. This process was repeated until the absolute value of the error fell below the user imposed 100 ft threshold.

5.4 Strategy 2: Changing the Size of the HAC

The second strategy that may be employed to match the two range-to-go values includes changing the size of the HAC. For example, if the WLE range is greater than the maximum possible range for the vehicle, the HAC radius will be decreased. This modification will result in a shorter actual range as well as a shorter WLE range for the vehicle. A smaller HAC radius is completed because the driving variable behind HAC radius is bank angle. The bank angle of the vehicle is increased in order to create a tighter HAC turn. Conversely, if the WLE range is less than the maximum possible range for the vehicle, the HAC size is increased. The vehicle accomplishes this larger turn by employing a lesser bank angle. This larger HAC turn accomplishes the need for a longer

WLE range. For both of these cases, the HAC location in the x-direction is a constant. The HAC location in the y-direction will vary with the final radius of the HAC.

5.4.1 Secant Method

The process of finding the optimal solution, which will match the WLE range with the maximum possible range, is essentially a root-finding problem. The independent variable in this root finding problem is the bank angle of the vehicle. The dependent variable is the variable that is driven to zero, which in this case is the error between the two range values. Specifically, the error is defined by Eq. (80).

It was determined that the secant method would be used in order to find the optimal bank angle value. The secant method requires two initial values for the independent variable before an approximation to the solution can be made. After two initial values are found, an iteration process is completed in order to drive the error between the two range values to a value less than plus or minus 100 ft. This 100 ft error envelope will provide the vehicle with an extremely well-planned trajectory. In the sense of this model, 100 ft is a small value. This process is simply illustrated by Fig. 36. Within Fig. 36, the curved line represents the function, which relates the independent variable, the bank angle, to the dependent variable, the range error. The first and second range error values are obtained by evaluating x_1 and x_2, as seen in Fig. 36. The values of $f(x_1)$ and $f(x_2)$ are connected by a straight line and, at the point where that line crosses the x-axis, the function is evaluated to find the range error value corresponding to x_3. The values $f(x_2)$ and $f(x_3)$ are then connected by a straight line and the process is repeated.

This process is carried out until the range error value falls below the 100 ft, user-defined, threshold.

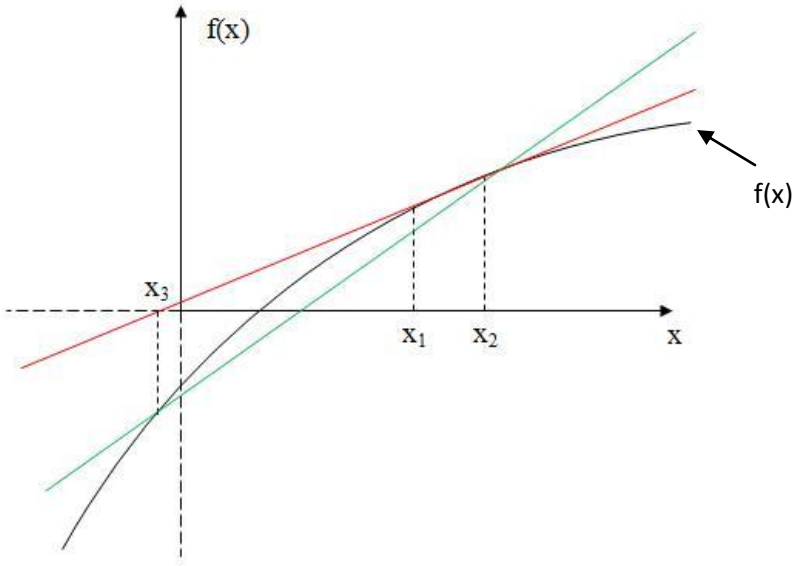

Fig. 36. Simplified illustration of the secant method.

The first initial value for bank angle is the nominal value of 30 deg. If, the first time through the iteration process the error between the two ranges is a positive value, 5 deg is subtracted from the nominal value of 30 deg. In this case, the maximum possible range is greater than the WLE range; therefore, the WLE range needs to be made longer, which is accomplished with a larger HAC turn. A larger HAC turn requires a shallower bank angle from the vehicle. Conversely, if the resulting error value would have been negative, then 5 deg would have been added to the initial value of 30 deg and the first two bank angle values would have been 30 and 35 deg. In order to maintain consistency, this example will be carried out assuming a positive error value.

After this first iteration two bank angle values are present, 30 and 25 deg. From these two points, and their corresponding error values, the secant method can be applied.

The next time through the iteration process a new error value is obtained and, whether that error value is positive or negative, the secant method will automatically determine if the bank angle needs to be increased or decreased. There is no need to insert logic that corresponds to one solution if the error is positive and another solution if the error is negative. The secant method equation is illustrated by

$$x_{n+1} = x_n - f(x_n)\frac{x_n - x_{n-1}}{f(x_n) - f(x_{n-1})} \tag{82}$$

where the subscript *n* represents the index value of the looping iteration structure.

After a new bank angle value is obtained the iteration process is repeated in order to find an even more accurate value for bank angle. This process is repeated until the absolute value of the error between the two range values falls below the 100 foot threshold. Each time the process is repeated the numerical groundtrack planner program is called. This is the previously mentioned program that uses complicated geometry to calculate the actual range for the vehicle as it is completing the banked turns within TAEM. Since bank angle is the driving force behind these complicated calculations, the newest bank angle value obtained from the secant method is passed to this program in order to determine the newest error between the two ranges.

5.4.2 Modifying the HAC Location

While changing the size of the HAC may be the best solution to the groundtrack predictor problem, there is one slight issue with the strategy. If, for example, the vehicle enters TAEM at a point that is relatively near the runway, the vehicle will have to complete a large sweeping HAC turn in order to safely reach the runway. In order to

complete this HAC turn, the vehicle will more than likely have to complete a large S-turn in order to align itself with a tangent point of the HAC. When the initial S-turn is significant the accuracy of the simulation has the potential to be negatively affected. This issue is illustrated by Fig. 36. Shown with a simplified cylinder representing the HAC, the vehicle is required to complete a significant S-turn at the beginning of TAEM.

The solution to this problem is to move the location of the HAC in the x-direction. Unlike the strategy described by section 5.3, the HAC location will not be continuously moving in search of a solution that converges. This strategy will utilize a linear approximation that is a function of the straight-line distance from the vehicle starting point and ALI. The dependent variable is the offset distance, measured from ALI.

$$D_{offset} = -\frac{1}{6}D_{SL} + 73{,}333.3\overline{3} \tag{83}$$

Equation (83) illustrates this linear approximation where D_{offset} represents the offset distance, in ft, and D_{SL} represents the straight-line distance, in ft, from the vehicle to ALI.

For example, if it is found that the measured distance from the vehicle's initial position to ALI is 260,000 ft, using Eq. (83), it is found that the HAC should be located 30,000 ft away from ALI in the negative x-direction. Keeping with this example, Fig. 37 illustrates a general case where moving the HAC away from the runway would be desirable. Moving the HAC away from ALI and the runway would significantly decrease the S-turn. Figure 38 exemplifies the case where the vehicle has the same starting position but the HAC is moved to a location further away from the runway. As can be seen, the S-turn required at the beginning of TAEM is much less significant than the S-turn shown in Fig. 37.

It should be noted that the initial vehicle position was the only variable that affected the location of the HAC. The location of the HAC did not vary based on the energy of the vehicle. The energy of the vehicle has the potential to only change the size of the HAC while in search of matching range values.

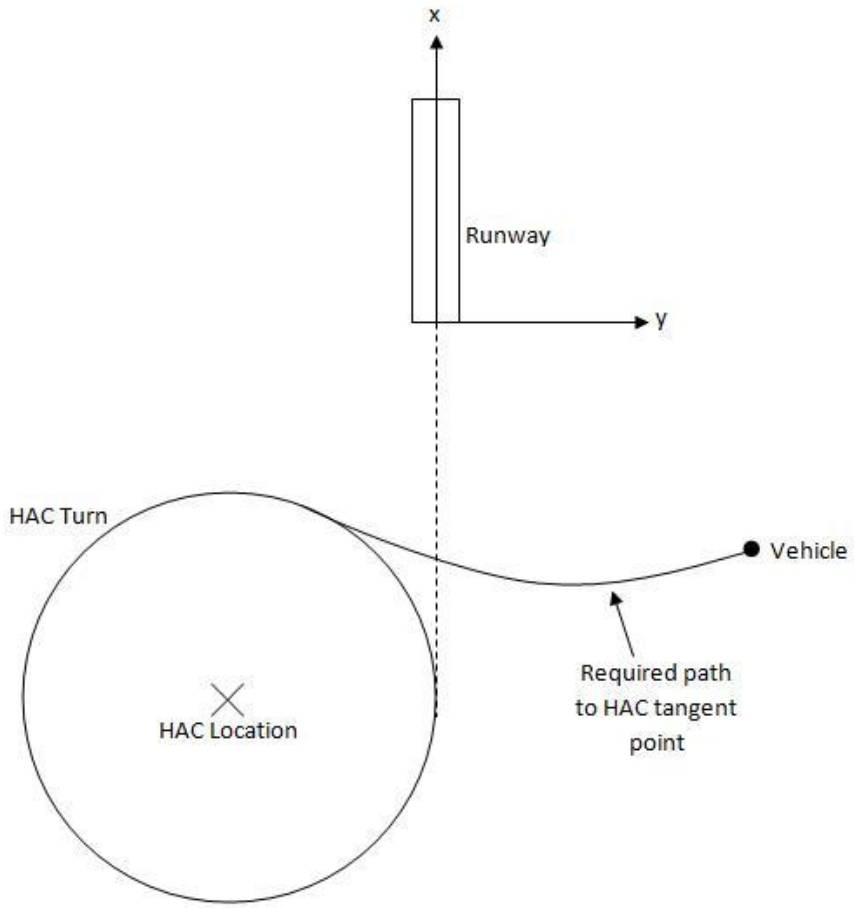

Fig. 37. Simplified illustration depicting the vehicle at a point too close to the runway centerline at the beginning of TAEM. Since the HAC location in the x-direction is too close to the runway the vehicle is required to complete a significant S-turn at the beginning of the trajectory. This is not desirable.

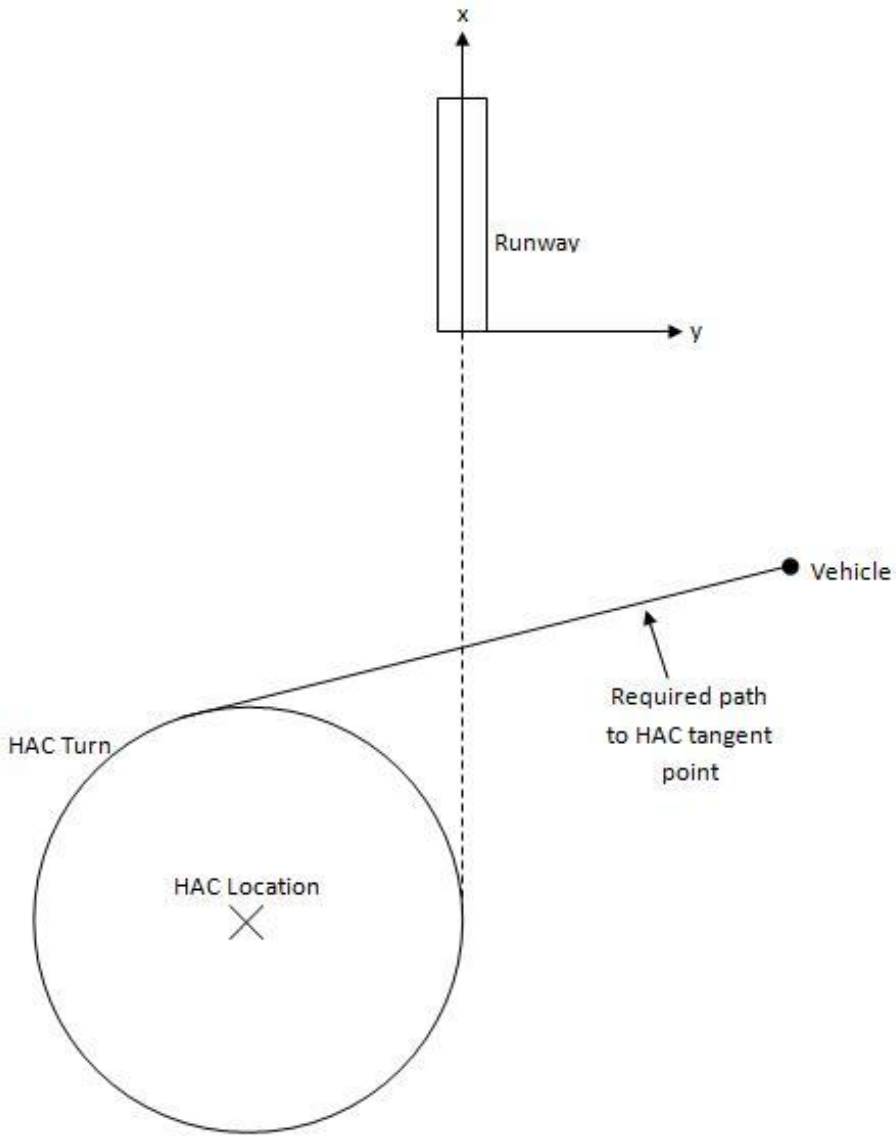

Fig. 38. Simplified illustration depicting the vehicle at the same initial point as it was in Fig. 37. The HAC location has been moved away from the runway in order to negate the need for an S-turn.

5.5 Using the Analytic Groundtrack Planner

After the groundtrack planner has obtained estimates for the variables that affect the size and location of the HAC, these estimates are used as the initial estimates within the on-line high-fidelity simulation. Since these estimates are extremely good, due to the

analytic groundtrack planner, a solution to the trajectory problem is converged upon very quickly. It cannot be overstated just how important a quick and accurate solution is to the overall success of the TAEM phase. Since the groundtrack planner is completed offline, it is not crucial that the program is completed extremely fast. The high-fidelity simulation, though, is being run on-line and in real-time as the vehicle is attempting to follow a prescribed path to the runway. The sooner a solution is found, the earlier the vehicle can track the correct prescribed trajectory, which will result in an accurate and safe transfer to ALI. It should be noted that the high-fidelity simulation was developed by Kluever et al [13]. The high-fidelity simulation uses a numerical integration method to determine a trajectory solution. The high-fidelity simulation is run however many iterations it takes to converge to an acceptable trajectory solution. The high-fidelity simulation has been proven and will not be viewed in detail within this text. For more information concerning the high-fidelity simulation refer to the cited text [13].

CHAPTER 6

GROUNDTRACK PREDICTION RESULTS

Using the strategies presented in Chapter 5, many trials were completed with the goal of determining which method, varying the HAC location or the HAC size, would produce the best results. The trials were divided into two different categories. The first set of trials was completed by using a variable initial vehicle position. Detailed results are shown for, what this paper will refer to as, the nominal case. Additionally, detailed results are shown for the cases where the vehicle initial position is -30% and +20% of the nominal case. Essentially, three locations in the general vicinity of each other were chosen in order to determine if the new logic within the simulation was robust enough to create a unique path to the runway that could be successfully tracked and followed.

The second set of trials was completed by was using a variable initial energy value for the vehicle. As a reminder, the energy of the vehicle is a function of altitude and velocity. Detailed results are shown for, what this paper will refer to as, the nominal

energy conditions. Detailed results are also shown for trials in which the vehicle possesses -20% and +15% of the nominal initial energy. All of trials were started from the same initial position. Essentially, the vehicle was placed at one position and the energy conditions of the vehicle were modified. The new logic within the simulation was then responsible for determining a path to the runway that could be followed by the vehicle.

For each of the two sets of trials the variable HAC size technique and the variable HAC location technique were employed. The results from these two techniques were compared to determine which one would be favorable over the other.

6.1 Initial Position Trials: Variable HAC Size Technique

6.1.1 Nominal Trial

The nominal case that defines the vehicle's initial position is a location that is locally south-east of the runway. As a point of reference, the runway threshold is placed at the origin of the x- and y-axes. The ALI is positioned on the centerline of the runway and placed 57,976.9 ft from the runway in the negative x-direction. The initial x-location of the vehicle is at –32,137.1 ft. The initial y-location of the vehicle is at 319,501.0 ft. The initial velocity of the vehicle is 2,000 ft per second at an initial altitude of 80,000 ft. The vehicle has an initial heading angle of 266.8 deg, measured clockwise from the positive x-axis. The initial flight path angle of the vehicle is -5 deg.

Using the initial position of the vehicle, the straight-line distance from the vehicle to ALI was measured. This value was determined to be 320,544.2 ft. Using Eq. (83), it is determined that the location of the HAC in the x-direction will be offset from ALI 19,909.3 ft.

The first program that this data was input to, the analytic groundtrack planner, was responsible for determining estimates for the HAC turn bank angle, the final radius of the HAC, and the quadratic coefficient of the HAC radius. The analytic groundtrack planner was completed offline. As a reminder, the bank angle was chosen using the secant method such that the absolute value of the error between the maximum possible range and the WLE range was less than 100 ft. The appropriate column within Table 6 summarizes the results obtained from the analytic groundtrack planner for this nominal case.

The estimates that were found by the analytic groundtrack planner were then input to the high-fidelity simulation, which was completed online and in real-time. The high-fidelity simulation was responsible for determining if the solution converged to the prescribed trajectory. Using the estimates for the components that make up the HAC size, the simulation allowed the solution to converge in one iteration. The results from the high-fidelity simulation for this nominal case are presented in the appropriate column within Table 7.

6.1.2 -30% Scaled Initial Position

After completing the nominal vehicle position trial the outermost bounds of the simulation were tested in order to find the most extreme, yet still plausible, initial position for the vehicle. Maintaining the same energy used during the nominal trial, the vehicle was moved 30% closer to the HAC in the x- and y-directions, with respect to the nominal. This was done by multiplying the initial nominal x-location value by 0.70. The same procedure was completed for the y-location value. The initial x-position of the vehicle is now -22,496.0 ft and the initial y-position of the vehicle is now 223,650.7 ft. This initial position translates to a straight-line distance to ALI of 226,447.7 ft. Using Eq. (83), it was found that the HAC should be placed 35,592.1 ft away from ALI in the negative x-direction.

Using this new initial position, the results from the analytic groundtrack planner may be viewed in the appropriate column of Table 6. The results from the analytic groundtrack planner were then input to the high-fidelity simulation and after two iterations the solution converged to the correct planned trajectory. The results from the high-fidelity simulation may be viewed in the appropriate column of Table 7.

6.1.3 +20% Scaled Initial Position

After testing the most extreme initial conditions characterized by the vehicle being very close to the HAC, the most extreme conditions exemplified by the vehicle being far away from the HAC were tested. The vehicle was moved to an initial position

that was 20% further from the HAC than the nominal case. The new x-location value was found by multiplying the nominal x-location value by 1.20. The y-location value was computed in a similar manner. The new x-position of the vehicle was -38,564.5 ft while the new y-position was 383,401.2 ft. These coordinates translated to a straight-line distance to ALI of 383,892.4 ft. Using Eq. (83), it was found that the HAC should be offset from ALI 9,351.3 ft in the negative x-direction.

Like the other trials, the results from the analytic groundtrack planner may be viewed in the appropriate column of Table 6. The results from the analytic groundtrack planner were input into the high-fidelity simulation and after two iterations the solution converged to the planned trajectory. The results from the high-fidelity simulation may be viewed in the appropriate column of Table 7. It was found that when the initial position of the vehicle was +20% greater than the nominal, the limits of the simulation were beginning to be reached. This is shown by the position of the HAC in the x-direction. As can be seen in Table 7, the HAC location is approximately 67,000 ft from the runway in the negative x-direction. The location of ALI is approximately 58,000 ft from the runway in the negative x-direction. The HAC location can never be closer to the runway than the ALI point; therefore, when the HAC location is encroaching upon ALI, it is known that the limits of the simulation are being reached.

6.1.4 Results and Analysis

Many more trials, other than just the extreme trials, were completed in order to make sure the simulation was robust enough to handle any range of initial vehicle

conditions. The results from these many trials are presented in Tables 6 and 7. Table 6 illustrates a very intuitive characteristic about the system. As the vehicle was moved closer to the HAC, the size of the HAC increased. This is known to be correct because in order to fly a longer path to compensate for the close location, the size of the HAC should be increased. The HAC is also moved away from the runway to help compensate for the close initial position. Conversely, when the vehicle starts TAEM from a relatively far away distance, the HAC size is made smaller and the HAC is moved closer to the runway. This compensates for the extra distance that the vehicle has to fly in order to reach the HAC. Another intuitive observation is that the HAC turn bank angle is greater when the vehicle must fly a smaller radius. Using the same logic, the HAC turn bank angle is less when the vehicle must fly a large HAC radius.

Table 6. Results produced by the analytic groundtrack planner using the same initial energy for the vehicle while varying the initial position.

% Change in position	R_F (ft)	R_2 (ft/deg^2)	X-HAC (ft)	Bank angle (deg)
-30%	21,133.8	0.5673	-93,569.1	17.27
-20%	19,910.3	0.4023	-88,372.2	17.79
-5%	16,755.2	0.2097	-80,516.2	19.83
Nominal	15,404.0	0.1623	-77,886.1	21.29
+5%	13,982.4	0.1197	-75,251.9	23.31
+20%	8,049.2	0.0381	-67,328.1	35.07

Table 7. Results produced by the high-fidelity simulation using the estimates provided by the analytic groundtrack planner.

% Change in position	R_F (ft)	R_2 (ft/deg^2)	X-HAC (ft)	Max bank angle during S-turn (deg)	Downtrack error at ALI (ft)	Crosstrack error at ALI (ft)
-30%	19,835.4	0.5673	-93,921.2	2.0	4.00	0.03
-20%	18,985.6	0.4023	-88,552.5	0.2	8.60	0.08
-5%	16,138.1	0.2097	-80,516.2	0.5	119.40	0.98
Nominal	14,807.1	0.1623	-77,886.2	0.5	75.00	1.93
+5%	13,290.2	0.1197	-75,251.9	0.1	104.70	0.85
+20%	7,278.5	0.0381	-67,420.9	1.1	89.80	35.77

It can be seen from the results that the analytic groundtrack planner accomplished the task of providing an excellent estimation of the HAC turn bank angle. The final radius and quadratic coefficient for the HAC radius were calculated in the analytic groundtrack planner using the estimated HAC turn bank angle. The final radius values calculated by the analytic groundtrack planner compare very well with the high-fidelity simulation final radius values. In most cases the final radii are well within 1,000 ft of each other. This similarity proves that the simulation had no problem converging quickly to a solution that matched the planned trajectory.

The analytic groundtrack planner also provided excellent estimates for the location of the HAC in the x-direction. These values compare favorably to the values actually used in the simulation. Again, this proves that the high-fidelity simulation had no problem converging to a solution when using the estimates provided by the analytic groundtrack planner. It is critical that the high-fidelity simulation be able to converge quickly to a solution. A quick and efficient program is essential to the vehicle being able to fly a safe reentry trajectory. In nearly all of the cases that were tested, the solution converged in one or two attempts. It should be noted that the size and location of the

HAC were, essentially, fine-tuned during this convergence process. No significant changes needed to be made to the size and location of the HAC because of the extremely good estimates provided by the analytic groundtrack planner. The logic and calculations behind the high-fidelity simulation were established prior to this research and were used as is [13]. The simulation that was used has been proven to be effective by Kluever et al [13].

The bank angle profile for the vehicle during the length of TAEM was a very informative parameter. From Fig. 39 it can be seen that the HAC turn began at a time of 350 seconds and ended at a time of 520 seconds, for the nominal trial. During the HAC turn the vehicle utilized a bank angle value of approximately 22 deg. This matches within 0.8 deg of the estimated value provided by the analytic groundtrack planner. This once again proves that the data provided by the analytic groundtrack planner was instrumental in a successful TAEM trajectory. It was noticed from the bank angle profile that during the HAC turn there is a significant amount of "chatter" in the data. These discontinuities do not significantly affect the path of the vehicle because the bank angle command is integrated a number of times before the path is planned. Each of the integrators acts as a "smoother," which will negate the effect of the discontinuities. The bank angle during the HAC turn was interpreted as being the mean value line between the peaks and valleys of the chatter. It should be noted that the bank angle profile exhibited by Fig. 39 was obtained from the nominal trial, as well as the two extreme trials.

It can also be seen within Fig. 39 that there is a significant transient response at the beginning of the HAC turn for all of the trials. This transient suggests that the system is over-gained by the control-design. When the values of natural frequency and damping

ratio were relaxed, in an attempt to decrease the large transients, the accuracy of the simulation was negatively affected before the transients were reduced. It is suggested that a “limiter” could be placed on the system at the beginning of the HAC turn in order to help control the large transient response.

Figure 39 provides excellent insight into how changing the bank angle of the vehicle affects the HAC turn for the trajectory. Obviously, it can be seen when viewing Figs. 39 and 46 simultaneously, when the bank angle for the vehicle during the HAC turn is small, the HAC size is large. Conversely, when the bank angle during the HAC turn is large, the HAC size is small.

The goal of minimizing the bank angle required during the S-turn subphase was also accomplished using the varying HAC location method, namely Eq. (83). As can be seen from Table 5, the largest bank angle required during the S-turn for any of the cases is only 2 deg. This small of a value will not significantly affect the accuracy of the simulation.

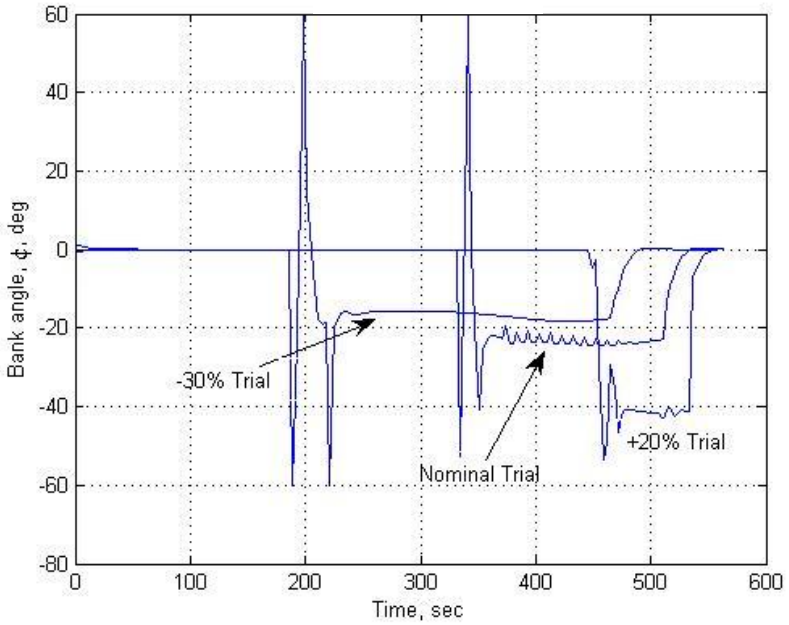

Fig. 39. Bank angle profile for the nominal trial and the two extreme position trials.

One of the most important details provided by Table 7 is the absolute error values for both the x and y-directions. It can be seen that the crosstrack error, or error in the y direction, is never greater than 2 ft except for one trial. This error is extremely small for the relative size of the system. The error in the x-direction, or the downtrack error, is also very good. Although more significant than the crosstrack error, the downtrack error is not as important of a characteristic to the system overall. The downtrack error is not as important because obviously a runway is longer than it is wide. If the vehicle possesses some downtrack error along the runway centerline then the vehicle will simply land a little further up or down the runway. If the vehicle has significant crosstrack error then the vehicle may not land on the runway at all, let alone the centerline. This fact notwithstanding, 100 ft of downtrack error for a system of this magnitude is incredibly small.

For each of the different trials completed, many plots illustrating important parameters were constructed. These plots include parameters such as vehicle velocity, flight path angle, angle of attack, energy, dynamic pressure, lift-to-drag ratio, and many more. These plots are generally similar for all of the trials completed; therefore, only the plots from the nominal case will be shown as Figs. 40-45.

The dynamic pressure for the vehicle, illustrated by Fig. 42, is shown to track the reference dynamic pressure very well. The reference dynamic pressure is calculated within a solver that assumes quasi-equilibrium glide. The dynamic pressure is tracked best during the acquisition subphase, which occurs between an altitude of approximately 70,000 and 30,000 ft. Figure 45 is similar in the sense that the actual flight path angle is compared to the flight path angle found by the quasi-equilibrium glide solver. Again, the flight path angle is tracked best during the acquisition subphase.

Figure 43 illustrates the lift-to-drag ratio for the vehicle as compared to the maximum possible lift-to-drag ratio. As can be seen, the vehicle flies at nearly the maximum lift-to-drag ratio for the entirety of TAEM. Figure 44 illustrates the angle of attack for the vehicle, which represents a range of very practical values.

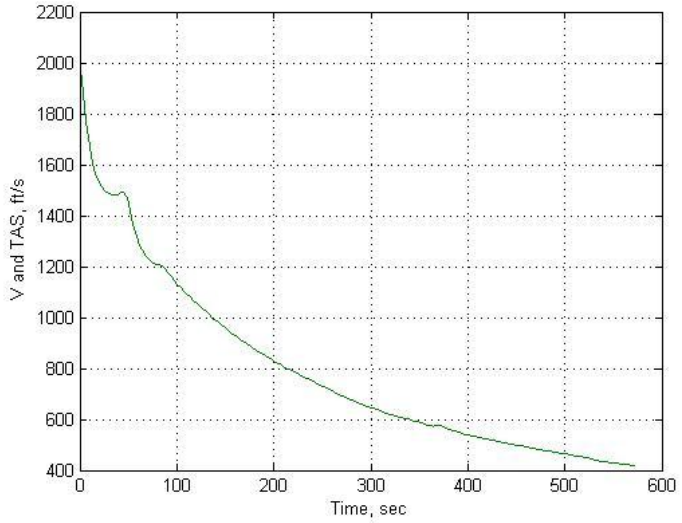

Fig. 40. Velocity versus time for the nominal trial.

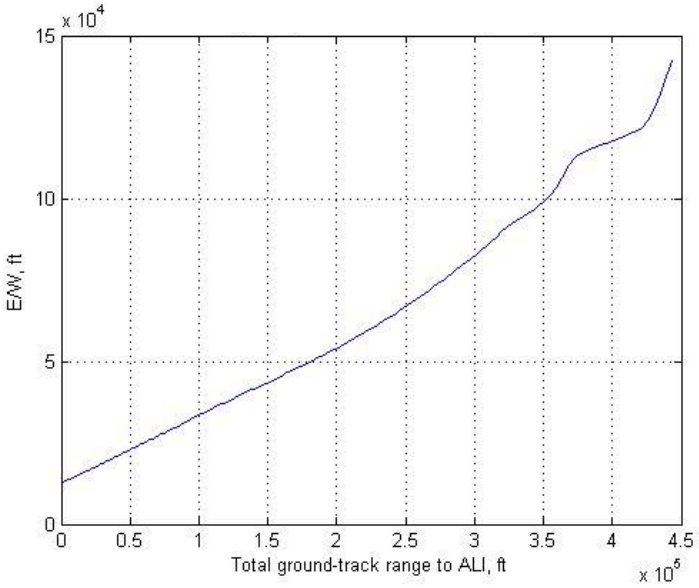

Fig. 41. Energy height versus range-to-go for the nominal trial.

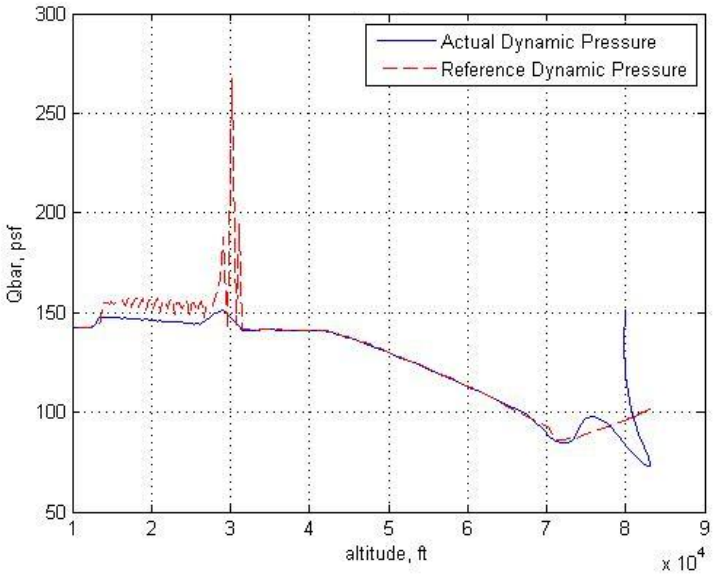

Fig. 42. Vehicle dynamic pressure compared to the reference dynamic pressure obtained from the quasi-equilibrium glide solver.

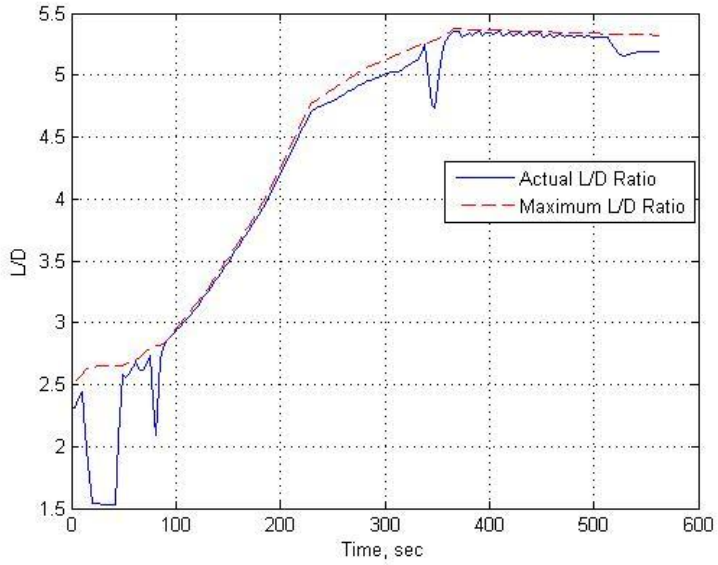

Fig. 43. Vehicle lift-to-drag ratio compared to the maximum possible lift-to-drag ratio.

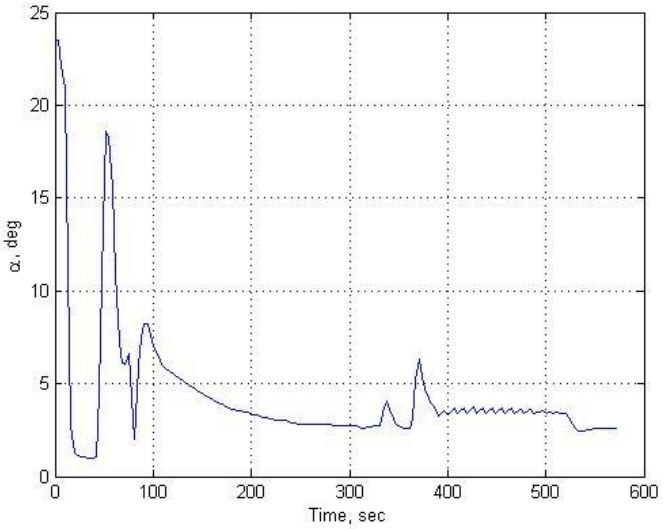

Fig. 44. Angle of attack versus time for the nominal case.

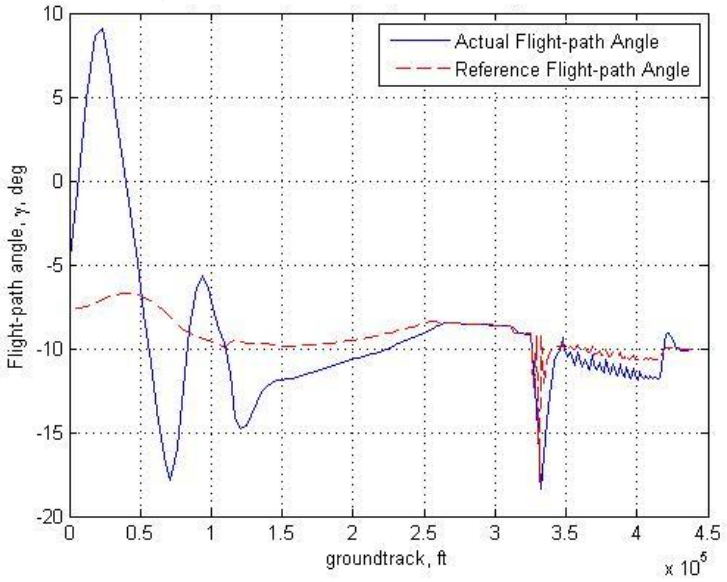

Fig. 45. Vehicle flight path angle compared to the reference flight path angle determined by the quasi-equilibrium glide solver.

One of the most important plots shows the groundtrack for the vehicle. The groundtrack for the vehicle varies considerably between each of the many trials. Figure 46 illustrates the groundtrack for the nominal trial, as well as the two extreme trials. As can be seen in Fig. 46, not only does the HAC size vary, but the HAC location varies

depending on the initial position of the vehicle. All of the trials result in the vehicle being accurately positioned at ALI.

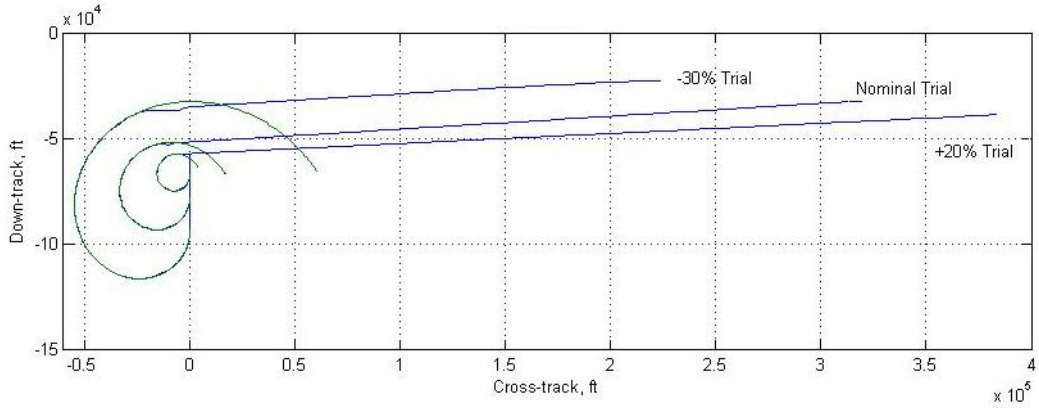

Fig. 46. Illustration representing three different trials using varying initial positions. The bank angle is varied according to the initial position of the vehicle.

6.2 Initial Energy Trials: Variable HAC Size Technique

6.2.1 Nominal Trial

The same nominal trial vehicle conditions were used for the energy modification case as they were for the position modification case, described by section 6.1.1. The location of ALI is also consistent from previous trials. Because of this consistency the results for this nominal trial are the same as they were in section 6.1.1. As a reminder, the vehicle conditions that directly affect the energy of the vehicle are velocity and altitude. The nominal trial velocity for the vehicle is 2,000 ft per second. The nominal trial altitude for the vehicle is 80,000 ft. These energy characteristics will be varied while the initial

position of the vehicle will remain constant. The initial heading angle of the vehicle will also remain constant.

6.2.2 -20% Scaled Initial Energy

It was found that the energy of the vehicle could be decreased to 80% of the nominal trial value and still reach the runway safely when utilizing a variable HAC size. This value was found to be near the lower limit and, therefore, provides an extreme case to test. The resulting initial velocity after scaling the energy by -20% of the nominal is a value of 1,789 ft per second. The resulting altitude is 64,000 ft. It was found that 20% less energy than the nominal was the lower limit of the simulation because the bank angle that the analytic groundtrack planner determined was approximately 62 deg. The vehicle that is being utilized for this simulation has a bank angle limiter, which limits the allowable bank angle to a value of less than 60 deg. Because of this, the desired path determined by the analytic groundtrack planner could not be flown. However, the high-fidelity simulation was robust enough to compensate for the error produced by the analytic groundtrack planner. The high-fidelity simulation increased the final radius value to 5,000 ft, which is also a limit for the system. With the final radius value set to 5,000 ft, the simulation then modified the location of the HAC in the x-direction in order to allow the trajectory to converge to a solution. The appropriate columns of Tables 8 and 9 show the results from the analytic groundtrack planner and from the high-fidelity simulation, respectively.

6.2.3 +15% Scaled Initial Energy

The most extreme case exhibited by the vehicle possessing too much energy was found when the vehicle had an energy level 15% greater than the nominal case. During this trial the vehicle had an initial velocity of 2,144.8 ft per second and an initial altitude of 92,000 ft. This level of energy was determined to be the upper limit of what the simulation could handle because, while the analytic groundtrack planner provided estimates for the high-fidelity simulation, the high-fidelity simulation had to utilize over 20 iterations before a trajectory was found. Even after all of the iterations, the high-fidelity simulation did not converge to an acceptable solution. The downtrack error of more than 2,000 ft is unacceptable for this application. Because of this, the variable HAC size technique was proven to not be able to provide a good solution in cases where the energy of the vehicle was much greater than the nominal case. As a reminder, the nominal initial energy is a value which defines the vehicle to be within the TAEM phase of reentry. It is unlikely that the vehicle will reach a point close to the runway with an excessive amount of energy because the stages of reentry before TAEM will not allow this to happen. However, it is reassuring to know that the vehicle is able to possess between -20% and +15% of the nominal energy and still reach ALI accurately.

6.2.4 Results and Analysis

The results produced by the variable HAC size technique when the energy of vehicle was modified considerably are acceptable in many cases. As shown by Tables 8

and 9, the results are much more accurate for cases where the energy is less than the nominal. For these cases the final radius values and the HAC location values produced by the analytic groundtrack planner are extremely similar to the respective values utilized in the high-fidelity simulation. Any trial where the vehicle possesses between -20% of the nominal energy and the nominal energy provide excellent tracking results. However, when the energy of the vehicle is any value greater than the nominal, the vehicle trajectory strays from the estimates provided by the analytic groundtrack planner in order to provide a correct solution. The final radius and HAC location values determined by the analytic groundtrack planner are not close to the respective values used in the high-fidelity simulation. While the crosstrack error for these high energy cases is negligible, the amount of iterations required for the trajectory to converge to a solution was great. Again, the more efficient the simulation is, the faster a solution is determined. Saving time is extremely important in a situation such as this.

Table 8. Results produced by the analytic groundtrack planner using the same initial vehicle position while varying the initial energy of the vehicle.

% Change in initial energy	R_F (ft)	R_2 (ft/deg^2)	X-HAC (ft)	Bank angle (deg)
-20%	3,154.1	0.0098	-77,886.2	62.21
-10%	10,302.4	0.0652	-77,886.2	30.14
Nominal	15,404.2	0.1623	-77,886.2	21.29
+5%	17,577.1	0.2320	-77,886.2	18.91
+15%	20,503.3	0.4414	-77,886.2	16.37

Table 9. Results produced by the high-fidelity simulation using the estimates provided by the analytic groundtrack planner.

% Change in initial energy	R_F (ft)	R_2 (ft/deg^2)	X-HAC (ft)	Max bank angle during S-turn (deg)	Downtrack error at ALI (ft)	Crosstrack error at ALI (ft)
-20%	5,000.0	0.0098	-68,992.2	6.0	176.10	37.80
-10%	9,542.6	0.0652	-77,886.2	6.0	6.80	1.80
Nominal	14,807.1	0.1623	-77,886.2	0.5	75.00	1.93
+5%	13,950.0	0.2320	-87,149.2	3.0	199.60	0.00
+15%	16,384.1	0.4414	-85,667.1	10.0	2080.40	0.00

Figure 47 shows the groundtrack for the vehicle for three different energy trials, each labeled appropriately. As can be seen, the vehicle had the same initial position for all of the trials. Based on the energy of the vehicle the HAC size was modified accordingly, such that the total possible range for the vehicle would match with the WLE range. It is intuitive that if the vehicle possesses too much energy, the HAC will be larger in size in order to provide a longer range for the vehicle to fly, and thus bleed off the excess energy. Conversely, if the vehicle does not have enough energy, the HAC turn will be small so that the vehicle does not waste energy flying an unnecessarily large HAC turn. These intuitive ideas are realized within the simulation and can be seen, for the nominal and extreme energy trials, within Fig. 47. It should be noted that since the initial position of the vehicle was the same for all of these trials, the HAC location was not varied within the analytic groundtrack planner. The only modification to the HAC location occurred during the high-fidelity simulation when the simulation was iterating in order to converge on a solution to the trajectory. Except during the extreme trials, the HAC location generally ended up in the same location. This was due to the straight-line

distance from the initial position of the vehicle to the ALI point always being the same value. It should be noted that the trial with 15% more energy than the nominal did not converge to a trajectory solution using the high-fidelity simulation. This is seen within Table 9 as the downtrack error value being greater than 200 ft. The nonconvergence is also exhibited in Fig. 47 by the slight bank angle variance at the very end of the trial with 15% greater energy than the nominal HAC turn. If the trial had converged, this slightly rough area would be smooth.

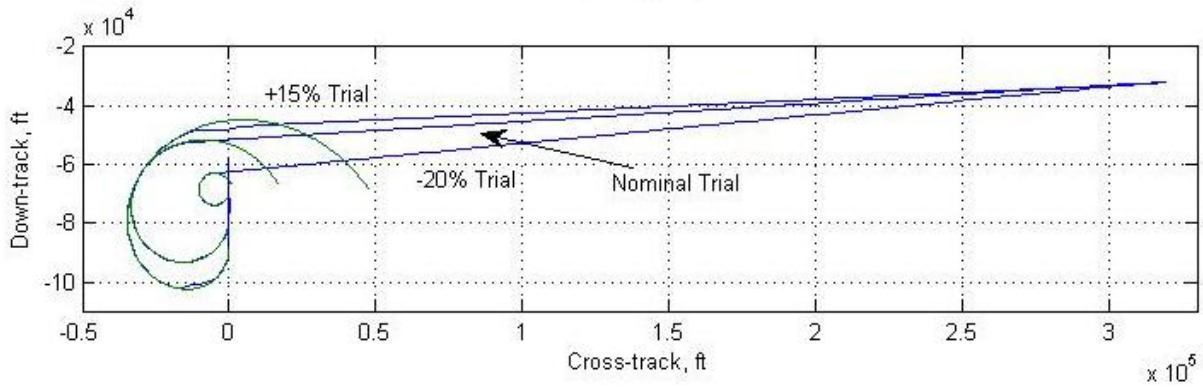

Fig. 47. Illustration representing three different trials using varying initial energy values. The bank angle of the vehicle is modified based on the energy of the vehicle.

The other plots that further illustrate the vehicle's reentry are nearly identical to Figs. 40-45. This is mainly due to the fact that, while the trajectory of the vehicle is different for each and every trial, the trials are similar enough that Figs. 40-45 represent the general characteristics of reentry for each trial well. The exception to this rule is the plots representing the bank angle of the vehicle during TAEM. The bank angle plot for each trial has the same shape; however, the HAC turn bank angle for each case is a little bit different depending on which bank angle was chosen for the vehicle during the completion of the analytic groundtrack planner. Other than the bank angle value at which

the vehicle completes the HAC turn being different, the other characteristics of the plot are similar.

6.3 Initial Position Trials: Variable HAC Location Technique

The second technique used to find an accurate solution to the trajectory problem included varying the location of the HAC. While the HAC location was varied within the first technique of varying the HAC size, the HAC location was not the primary variable that caused the two range values to match. Moving the HAC location within the structure of varying the HAC size was done only to avoid a significant bank angle value during the S-turn subphase.

Much like the process described in sections 6.1 and 6.2, many trials were completed in order to determine how robust the program was when it was required to find a solution to each unique trajectory problem. The initial position of the vehicle was varied using the same range of -30% to +20% of the nominal trial in order to best determine which technique is optimal.

6.3.1 Results and Analysis

All of the trials converged to a solution quickly and efficiently using the HAC location as the primary variable that was modified. Tables 10 and 11 show the results of the analytic groundtrack planner and the high-fidelity simulation, respectively. It can be seen that the final radius and HAC location values produced by the analytic groundtrack

planner match extremely well with the respective values that were produced by the high-fidelity simulation.

Tables 10 and 11 also prove that this technique of varying the location of the HAC has upper and lower limits for the initial position of the vehicle of approximately -30% and +20% of the nominal, respectively. The lower limit is known to be about -30% of the nominal position because the bank angle required during the S-turn is extremely large. While the crosstrack and downtrack errors for this -30% trial are negligible, a high bank angle value during the S-turn is not desirable because it is possible that the estimates produced by the analytic groundtrack planner have a significant amount of error. This leads to error being introduced to the high-fidelity simulation and then the high-fidelity simulation is required to complete more iterations in order to negate the introduced error. The overall efficiency of the simulation is affected significantly. The upper limit is known to be about +20% of the nominal position because the HAC location is approaching the ALI point. As a reminder, the HAC location can never be closer to the runway than the ALI point; therefore, when the HAC location is getting close to ALI it is known that the limits of the simulation are being reached.

Table 10. Results produced by the analytic groundtrack planner using the same initial vehicle energy while varying the initial position of the vehicle. The HAC location was the primary variable.

% Change in initial position	R_F (ft)	R_2 (ft/deg^2)	X-HAC (ft)	Bank angle (deg)
-30%	14,948.5	0.2099	-140,686.5	30
-20%	13,932.7	0.1607	-128,846.5	30
-10%	12,272.7	0.1040	-107,268.3	30
Nominal	11,707.1	0.0910	-99,045.3	30
+5%	11,124.9	0.0792	-90,122.8	30
+20%	9,362.9	0.0504	-59,749.0	30

Table 11. Results produced by the high-fidelity simulation using the estimates provided by the analytic groundtrack planner.

% Change in initial position	R_F (ft)	R_2 (ft/deg^2)	X-HAC (ft)	Max bank angle during S-turn (deg)	Downtrack error at ALI (ft)	Crosstrack error at ALI (ft)
-30%	15,289.9	0.2099	-142,035.6	48.0	119.80	0.00
-20%	14,331.1	0.1607	-130,243.3	36.0	26.10	0.00
-5%	12,625.3	0.1040	-108,489.1	20.0	14.00	0.00
Nominal	12,057.7	0.0910	-100,110.3	15.0	3.98	0.00
+5%	11,442.6	0.0792	-91,093.7	10.0	84.05	0.05
+20%	9,545.9	0.0504	-60,321.3	5.0	164.56	18.13

For all of the cases, it can be seen in Table 9 that the crosstrack error is nearly 0 ft for every trial. This is a very desirable quality of the system, which can be attributed to the accuracy of the control design. It is also seen that the downtrack error is very small for all cases. The crosstrack and downtrack errors for this set of trials using the variable HAC location technique compare similarly to the respective errors using the variable HAC size technique. When comparing the error results, in order to compare similar sets of data both of the variable position sets of data should be compared; therefore, Tables 11 and 7 were be compared. The crosstrack error values produced by the variable HAC location technique were smaller than the error values produced by the variable HAC size technique; however, both techniques produced error values that were negligible. The downtrack errors produced by the variable HAC location technique were less than the error values produced by the variable HAC size technique, but again, both sets of error values were extremely small and would be more than acceptable for any simulation.

One of the undesirable characteristics of the variable HAC location technique includes the required bank angle during the S-turn subphase. As can be seen in Table 11,

the smallest required bank angle during the S-turn is 5 deg. This small value is acceptable; however, the bank angle values ranged from this small value all the way up to 48 deg. A large S-turn bank angle value will be detrimental to the accuracy of the analytic groundtrack planner. This will cause the analytic groundtrack planner to introduce some error to the high-fidelity simulation. For nearly all of the trials, the solution did not converge in one iteration, but rather the simulation was required to iterate twice before converging on an appropriate solution. This observation tells the user that the initial estimates provided by the analytic groundtrack planner were not good enough for the high-fidelity simulation.

This observation is also observed by viewing the discrepancies between the values of parameters such as final HAC radius and HAC location provided by the analytic groundtrack planner and the respective final values that were used by the high-fidelity simulation. Using the data provided by Tables 6-7 and 10-11, it was found that the average difference between the HAC location estimate and the actual value was approximately 104 ft when the variable HAC size technique was used. The average difference between the final HAC radius estimate and the actual value was approximately 817 ft when the variable HAC size technique was used. When the variable HAC location technique was used the average difference in HAC location was almost 1,100 ft while the average difference in final HAC radius was about 323 ft. These results prove that the variable HAC size technique is only marginally better at producing a solution than the variable HAC location technique.

The variable HAC location technique was effective in requiring the vehicle to maintain a relatively constant bank angle of 30 deg while traveling around the HAC.

Illustrated by Fig. 48, which is the bank angle profile for the nominal trial, it can be seen that there is no chatter in the bank angle profile like there was when the HAC size was varied. This is a desirable characteristic; however, there was no great effect on the accuracy of the simulation because of it. As shown by the crosstrack and downtrack errors in Table 7, the chatter did not have a detrimental effect on accuracy. Figure 48 also highlights the significant required bank angle of nearly 15 deg during the S-turn. It should be noted that the bank angle plots could be produced for the extreme position trials; however, the bank angle is always set to a nominal value of 30 deg so the plots would all look relatively alike.

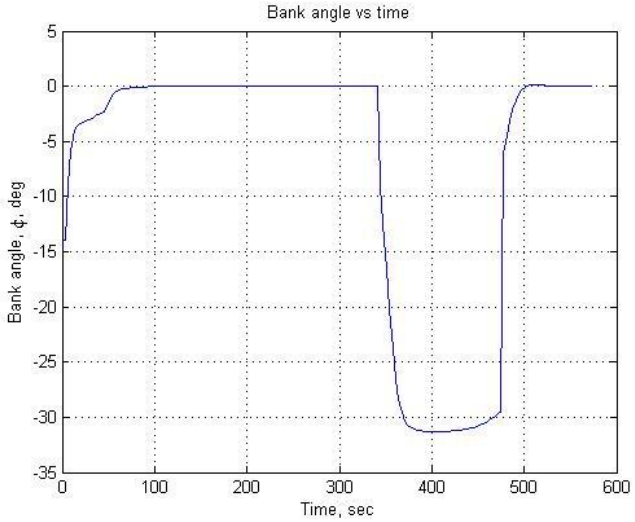

Fig. 48. Bank angle profile for the vehicle, for the nominal trial, when utilizing the variable HAC location technique.

The groundtrack for the vehicle is illustrated for three different trials in Fig. 49. Not only is the nominal case shown, but the two extreme position cases of 70% and 120% of the nominal are shown. It can be seen that main range modifier is the location of the HAC. As the vehicle's initial position is moved closer to ALI the HAC is moved away from the runway. Conversely, as the initial position is moved further away the HAC

is moved closer to the runway. While the size of the HAC does change, this change in size is not the driving variable behind the range values matching. The size of the HAC is only varied as a by-product of the bank angle needing to remain constant. Intuitively, when the vehicle's initial position is closer to ALI, the speed is greater than it should be; therefore a larger HAC radius is needed in order to allow the vehicle to bank at the specified value of 30 deg. The opposite is true as well. When the vehicle's initial position is further away, the speed is less than it should be. When the vehicle reaches the HAC the vehicle speed is still less than it should be; therefore a smaller radius turn is required in order to maintain a 30 deg bank.

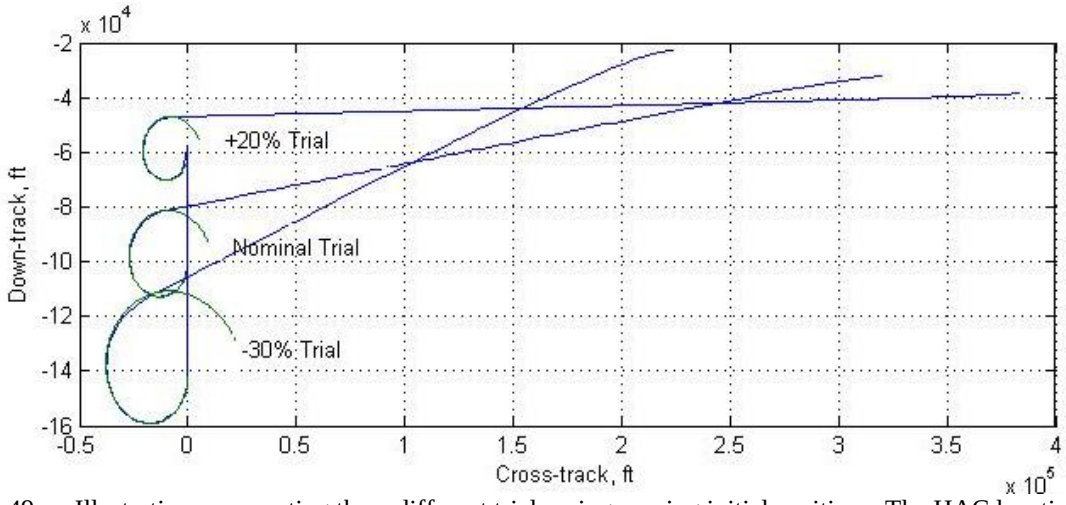

Fig. 49. Illustration representing three different trials using varying initial positions. The HAC location is varied according to the initial position of the vehicle. The HAC turn bank angle is maintained at 30 deg.

It should be noted that the other plots that illustrate the trajectory of the vehicle as it completes TAEM are extremely similar for all trials. Figures 40-45 are all representative of the general characteristics of each and every trajectory. The bank angle plots for all of the trials that were completed using the variable HAC location technique are nearly the same as Fig. 48. The only main difference between bank angle plots is the S-turn bank angle value at the beginning of TAEM.

6.4 Initial Energy Trials: Variable HAC Location Technique

Much like the process carried out in section 6.2, the energy of the vehicle was the main variable that was modified and the trajectory was solved using the variable HAC location technique. The initial position of the vehicle remained constant while the energy was varied on either side of the nominal case. The initial position of the vehicle was set to be at -32,137.1 ft in the x-direction and 319,501.0 ft in the y-direction. The heading angle of the vehicle was also kept constant at 266.8 deg. Much like section 6.2, for these trials the nominal energy was characterized by an initial vehicle velocity of 2,000 ft per second and an initial vehicle altitude of 80,000 ft.

6.4.1 Results and Analysis

It was found that the initial vehicle energy could not be modified to be -20% of the nominal value, as it was in section 6.2. When the initial vehicle energy was modified to be -20% of the nominal energy the vehicle was unable to reach the runway using the variable HAC location technique and an overhead HAC. The least possible amount of energy that the vehicle could have and still fly a converged solution was -5% of the nominal. The results from this extreme energy case are shown in the respective columns of Tables 12 and 13.

While the variable HAC location technique was not able to handle low initial energy cases well, the technique was able to handle high initial energy cases much better

than the variable HAC size technique. As was seen in section 6.2, the variable HAC size technique was only able to provide a converged solution when the initial energy of the vehicle was less than +15% of the nominal. Using the variable HAC location technique the initial energy was able to be set to +25% of the nominal and still provide a converged solution. The results from this high initial energy trial may be seen in the respective columns of Tables 12 and 13.

Table 12. Results produced by the analytic groundtrack planner using the same initial vehicle position while varying the initial energy of the vehicle. The HAC location was the primary variable.

% Change in initial energy	R_F (ft)	R_2 (ft/deg^2)	X-HAC (ft)	Bank angle (deg)
-5%	10,899.1	0.0744	-86,163.0	30
Nominal	11,707.1	0.0910	-99,045.4	30
+5%	12,712.3	0.1139	-113,060.5	30
+15%	12,151.2	0.1715	-131,600.0	30
+25%	15,026.0	0.2176	-141,860.0	30

Table 13. Results produced by the high-fidelity simulation using the estimates provided by the analytic groundtrack planner.

% Change in initial energy	R_F (ft)	R_2 (ft/deg^2)	X-HAC (ft)	Max bank angle during S-turn (deg)	Downtrack error at ALI (ft)	Crosstrack error at ALI (ft)
-5%	11,166.1	0.0744	-86,977.2	10.0	15.92	0.04
Nominal	12,057.7	0.0910	-100,110.3	15.0	3.98	0.00
+5%	13,107.4	0.1139	-114,419.8	20.0	12.64	0.00
+15%	14,349.4	0.1715	-132,519.7	32.0	180.15	0.00
+25%	15,117.0	0.2176	-142,130.1	35.0	20.05	0.00

When comparing the results from the variable HAC location technique and the variable HAC size technique it is easiest to evaluate how each of the simulations ended the TAEM phase of flight. As can be seen in Table 13, the final crosstrack error for the

vehicle was very small for all cases. A conclusion could be drawn that perhaps the variable HAC location technique is best utilized when the vehicle has more energy than the nominal case, as the crosstrack error for these high-energy trials is negligible. The final downtrack error for the vehicle fell well within the acceptable limits for all trials. The results from the variable HAC size technique, shown in Table 9, were nearly identical to the results produced by the variable HAC location technique. Because of the similarity in final position results for each technique another factor was employed to determine which technique was best.

With the overall goal of producing a time efficient trajectory solution, the estimates on system parameters produced by the analytic groundtrack planner were evaluated. If the analytic groundtrack planner is able to provide a good initial estimate for the size and location of the HAC, the high-fidelity simulation is able to converge quickly to a solution. It was found that the average difference between the final radius estimate provided by the analytic groundtrack planner and the actual final radius using the variable HAC size technique was approximately 2,200 ft. The average difference between the two HAC location values using the variable HAC size technique was approximately 5,200 ft. On the contrary, when using the variable HAC location technique, the average difference between the two final radius values was approximately 230 ft. The average difference between the two HAC location values was approximately 810 ft when using the variable HAC location technique. These statistics reveal that the variable HAC location technique is much preferred over the variable HAC size technique when the initial vehicle energy is the modified parameter. The smaller differences between both the final radius values and the HAC location values suggest that the estimates provided by the analytic groundtrack

planner are superior when utilizing the variable HAC location technique. When the estimates provided by the analytic groundtrack planner are extremely good the high-fidelity simulation is able to converge on a trajectory solution quickly and efficiently. If the high-fidelity simulation is responsible for further modification of the final HAC radius and location more iterations will be required before a solution is converged upon.

Figure 50 illustrates the nominal and extreme trials using the variable HAC location technique. As can be seen, the initial position of the vehicle is the same for all trials. It is also seen that during the low-energy trial the vehicle is not able to fully complete the HAC turn in order to reach ALI. This suggests that, when using this technique, the vehicle needs to have an initial energy value at least -5% of the nominal. Each of the HAC turns illustrated requires the vehicle to fly at a bank angle of 30 deg. Figure 51 proves that the vehicle completes the HAC turn using the prescribed 30 deg bank angle. It should be noted that Fig. 51 is the vehicle bank angle profile that was produced when the vehicle possessed an initial energy of +25% of the nominal; however, the bank angle profile for all of the trials is similar due to the fact that the vehicle is attempting to follow the HAC with a nominal bank angle of 30 deg. Also seen within Fig. 51 is the very high bank angle required during the S-turn subphase. While a large bank angle during the S-turn is not desirable, it is acceptable in extreme cases.

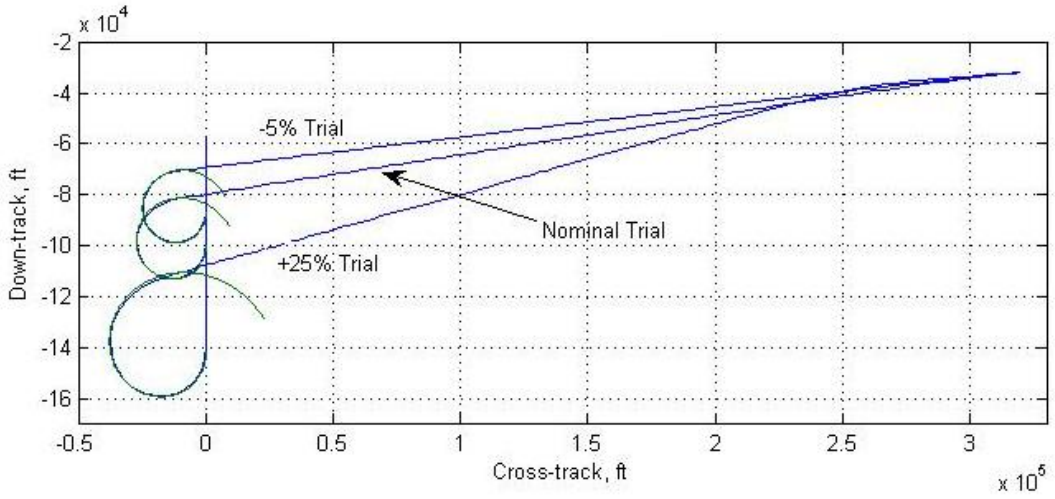

Fig. 50. Illustration representing three different trials using variable initial vehicle energy. The HAC location is varied according to the initial energy of the vehicle. The HAC turn bank angle is maintained at 30 deg.

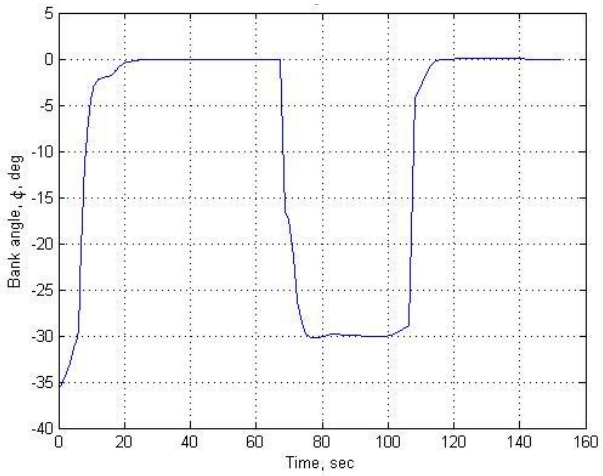

Fig. 51. Vehicle bank angle profile for the 125% energy trial using the variable HAC location technique.

6.5 Final Testing

After the upper and lower limits of the simulation were determined for both solution techniques, many trials were completed in order to fully test the solving ability

of the simulation. Specifically, the variable HAC size technique and the variable HAC location technique were tested with fifty trials each. Each of the fifty trials forced the vehicle to have a unique initial position, as well as initial energy and initial heading angle. The initial conditions of the vehicle were shared between the two solving techniques. For example, the vehicle was placed at an initial position with a specific heading and energy. The simulation was then completed using the variable HAC size technique. Results were recorded and then the vehicle was reset to the same initial conditions. The simulation was completed again using the variable HAC location technique. After the results were recorded, another unique location was chosen as well as a new heading angle and initial energy. This process was repeated fifty times. It should be noted that the fifty initial positions, heading angles, and energy values were chosen randomly. Also, all fifty trials begin from the right side of the runway centerline, when viewed from above. The left side was not tested extensively because the simulation is symmetric about the runway centerline. The solution for each side, provided the initial conditions are exactly alike, is the same except a right-hand-turn about the HAC is required when starting from the left side of the runway centerline while a left-hand-turn is required when starting from the right side of the runway. All values throughout each symmetric trial are the same with the only difference coming in the form of a couple of sign reversals. It should be noted that the simulation is able to deal with any possible initial conditions, no matter if the vehicle needs to complete a right or left-hand turn about the HAC. With the purpose of proving the symmetry about the runway centerline, one trial positioned the vehicle on the left side of the runway with the exact same initial position and energy characteristics as a trial on the right side of the runway. The initial

heading angle was mirrored about the runway centerline. These mirrored trials can be observed within Tables 16 and 17, in the appendix, as trial numbers 5 and 7. As can be seen, the results for each trial are exactly the same. To further help define the fifty trials that were completed, Fig. 52 was created to provide a visual representation of all fifty initial positions. The fifty initial positions are represented by the circle markers. Also contained within Fig. 52 is the runway, represented by the square symbol, and the ALI point, represented by the x symbol.

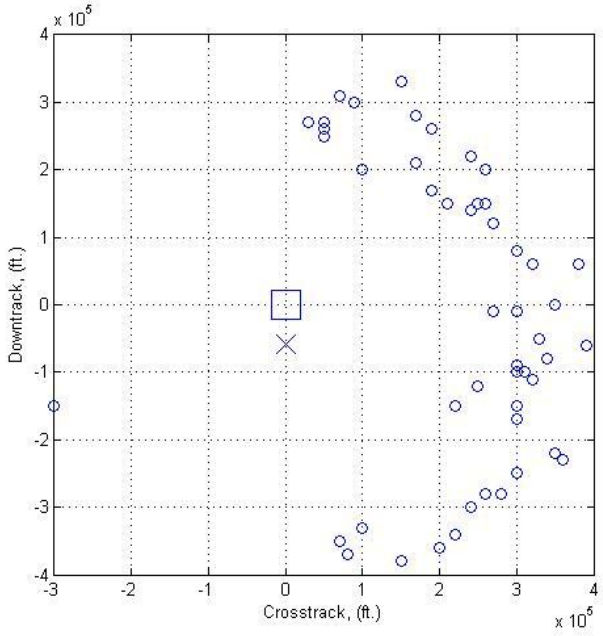

Fig. 52. Initial vehicle positions used for the fifty trials.

While it would be unrealistic to illustrate the full trajectories for all fifty trials on the same plot, seven of the trajectories spanning the entire right side of the runway are shown in Fig. 53. Figure 53 was produced using the variable HAC size technique. Figure 54 illustrates the same trials and their trajectories using the variable HAC location technique. It is easy to see the different HAC sizes and locations produced by the two techniques by observing Figs. 53 and 54. Also seen within Figs. 53 and 54 is trial number

7, which was completed after starting the vehicle on the left side of the runway. This trajectory is a mirror image of trial 5.

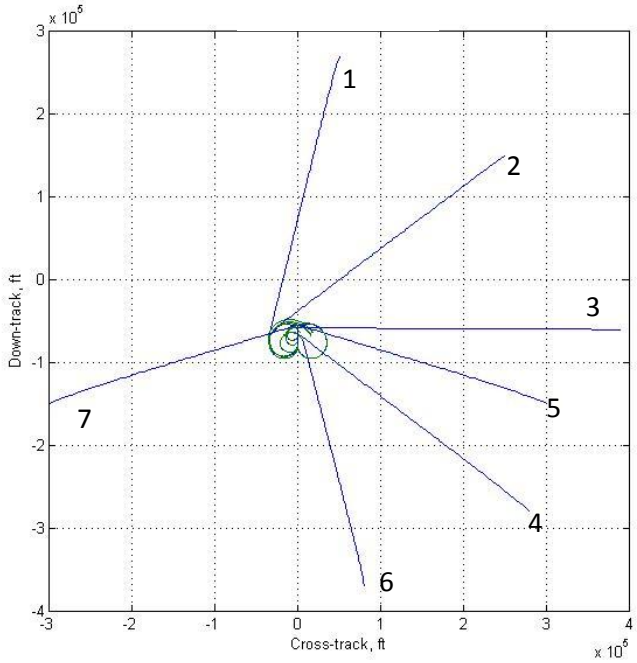

Fig. 53. Seven trials that span the extents of testing using the variable HAC size technique.

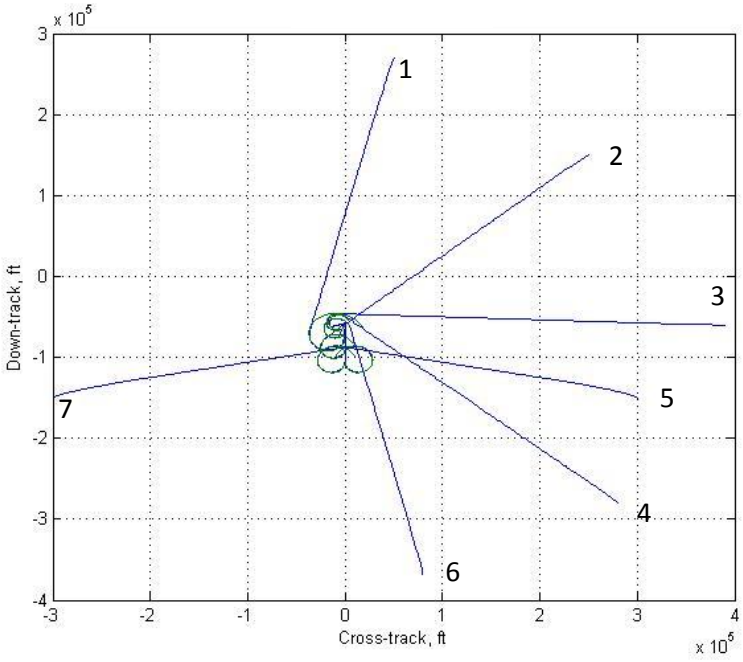

Fig. 54. Seven trials that span the extents of testing using the variable HAC location technique.

As can be seen from Figs. 52-54 and from Tables 14-17, the vehicle was tested extensively, which included trajectories that were close to the vehicle limits in terms of PSHA turns. When the initial position of the vehicle is near the runway centerline and approaching from the opposite direction as compared to the landing direction, the vehicle is required to complete a HAC turn with a PSHA value nearing 180 deg. This PSHA value is the lower limit that still allows for an overhead HAC. The trials that test near the lower PSHA limit can be seen by observing the initial positions locally north of the runway in Fig. 52. When the vehicle has an initial position near the runway centerline and is flying in the same direction as the landing direction, the vehicle is required to complete a HAC turn with a PSHA value nearing 360 deg. The trials that test near this limit can be observed by viewing the initial positions locally south of the runway in Fig. 52. To further prove that a wide range of test cases was used, Tables 14-17 have columns dedicated to providing the PSHA value for the HAC turn that was completed. Seen within the context of this paper, Tables 14 and 15 provide data for only ten trials, which is a subset of the fifty trials completed. Within the appendix, Tables 16 and 17 provide the raw data for all fifty trials. As can be seen, the PSHA value ranges from 192 to 347 deg with a good distribution of values in between. It should also be noted that the energy values of the vehicle were chosen using a standard normal distribution centered at 100% and spanning the interval of -20% and +15% of the nominal. These limits were determined previously in sections 6.2 and 6.4. A histogram of PSHA values and energy values may be observed in Figs. 55 and 56, respectively. The distribution of the PSHA histogram proves that many PSHA values were used over the range of 180 to 360 deg.

The distribution of the energy histogram resembles a normal distribution centered at 100% energy, where the percentage of energy is measured against the defined nominal. As a reminder, the nominal energy was defined as the vehicle having an initial velocity of 2,000 ft per second at an initial altitude of 80,000 ft.

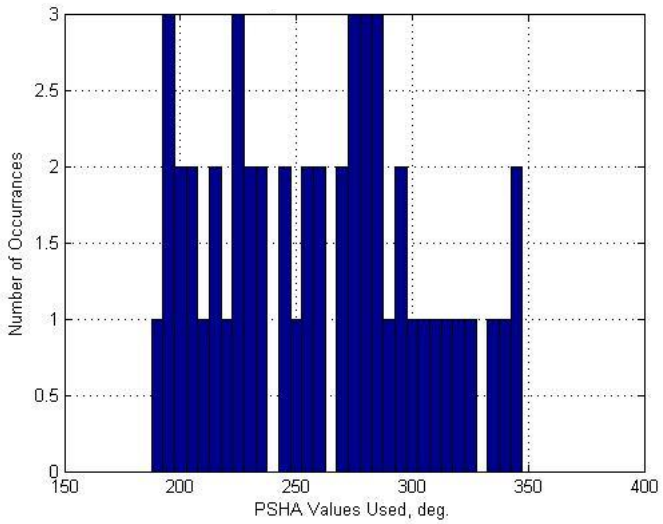

Fig. 55. Histogram of PSHA values used during the fifty executed trials.

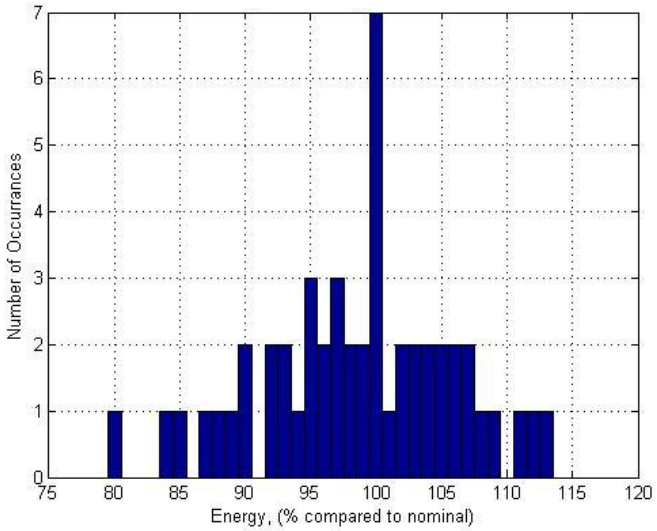

Fig. 56. Histogram of energy values used during the fifty trials. The energy histogram generally represents a normal distribution centered at 100%.

Previously, it was determined that the two solving techniques were very similar based on the final results that were produced. Because of this, a new set of parameters was observed in order to help differentiate between the two techniques. First, the difference between the final radius value estimated by the analytic groundtrack planner and the final radius value used in the high-fidelity simulation was found. Similarly, the difference between the two HAC location values was found. These values allow some insight into how fast the high-fidelity simulation may be converging on a solution based on the initial estimates provided by the analytic groundtrack planner. A good estimate should allow the high-fidelity simulation to converge to a solution quickly and efficiently. Another telling value that was observed was the number of iterations required by the high-fidelity simulation in order to converge to an acceptable solution. A small number of iterations translates into the shortest possible amount of time required for computing.

Table 14 is responsible for presenting the results produced by the variable HAC size technique. Table 15 is responsible for the HAC location technique. First, the initial position, initial heading angle, and initial energy are defined for each trial. These initial conditions represent the values that were treated as the independent variables of the system. The bank angle found by the analytic groundtrack planner was then identified. The final radius and HAC location values produced by the analytic groundtrack planner were recorded but are not seen explicitly in Tables 14 and 15. The high-fidelity simulation then produced the remaining results. The number of iterations required in order to find a converged solution using the high-fidelity simulation, the crosstrack and downtrack error values, and the PSHA angle completed are all very important results

produced by the simulation. Also, the final radius and HAC location values used during the high-fidelity simulation were recorded but are not explicitly seen within Tables 14 and 15. The final radius and HAC location differences were calculated and can be seen in the last two columns of Tables 14 and 15. These differences were found in order to help identify which strategy converged to a solution in the least amount of time.

Table 14. Subset of the data produced by the fifty trials completed using the variable HAC size technique.

Trial #	X_0 (ft)	Y_0 (ft)	Psi_0 (deg)	Initial energy	ϕ_{HAC} (deg)	I	Final crosstrack error (ft)	Final downtrack error (ft)	PSHA (deg)	ΔRF (ft)	ΔX_{HAC} (ft)
11	-10000	300000	262	100%	19.6	6	0.04	8.00	262	3423	4023
12	-10000	270000	260	95%	19.8	1	0.34	145.62	257	653	0
13	-50000	330000	268	99%	23.2	2	1.34	1.62	269	442	118
14	-80000	340000	275	96%	28.0	2	0.13	39.17	273	735	0
15	-100000	300000	280	90%	26.1	1	1.41	25.72	276	440	0
16	-110000	320000	280	92%	28.5	2	1.64	110.89	278	723	0
17	-90000	300000	278	85%	31.4	3	1.54	102.17	274	797	0
18	-120000	250000	282	80%	26.1	1	0.12	177.62	279	457	0
19	-150000	220000	300	88%	20.8	1	0.00	192.46	287	333	0
20	-170000	300000	290	94%	25.7	1	1.76	123.92	288	605	0

Table 15. Subset of the data produced by the fifty trials completed using the variable HAC location technique.

Trial #	X_0 (ft)	Y_0 (ft)	Psi_0 (deg)	Initial energy	ϕ_{HAC} (deg)	I	Final crosstrack error (ft)	Final downtrack error (ft)	PSHA (deg)	ΔRF (ft)	ΔX_{HAC} (ft)
11	-10000	300000	262	100%	30.0	2	0.00	26.58	256	336	1230
12	-10000	270000	260	95%	30.0	2	0.00	40.15	254	315	1210
13	-50000	330000	268	99%	30.0	1	0.01	20.41	265	272	838
14	-80000	340000	275	96%	30.0	1	0.44	58.47	272	244	776
15	-100000	300000	280	90%	30.0	2	0.09	12.01	276	337	1079
16	-110000	320000	280	92%	30.0	1	0.88	118.68	278	184	596
17	-90000	300000	278	85%	30.0	1	15.74	133.26	276	220	706
18	-120000	250000	282	80%	30.0	1	0.23	100.02	280	138	451
19	-150000	220000	300	88%	30.0	2	0.00	35.27	283	542	1770
20	-170000	300000	290	94%	30.0	2	0.00	32.87	288	291	971

First, it should be noted that the high-fidelity simulation was allowed to iterate 10 times in search of a solution. If the high-fidelity simulation was not able to converge to a solution after 10 iterations, then the trial was deemed to be a failure. The simulation was carried out using the values determined during the tenth iteration; this leads to high error values throughout the results. After the fifty trials were completed, the most obvious measure of performance was determining how many simulations were able to find a converged solution to the trajectory. Utilizing the variable HAC size technique, 43 out of 50 of the trials produced a converged solution. Each of the 43 converged solutions possessed extremely low error values; however, seven failures is an extremely high number. The success rate using this technique was only 86%, which is extremely low for an application of this nature. The average difference between final radius values was nearly 1,500 ft. The average difference between HAC location values was approximately 1,000 ft. The average crosstrack error value using the variable HAC size technique was approximately 8 ft, which is very good. The average downtrack error value was approximately 250 ft, which is acceptable but not outstanding. These values were skewed slightly because of the seven failure trials; however, in order to fairly analyze the two techniques, the failure results were not omitted. The final quality of the high-fidelity simulation that was observed was the average number of iterations required to converge to a trajectory solution, which was about 4 using the variable HAC size method.

Observing Tables 15 and 17, it is seen that all 50 trials converged to a trajectory solution using the variable HAC location technique, which represents a 100% success rate. The average difference in final radius and HAC location values are approximately 350 ft and 1,200 ft, respectively. The final radius difference compares very favorably to

the variable HAC size method. The HAC location difference is comparable to the variable HAC size technique. The average crosstrack and downtrack error values produced using the variable HAC location method were approximately 8 ft and 80 ft, respectively. Both of these positional error values are exceptionally good. A histogram illustrating the downtrack and crosstrack error values may be seen as Figs. 57 and 58, respectively. Figures 57 and 58 both show data using the two techniques. Figure 57 illustrates all of the downtrack error values found using the variable HAC location technique fall within the acceptable error range of 200 ft. However, Fig. 57 also illustrates the many outlying trials that had a large amount of error at the end of the TAEM phase. These outlying trials move the average downtrack error value using the variable HAC size technique to over 250 ft. It should be noted that the standard deviation for the downtrack error using the variable HAC location technique was approximately 50 ft. The standard deviation using the variable HAC size technique was almost 500 ft.

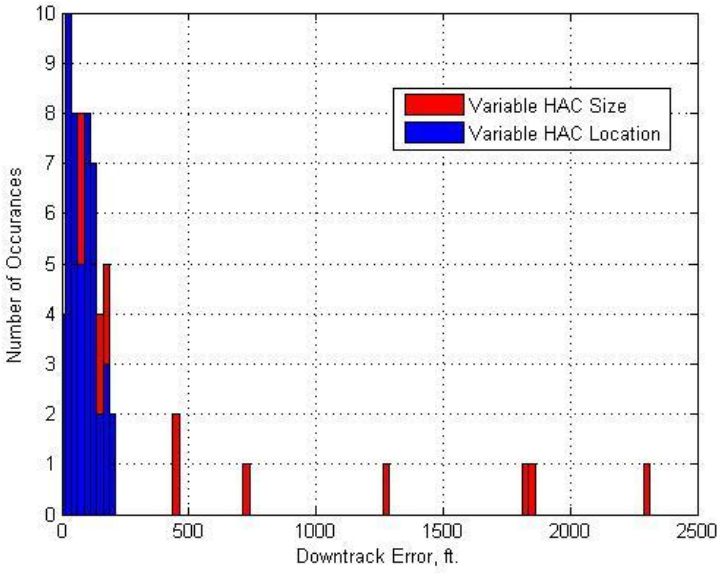

Fig. 57. Histogram of downtrack error values using both techniques.

Figure 58 illustrates the performance of the lateral tracking portion of this paper. As can be seen in Fig. 58, save for a few outlying points, all of the crosstrack error values are less than 10 ft. The outlying points can be attributed to the location of the HAC being placed too close to ALI. Because of this, the prefinal subphase is extremely short and there is not enough time to completely damp out all of the error within the trajectory. All of the crosstrack error values illustrated in Fig. 58 are acceptable values and prove the extraordinary lateral tracking control-design within the system.

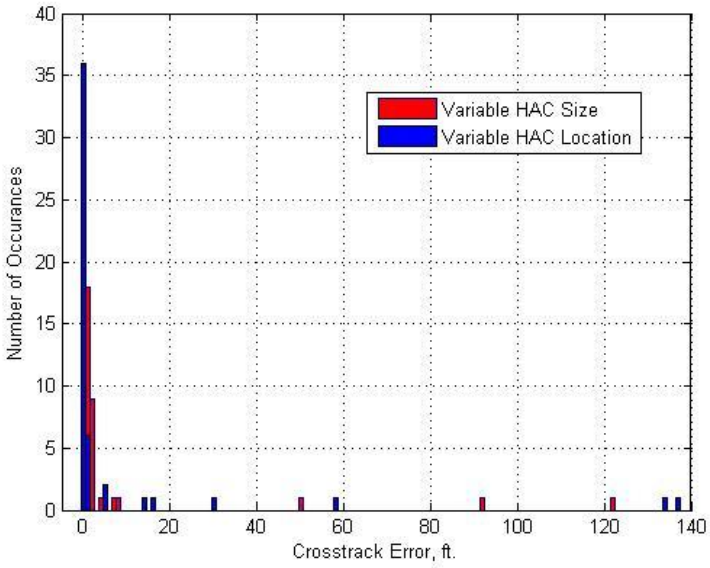

Fig. 58. Histogram of crosstrack error values using both techniques

It should also be noted that the average number of iterations required by the high-fidelity simulation to converge to a solution was only 2 using the variable HAC location technique, as opposed to the 4 required using the variable HAC size technique. A visual interpretation of the number of iterations required by the high-fidelity simulation when using the two different techniques may be seen as Fig. 59. As can be seen in Fig. 59, the variable HAC size technique has a higher mean value of iterations. The amount of time it

takes to run 2 iterations using the high-fidelity simulation is approximately 15 seconds. On the other hand, it takes approximately 30 seconds to run 4 iterations using the high-fidelity simulation. Comparatively, it only takes approximately 0.001 seconds to obtain the very good estimates of the required parameters using the analytic groundtrack planner. These quantitative time results were obtained using an AMD Turion 64 X2 Mobile Technology TL-64 2.20 GHz Processor with 3.00 GB of RAM and a 32-bit operating system.

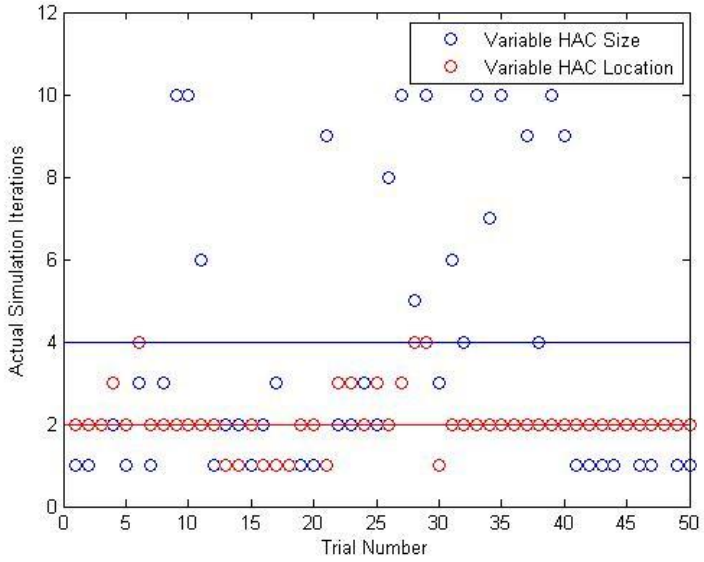

Fig. 59. Visual interpretation of the number of iterations required by the high-fidelity simulation for the two techniques.

In search of an explanation for why the variable HAC location technique consistently converged to a solution in less iterations than the variable HAC size technique, another qualitative simulation characteristic was observed. The variable HAC location technique was observed first. Since the main goal of the analytic groundtrack planner is to find and decrease the range-to-go error, this error value was set to be the dependent variable. The independent variable was set to be the location of the HAC in the

x-direction. The location of the HAC was placed at ALI and the range-to-go error was recorded. The HAC was then moved away from ALI 75 ft and the range-to-go error was recorded again. This process was completed 1,000 times, which equates to the range of HAC locations varying by 75,000 ft. Each HAC location value along with its accompanying range-to-go error value was plotted and can be observed in Fig. 60.

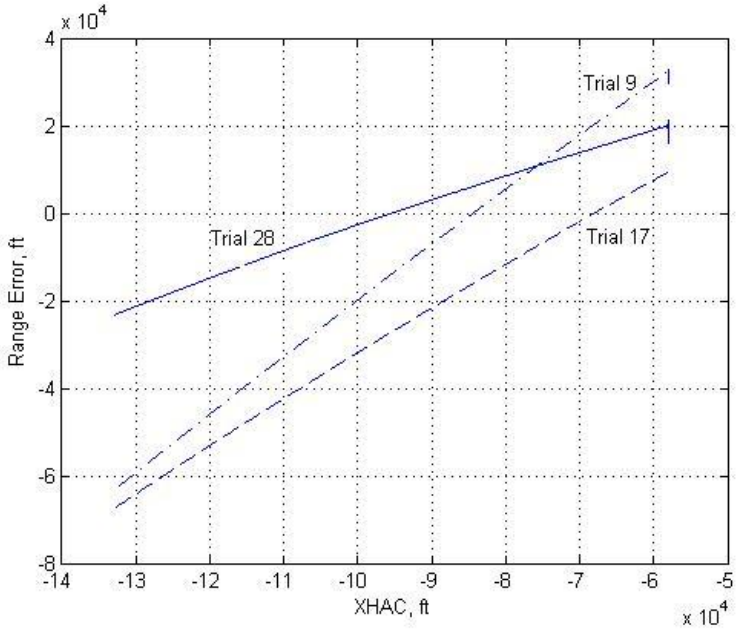

Fig. 60. For three different trials, the location of the HAC was varied and the corresponding range-to-go error value was recorded.

This plotting procedure was completed for 3 different trials. Figure 60 is interpreted by finding where each line crosses the x-axis, where the range-to-go error is zero. The corresponding x-direction HAC location is the location that the analytic groundtrack planner declares will provide the simulation with the best chance to converge to a solution quickly. It should be noted that Trials 9, 17, and 28 converged in 2, 1, and 4 iterations, respectively, when run through the high-fidelity simulation.

Figure 60 also shows that range-to-go error is a nearly linear function of HAC location, for all trials. This is an important observation because it suggests that a solution

will always be found no matter how bad the initial HAC location estimate is. While the secant method was not used for the variable HAC location technique, it would be another excellent method to use, because of the linearity, in order to find the location value that corresponds to the smallest range-to-go error value. However, the secant method is not needed to produce excellent results; the method that was used, which included modifying the HAC location based on scaling the range-to-go error, produced extremely good estimates for the high-fidelity simulation.

Next, the variable HAC size technique was observed. Again, range-to-go error was used as the dependent variable while HAC bank angle was used as the independent variable. The HAC bank angle was forced to start at 10 deg, which would result in the vehicle completing a large sweeping HAC turn, and was incremented 0.1 deg. The HAC bank angle was incremented 500 times producing a HAC bank angle range from 10 deg to 60 deg. A bank angle of 60 deg is the realistic limit for the vehicle that was used. Figure 61 illustrates the results produced by the same 3 trials that were observed using the variable HAC location technique.

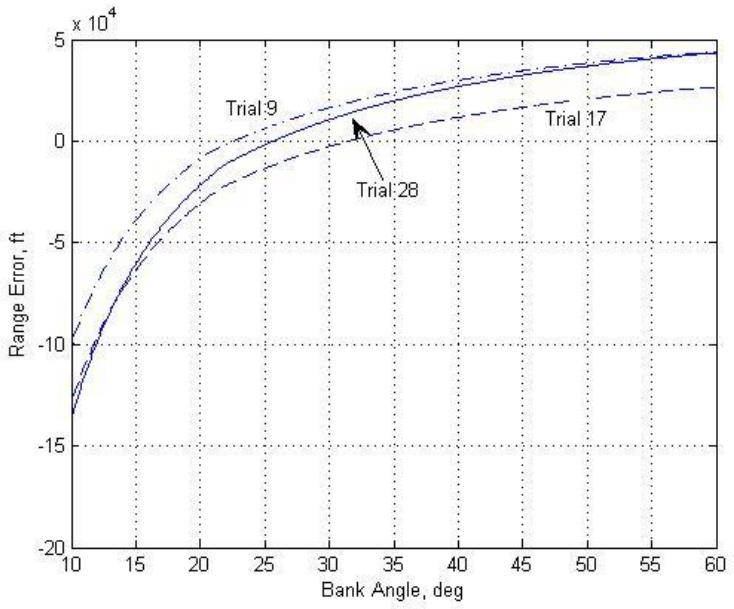

Fig. 61. For three different trials, the bank angle of the HAC was varied and the corresponding range-to-go error value was recorded.

It can be seen in Fig. 61 that the point where each function crosses the zero-error x-axis provides the analytic groundtrack planner with the HAC bank angle estimate. This bank angle estimate is the value that is relayed to the high-fidelity simulation. Because of the high number of iterations carried out by the high-fidelity simulation to find a converged solution, it is known that these bank angle estimates are not being found as accurately as would be hoped. It should be noted that Trials 9, 17, and 28 converged in 10, 3, and 5 iterations, respectively, when run through the high-fidelity simulation. Trial 9 was forced to run after a solution was not actually converged on after 10 iterations.

Figure 61 clearly illustrates that range-to-go error is not a linear function of bank angle. Because of this nonlinearity it is possible that the secant method is not obtaining the best possible estimate of bank angle. This could be because the secant method is inheriting and magnifying slight errors in the bank angle profile. While it may not be very

efficient, it may be advantageous to use a guess-and-check method to determine the best possible estimate of HAC bank angle.

After observing Figs. 60 and 61, along with reviewing all of the other evidence, it was determined that the variable HAC location technique was the superior of the two techniques. The crosstrack and downtrack error values using the variable HAC location technique were better than the variable HAC size technique. Additionally, the number of iterations required by the high-fidelity simulation was half as many when using the variable HAC location technique as opposed to the variable HAC size technique. Finally, Figs. 60 and 61 suggest that the variable HAC location technique is more consistent in producing good estimates for the high-fidelity simulation.

CHAPTER 7

CONCLUSIONS AND RECOMMENDATIONS

7.1 Lateral Tracking

It was found that dynamic lateral trajectory tracking was not only possible, but that it was actually superior to previously used static methods. Previous methods utilized static gains in order to help correct the bank angle of the vehicle in order to guide it onto a prescribed path. It was found that dynamic gains were able to adjust to vehicle conditions and vary accordingly. This dynamic nature of the gains allowed the vehicle to maneuver to the correct path very quickly and efficiently.

In order to find dynamic gains for the system in the simplest manner, the highly nonlinear system was linearized. Linearization of the system was determined to be a procedure that simplified the system considerably while still allowing for an accurate

representation. With the system linearized, state variables were chosen that best characterized the system and the system was expressed in terms of a state-space representation. Linearization and state-space representation of the system allowed for pole-placement to be the basis behind the control-design.

Since pole-placement was used to determine the dynamic gains, the controlling parameters for the system were simply the natural frequency and damping ratio. It is possible to modify the system in a variety of ways by simply varying these two parameters. For example, if a faster response time is desired the natural frequency simply needs to be increased by the user of the system. If the percent overshoot of the response needs to be decreased, then the user would simply increase the damping ratio. The system is extremely versatile and can be adjusted to the user's preferences. Succinctly, the system is a second-order damped system and possesses all of the qualities associated with such.

One of the main attractions to using such a simple control-design strategy such as pole-placement was that the strategy was extremely simple. This technique did not place a heavy load on the computers, which were already attempting to provide the vehicle with on-line, real-time tracking. Linear quadratic regression (LQR) would have also provided an effective control-design strategy; however, LQR requires a much more complex approach to the problem without a significant improvement in final results. The simplicity of pole-placement is an extremely attractive attribute of the control-design strategy.

Implementing a bank angle bias value for the vehicle as it attempted to track the HAC was also a new strategy, which performed extremely well. It has already been

proven that the vehicle is able to track a cylindrical HAC well. When the HAC is modified to be cone shaped, the vehicle has difficulty accurately tracking the prescribed trajectory using just open and closed-loop bank angle commands. There was a need for an increased bank angle when the PSHA value was large. As the vehicle completed the HAC turn, PSHA decreased along with the need for an increased bank angle. Many different functions of bank angle bias compared to PSHA-to-go were compared. An ideal function provided a large bank angle bias value when PSHA-to-go was large; ideally the bank angle bias value would decrease as PSHA-to-go decreased. After extensive testing, it was determined that the bank angle bias value should be an exponential function of PSHA. The maximum bank angle bias value was determined to be 4 deg and the exponential tuning parameter was set at 0.01.

There were a few negative effects that were found after laterally testing the vehicle. Because the gains were dynamically changing with respect to vehicle position and velocity, they sometimes created a "chattered" response with respect to the bank angle commanded. The "chatter" was not severe enough to detrimentally affect the trajectory of the vehicle. The commanded bank angle is run through a series of integrators in the high-fidelity simulation in order to determine the groundtrack of the vehicle. As the simulation progresses through these many integrations the "chatter" is essentially damped out and does not negatively affect the vehicle trajectory.

Another characteristic of the system that has room for improvement involves the transition from the HAC turn subphase to the prefinal subphase. Since both subphases utilized the dynamic gain tracking method there was always a possibility that the bank angle commanded at the end of the HAC turn would not match well with the bank angle

commanded at the beginning of the prefinal subphase. This was not a significant issue within the many tests that were conducted; however, there is a possibility for error at this transition in the future. It is known, though, that NASA employs the use of a "fader" to help correct these very such issues. The "fader" very simply takes the last bank angle value commanded by the HAC subphase and blends it seamlessly with the first bank angle value commanded by the prefinal subphase. Therefore, there is no discontinuity at this point in the trajectory for the vehicle.

Overall, the use of dynamic gains and a bank angle bias value provided the vehicle with a very simple, yet accurate, control-design package. The use of linearization and pole-placement was significant in maintaining the simplicity of the system. This lateral tracking control package integrated seamlessly with the groundtrack predictor system that was also developed for the vehicle.

7.2 Groundtrack Prediction

A very effective groundtrack predictor has been developed for the vehicle. This predictor is very simple, yet provides extremely accurate results. The simplicity of the predictor is presented in the form of energy equations that do not need to be integrated in order to find the range of the vehicle. First of all, it should be noted that the acquisition and prefinal subphases were not affected by the simplification. This is because the vehicle progresses through the acquisition and prefinal subphases with wings-level and at maximum lift-to-drag ratio. Therefore, the range for each of these two subphases is extremely easy to determine.

However, the S-turn and HAC turn portions of TAEM presented a new problem. Since the vehicle is banked at a specified angle throughout the S-turn and HAC turn, a new simple method needs to be found to find the range of the vehicle. In the past, the range was calculated for these two subphases by integrating a complex energy equation. This energy integration process required a significant amount of computing time and power to be devoted to just this calculation. It has been determined that it is much simpler, yet still very accurate, to use a simple scaling factor when dealing with the S-turn and HAC turn subphases. The actual groundtrack range-to-go is multiplied by the scaling factor, which produces the WLE range for the vehicle. After the WLE range is summed for each subphase, this total value is compared to the maximum possible range for the vehicle. Depending on how these values compare, the HAC location or size will be varied in order to allow these two range values to match.

This leads to the next conclusion that was drawn from this research. It was found that varying the HAC location provided the most accurate and consistent results, as opposed to varying the HAC size. It was found that when the variable HAC location technique was used a trajectory solution was determined 100% of the time. The average crosstrack error value was 8 ft and the average downtrack error value was 80 ft. Both of these error values are extremely small and represent very successful trials. Also, it should be noted that the high-fidelity simulation required, on average, about two iterations to converge to a solution. This small value suggests that it requires very little time to determine a plausible path to ALI. In this application, it cannot be overstated, conserving time is extremely important. Conversely, when the variable HAC size technique was applied a trajectory solution was found only 86% of the time. The average crosstrack and

downtrack error values were 8 ft and 250 ft, respectively. While these error values are certainly acceptable, the high-fidelity simulation required more than twice the amount of iterations in order to converge to a solution. It was found that the variable HAC size technique required more iterations in order to converge because of the shape of the function relating downtrack error to HAC bank angle. The function is not linear and actually has a couple of unpredictable portions throughout the range of bank angle values. Because of this, the secant method may have a hard time finding the bank angle that will produce the most accurate results. On the other hand, the variable HAC location technique required less iterations because the function relating downtrack error to HAC location in the x-direction is nearly linear. This linearity is very predictable; therefore, the error scaling method used to find the best estimate for the location of the HAC was very accurate. Since the variable HAC location technique was able to provide the high-fidelity simulation with better initial estimates for HAC location and size, the result was a trajectory that converged very quickly to a solution.

It should be noted that even though 14% of the trials involving the variable HAC size technique were said to be failures, these trials would actually have more time to correct any error due to the vehicle ending TAEM at ALI. The vehicle would still have the entire approach and landing phase to negate any major errors. However, it is possible for the vehicle to have a minimal amount of error at the end of TAEM; therefore, it is unacceptable for the vehicle to carry any significant amount of error in to the approach and landing phase.

While the variable HAC location technique possessed many desirable qualities that the variable HAC size technique did not, there were some facets of the variable HAC

location approach that were not desirable. For example, the energy range for the vehicle was only able to be -5% to +25% of the nominal energy state using the variable HAC location technique. Any energy value outside of this range did not allow the vehicle to find a trajectory solution. The variable HAC size technique was able to find a converged trajectory solution when the energy ranged from -20% to +20% of the nominal. Because of this, the variable HAC size technique would be the best technique to utilize if the vehicle were to possess less than -5% of the nominal energy upon transfer to the TAEM phase. While this is a significant advantage in favor of the variable HAC size technique, it is not enough to conclude that the variable HAC size technique should be used in favor of the variable HAC location technique. Overall, the variable HAC location technique provides much better performance when compared with the variable HAC size technique.

REFERENCES

[1] Lockheed Martin SkunkWorks, "X-33 Guidance, Navigation, and Control Design Description," SSTO 604D0034K_3, Vol. 3, 1997.

[2] Hull, J. R., Gandhi, N., and Schierman, J. D., "In-Flight TAEM/Final Approach Trajectory Generation for Reusable Launch Vehicles," AIAA Paper 2005-7114, Sept. 2005.

[3] Moore, T. E., "Space Shuttle Entry Terminal Area Energy Management," NASA TM-104744, Nov. 1991.

[4] Vernis, P., and Ferreira, E., "On-Board Trajectory Planner for the TAEM Guidance of a Winged-Body,"*AAAF 4th International Symposium on Atmospheric Reentry, Vehicles, and Systems*, AAAF, Arcachon, France, 2005.

[5] Kluever, C. A., "Unpowered Approach and Landing Guidance Using Trajectory Planning," *Journal of Guidance, Control, and Dynamics*, Vol. 27, No. 6, 2004, pp. 967-974.

[6] Fliess, M., Levine, J., Martin, P., and Rouchon, P., "Flatness and Defect of Non-Linear Systems: Introduction Theory and Examples," *International Journal of Control*, Vol. 61, 1995, pp. 1327-1361.

[7] Morio, V., Falcoz, A., Vernis, P., and Cazaurang, F., "On the Design of a Flatness-Based Guidance Algorithm for the Terminal Area Energy Management of a Winged-Body Vehicle," 2007.

[8] Burchett, B. T., "Fuzzy Logic Trajectory Design and Guidance for Terminal Area Energy Management," *Journal of Spacecraft and Rockets*, Vol. 41, No. 3, 2004, pp. 444-450.

[9] Ridder S. D. and Mooij, E., "Optimal Terminal-Area Strategies and Energy-Tube Concept for a Winged Re-Entry Vehicle," AIAA Paper 2009-5769, August 2009.

[10] Pamadi, B. N., 2004, *Performance, Stability, Dynamics, and Control of Airplanes: Second Edition*, AIAA Education Series, Reston, VA, pp. 126-128.

[11] Chartres, J. T. A., Grablin, M. H., and Schneider, G., "Optimisation of the Terminal Flight Phase for a Future Reusable Launch Vehicle," *AIAA Guidance Navigation and Control Conference*, AIAA, 2005, pp. 1-12.

[12] Ogata, K., 2008, *MATLAB for Control Engineers*, Pearson Prentice Hall, Upper Saddle River, NJ, pp. 305-307.

[13] Kluever, C. A., Horneman, K. R., and Schierman, J. D., "Rapid Terminal-Trajectory Planner for an Unpowered Reusable Launch Vehicle," *AIAA Guidance Navigation and Control Conference*, AIAA, 2009.

APPENDIX

Table 16. Data obtained using the variable HAC size technique from all fifty-trials.

	X_0 (ft)	Y_0 (ft)	Psi_0 (deg)	Energy	ϕ_{HAC} (deg)	I	Crosstrack Error (ft)	Downtrack Error (ft)	PSHA (deg)	ΔRF (ft)	ΔX_{HAC} (ft)
1	270000	50000	200	95%	21.5	1	1.19	38.95	193	211	0
2	150000	250000	235	98%	22.0	1	1.21	23.43	231	264	0
3	-60000	390000	270	100%	38.4	2	58.12	31.20	271	793	91
4	-280000	280000	315	93%	38.6	2	6.88	131.32	307	537	0
5	-150000	300000	300	100%	21.8	1	1.41	87.21	285	302	0
6	-370000	80000	355	90%	30.2	3	1.71	175.25	346	718	0
7	-150000	-300000	60	100%	21.8	1	1.41	87.21	285	302	0
8	60000	320000	260	102%	22.4	3	0.28	102.33	251	2126	1763
9	60000	380000	260	111%	22.6	10	0.77	2308.00	255	3117	1769
10	0	350000	265	105%	21.8	10	0.31	1839.51	262	3825	2975
11	-10000	300000	262	100%	19.6	6	0.04	8.00	262	3423	4023
12	-10000	270000	260	95%	19.8	1	0.34	145.62	257	653	0
13	-50000	330000	268	99%	23.2	2	1.34	1.62	269	442	118
14	-80000	340000	275	96%	28.0	2	0.13	39.17	273	735	0
15	-100000	300000	280	90%	26.1	1	1.41	25.72	276	440	0
16	-110000	320000	280	92%	28.5	2	1.64	110.89	278	723	0
17	-90000	300000	278	85%	31.4	3	1.54	102.17	274	797	0
18	-120000	250000	282	80%	26.1	1	0.12	177.62	279	457	0
19	-150000	220000	300	88%	20.8	1	0.00	192.46	287	333	0
20	-170000	300000	290	94%	25.7	1	1.76	123.92	288	605	0
21	-220000	350000	290	97%	46.1	9	122.13	139.45	295	436	3868
22	-330000	100000	340	100%	24.1	2	0.66	127.26	341	555	0
23	-350000	70000	345	93%	24.3	2	1.10	68.25	347	549	0
24	-250000	300000	310	98%	30.1	3	5.00	142.42	302	592	0
25	-280000	260000	320	100%	25.4	2	0.00	55.85	310	322	0
26	-300000	240000	330	112%	19.7	8	0.05	13.38	316	3969	4322
27	-340000	220000	335	106%	23.8	10	0.66	453.14	322	3293	4303
28	-360000	200000	335	104%	25.7	5	4.09	88.08	327	2854	486
29	-380000	150000	340	108%	22.4	10	0.23	1835.32	335	3717	3629
30	-100000	310000	280	102%	19.9	3	0.08	94.40	279	1621	1063

Table 16 Cont. Data obtained using the variable HAC size technique from the fifty-trials.

	X_0 (ft)	Y_0 (ft)	Psi_0 (deg)	Energy	ϕ_{HAC} (deg)	I	Crosstrack Error (ft)	Downtrack Error (ft)	PSHA (deg)	ΔRF (ft)	ΔX_{HAC} (ft)
31	-230000	360000	290	107%	29.7	6	7.58	109.44	296	2547	4132
32	250000	50000	175	104%	17.1	4	0.19	121.51	197	1998	1797
33	310000	70000	185	109%	16.6	10	0.81	456.63	198	3674	2019
34	300000	90000	195	113%	17.1	7	91.80	117.04	199	3498	1717
35	330000	150000	210	103%	35.7	10	50.22	714.52	203	2687	1583
36	280000	170000	215	107%	19.1	2	1.70	11.84	212	2988	683
37	260000	190000	220	105%	20.4	9	0.96	167.93	215	3433	1319
38	220000	240000	235	106%	20.7	4	2.07	73.02	224	2601	371
39	200000	260000	235	101%	26.1	10	2.33	1265.33	227	3557	3467
40	150000	260000	240	103%	19.5	9	0.02	147.32	234	4657	4921
41	140000	240000	245	99%	20.3	1	1.14	63.02	231	265	0
42	120000	270000	245	97%	23.2	1	1.50	184.00	237	195	0
43	80000	300000	250	95%	26.5	1	1.13	62.09	245	448	0
44	260000	50000	185	92%	23.6	1	1.63	50.16	192	41	91
45	270000	30000	182	96%	20.2	2	1.19	8.49	193	52	262
46	200000	100000	215	89%	20.6	1	0.36	66.32	204	283	0
47	210000	170000	230	87%	37.0	1	1.55	177.14	214	545	0
48	170000	190000	230	84%	33.5	2	1.30	73.80	221	653	0
49	150000	210000	235	97%	19.3	1	0.83	73.19	227	401	0
50	90000	310000	247	100%	23.5	1	0.49	96.99	244	509	0

Table 17. Data obtained using the variable HAC size technique from all fifty-trials.

	X_0 (ft)	Y_0 (ft)	Psi_0 (deg)	Energy	ϕ_{HAC} (deg)	I	Crosstrack Error (ft)	Downtrack Error (ft)	PSHA (deg)	ΔRF (ft)	ΔX_{HAC} (ft)
1	270000	50000	200	95%	30.0	2	1.25	4.66	195	152	917
2	150000	250000	235	98%	30.0	2	0.01	21.43	230	248	945
3	-60000	390000	270	100%	30.0	2	137.24	148.60	272	550	0
4	-280000	280000	315	93%	30.0	3	134.43	135.95	309	1573	0
5	-150000	300000	300	100%	30.0	2	0.00	119.30	282	469	1530
6	-370000	80000	355	90%	30.0	4	29.70	93.26	346	560	2257
7	-150000	-300000	60	100%	30.0	2	0.00	119.30	282	469	1530
8	60000	320000	260	102%	30.0	2	0.00	17.52	248	393	1423
9	60000	380000	260	111%	30.0	2	0.01	29.66	252	221	811
10	0	350000	265	105%	30.0	2	0.00	78.52	258	315	1330
11	-10000	300000	262	100%	30.0	2	0.00	26.58	256	336	1230
12	-10000	270000	260	95%	30.0	2	0.00	40.15	254	315	1210
13	-50000	330000	268	99%	30.0	1	0.01	20.41	265	272	838
14	-80000	340000	275	96%	30.0	1	0.44	58.47	272	244	776
15	-100000	300000	280	90%	30.0	2	0.09	12.01	276	337	1079
16	-110000	320000	280	92%	30.0	1	0.88	118.68	278	184	596
17	-90000	300000	278	85%	30.0	1	15.74	133.26	276	220	706
18	-120000	250000	282	80%	30.0	1	0.23	100.02	280	138	451
19	-150000	220000	300	88%	30.0	2	0.00	35.27	283	542	1770
20	-170000	300000	290	94%	30.0	2	0.00	32.87	288	291	971
21	-220000	350000	290	97%	30.0	1	0.00	163.32	296	318	0
22	-330000	100000	340	100%	30.0	3	0.00	179.30	337	427	1660
23	-350000	70000	345	93%	30.0	3	0.00	156.94	346	335	1350
24	-250000	300000	310	98%	30.0	2	5.08	193.51	302	478	1681
25	-280000	260000	320	100%	30.0	3	0.01	57.82	307	533	1904
26	-300000	240000	330	112%	30.0	2	0.00	74.57	309	369	0
27	-340000	220000	335	106%	30.0	3	0.00	124.43	318	624	2310
28	-360000	200000	335	104%	30.0	4	0.00	91.80	324	564	2126
29	-380000	150000	340	108%	30.0	4	0.00	93.35	332	669	2580
30	-100000	310000	280	102%	30.0	1	0.00	63.40	270	443	1390
31	-230000	360000	290	107%	30.0	2	0.45	89.91	295	380	1303
32	250000	50000	175	104%	30.0	2	0.00	104.60	197	278	1936
33	310000	70000	185	109%	30.0	2	0.02	104.76	197	157	1108
34	300000	90000	195	113%	30.0	2	0.00	199.44	200	165	1188
35	330000	150000	210	103%	30.0	2	58.39	95.07	204	169	1070

Table 17 Cont. Data obtained using the variable HAC size technique from all fifty-trials.

	X_0 (ft)	Y_0 (ft)	Psi_0 (deg)	Energy	ϕ_{HAC} (deg)	I	Crosstrack Error (ft)	Downtrack Error (ft)	PSHA (deg)	ΔRF (ft)	ΔX_{HAC} (ft)
36	280000	170000	215	107%	30.0	2	0.03	17.92	212	131	951
37	260000	190000	220	105%	30.0	2	0.74	168.02	216	140	1053
38	220000	240000	235	106%	30.0	2	0.51	42.91	225	212	1112
39	200000	260000	235	101%	30.0	2	0.77	57.17	227	207	1199
40	150000	260000	240	103%	30.0	2	0.08	48.05	235	207	1049
41	140000	240000	245	99%	30.0	2	0.05	135.46	234	237	1245
42	120000	270000	245	97%	30.0	2	0.03	84.83	236	285	1401
43	80000	300000	250	95%	30.0	2	0.07	2.38	245	290	1064
44	260000	50000	185	92%	30.0	2	0.76	31.83	196	254	1512
45	270000	30000	182	96%	30.0	2	0.36	60.96	192	238	1459
46	200000	100000	215	89%	30.0	2	0.12	73.13	208	190	1181
47	210000	170000	230	87%	30.0	2	14.15	51.78	215	332	1480
48	170000	190000	230	84%	30.0	2	4.69	34.04	222	248	1131
49	150000	210000	235	97%	30.0	2	0.02	24.45	229	194	1056
50	90000	310000	247	100%	30.0	2	0.02	2.45	244	228	818